Journal of Environmental Chemical Engineering 11 (2023) 110380

Contents lists available at ScienceDirect

Journal of Environmental Chemical Engineering

journal homepage: www.elsevier.com/locate/jece

Activation of persulfate and peroxymonosulfate for the removal of herbicides from synthetic and real waters and wastewaters

Enric Brillas

Laboratori d'Electroquímica dels Materials i del Medi Ambient, Secció de Química Física, Facultat de Química, Universitat de Barcelona, Martí i Franquès 1–11, Barcelona, Spain

ARTICLE INFO

Editor: Stefanos Giannakis

Keywords:
Catalytic activation
Electrochemical activation
Photocatalytic activation
UV activation
Thermal activation
Water treatment

ABSTRACT

Over the last decades, the quantity and quality of crops have been maintained by means of large and increasing amounts of synthetic herbicides, thus ensuring a world food production. The high recalcitrance and stability of these compounds at ambient conditions avoid their effective removal in municipal wastewater treatment facilities. Among the potential powerful oxidation treatments that are being developed for removing herbicide pollutants, sulfate radical ($SO_4^{\bullet-}$) based-advanced oxidation processes (AOPs) have experienced growing interest because they can compete with conventional AOPs only generating reactive oxygen species (ROS) like hydroxyl radical ($^{\bullet}OH$). This review presents a detailed, comprehensive, and critical analysis on the application of hybrid processes for the remediation of synthetic and real waters and wastewaters contaminated with herbicides at bench scale by using persulfate (PS) or peroxymonosulfate (PMS) as oxidant. Their activation originated $SO_4^{\bullet-}$, which is partially transformed into $^{\bullet}OH$. Other ROS like $O_2^{\bullet-}$ and were formed depending on the experimental conditions. The fundamentals and main reactions involved in the activation with thermal, catalytic (with iron ions, Fe, and other materials), UV (with and without Fe^{2+}), photocatalytic, and electrochemical processes are described. Papers with the application of each activation procedure to remove herbicide pollutants from each oxidant are summarized, being detailed for selected works their degradation and mineralization efficiency, the influence of scavengers, added inorganic anions, natural organic matter like humic acid, and water matrix. The by-products detected are reported as well. Comparative treatments with both oxidants and analogous processes with H_2O_2 were finally discussed.

1. Introduction

Many synthetic compounds are used as agrochemicals or pesticides that are industrially produced for controlling, preventing, or destroying animal or unwanted fungal pests. The target organism to be inactivated or destroyed by pesticides allows their classification into rodenticides, fungicides, insecticides, herbicides, and so on. Over the last decades, the intensive agriculture has used increasing amounts of herbicides to rise the world food production by maintaining the quantity and quality of crops. They can act in different ways over plants and fruits, e.g., as desiccants, defoliants, plant growth regulators, or for preventing the premature fall of fruits [1]. The properties of herbicides are closely related to their chemical structure and so, they are listed in families like triazine, urea, organophosphate, organochlorine, and chlorophenoxy acid, among others [2]. However, several phenomena including deposition, soil erosion, spray-drift, leaching, and run-off cause the entry of these substances into aquatic ecosystems [1]. It has been well documented the detection of herbicides residues and their metabolites at trace contents from ng L^{-1} to μg L^{-1} in natural waters like rivers, lakes, and seas. Despite their low concentration in aquatic systems, their potential chronic and acute toxicity can affect the ecosystems and human health, and for this reason, they are cataloged as priority persistent organic pollutants (POPs) [3,4]. Research efforts have been made to explore the effectiveness of powerful oxidation methods to remove herbicides from waters and wastewaters to avoid their environmental and health risks.

The majority of herbicides present a large chemical and photochemical stability at ambient conditions. This explains their hard destruction in municipal wastewater treatment plants (WWTPs) by conventional biological (aerobic and anaerobic) and physicochemical processes. To remediate contaminated soils, herbicides are previously extracted with surfactants and a flushing effluent is obtained for treatment [4]. The most efficient methods to remove herbicides from synthetic and real waters and wastewaters are the advanced oxidation

E-mail address: brillas@ub.edu.

https://doi.org/10.1016/j.jece.2023.110380
Received 25 April 2023; Received in revised form 25 May 2023; Accepted 14 June 2023
Available online 16 June 2023

processes (AOPs). The common feature of AOPs is the production of reactive oxygen species (ROS) on site like hydroxyl radical ($^{\bullet}OH$), with a standard reduction potential (E^{o}) as high as 2.72 V/SCE. This radical non-selectively reacts with most organics typically via hydroxylation and dehydrogenation processes until their mineralization is attained [5–7]. Other weaker ROS like superoxide ion ($O_2^{\bullet-}$) and singlet oxygen ($^1O_2$) can be formed depending on the aqueous matrix tested, operating conditions, and method applied. Environment-friendly processes generating ROS such as O_3-based treatments, gamma irradiation, pulse electric discharge plasma, UV/H_2O_2 photolysis, photocatalysis with TiO_2/UV or ZnO/UV, and electrochemical processes including electrochemical oxidation, electro-Fenton, photoelectro-Fenton, and photoelectrocatalysis have demonstrated their effectiveness for herbicides removal [4,5,8–11]. Other interesting and powerful procedures with emerging sulfate radical ($SO_4^{\bullet-}$)-based AOPs are being recently developed as well [12,13]. In situ produced $SO_4^{\bullet-}$ is another strong oxidant with an $E^{o} = 2.44$ V/SCE, comparable to that $^{\bullet}OH$ [5]. Since $SO_4^{\bullet-}$ possesses greater selectivity to attack organics and longer half-life (≈ 40 μs) than $^{\bullet}OH$ (≈ 20 ns) [13–15], sulfate radical based-AOPs have been postulated to have larger efficiency for the removal and mineralization of organic pollutants. Persulfate ($S_2O_8^{2-}$, PS) and peroxymonosulfate (HSO_5^-, PMS) are weak oxidants that can be easily activated to form $SO_4^{\bullet-}$, which can then evolve to $^{\bullet}OH$. Other ROS in more or less extent can be produced depending on the experimental conditions. Although both radicals can attack the organic pollutants in aqueous matrices, it has been reported that $SO_4^{\bullet-}$ prevails at pH < 7 while $^{\bullet}OH$ predominates in alkaline media, thus largely affecting the efficiency of sulfate radical based-AOPs [14,15]. Recent works have shown the great interest of removing herbicides by PS and PMS, where the activation method plays a fundamental role to explain their effectiveness. However, a detailed review of these treatments has not been reported yet in the literature.

This article presents a comprehensive and critical review on the activation processes of PS and PMS oxidants that have been applied to remediate synthetic and real waters and wastewaters contaminated with herbicides. Thermal, catalytic, UV, photocatalytic, and electrochemical activations have been summarized for each oxidant. For each activation method, the main reactions involved are described and selected works dealing with the removal of herbicides are analyzed with attention to their efficiency and the influence of scavengers, added inorganic anions, natural organic matter (NOM) like humic acid, and water matrix. Finally, comparative treatments with both oxidants and H_2O_2 are detailed and discussed.

2. Bibliometric analysis

The Scopus database was used to search the reviews and scientific papers that have been peer-reviewed for the activation of persulfate and peroxymonosulfate for the removal of herbicides from synthetic and real waters and wastewaters up to February 2023. The keyword “Herbicides” and “Persulfate” was introduced in it, followed by “Herbicides” and “Peroxymonosulfate”. A total of 2 reviews related to PS and 89, 67, and 13 scientific papers referring to PS, PMS, and both comparative treatments, respectively, were finally selected. Communications in congresses and articles do not written in English were excluded. The authors, title, and abstract of each retrieved publication were listed and individually analyzed before its acceptance in this review. Similar activation processes have been considered for both oxidants including thermal, catalytic (with iron ions, Fe, and other materials), UV (without and with Fe^{2+}), photocatalytic, and electrochemical treatments. The works usually described: (i) the synthesis and/or characterization of materials used to activate each oxidant, (ii) the influence of operating variables (temperature, pH, catalyst, oxidant, and herbicide concentrations, light irradiation, anodes and photoanodes, aqueous matrix, etc.) on herbicide degradation associated with its content decay measured by high-performance liquid chromatography (HPLC), (iii) the evolution of experimental parameters related to the herbicide mineralization such as total organic carbon (TOC) and chemical oxygen demand (COD) decay, (iv) the determination of energetic parameters, (v) the detection of the oxidizing radical species produced by means of electron paramagnetic resonance (EPR) or the inhibitory action of selected scavengers, (vi) the effect of added inorganic anions, NOM, and water matrix, and (vii) the identification of the by-products formed, usually by means of gas chromatography-mass spectrometry (GC-MS) or LC-MS/MS, with the proposal of a reaction sequence for the degradation or mineralization of the herbicide. The present review briefly exposes the fundamentals of each method applied to activate PS or PMS, followed by the analysis of the removal of selected herbicides using each oxidant or their comparison typically in synthetic solutions. Special emphasis over the operating variables, oxidizing species generated, and by-products detected is made. This review includes 4 tables and 19 figures, which have been designed to remark the findings described.

At present, few reviews have reported some specific examples over the destruction of herbicides only activated by PS. Gagol et al. [16] reviewed the characteristics of the hydrodynamic and acoustic cavitation technologies coupled to conventional activation methods to oxidize few herbicides, whereas Zhou et al. [17] presented a short review over the factors influencing the PS-based processes to remediate groundwaters and soils, with reference to the removal of several herbicides. However, any previous review has considered a comprehensive work summarizing the PS- and PMS-based AOPs to destroy herbicides from synthetic and real wasters and wastewaters up to February 2023, involving all the developing time of these oxidation technologies.

The above bibliometric analysis identified 102 scientific articles reporting PS-based processes, 89 of them regarding the use of PS alone and other 13 ones for comparison with PMS. Fig. 1a depicts that most publications (71 articles) have been published in the latter 5 years, since 2018, demonstrating the increasing and current interest of the application of PS-based AOPs to remove herbicides. Considering the PS activation, Fig. 1b makes evident that Fe activation with 18 articles (17.6%) has been the most applied method, followed by 17 articles (16.7%) with other catalytic or UV activation, 14 articles (13.7%) with photocatalytic activation, 13 articles (12.7%) with iron ions or electrochemical activation, and 10 articles (9.8%) with thermal activations. Concerning the PMS-based AOPs, a lower number of 67 articles have been published with this oxidant alone and other 13 ones by comparing with PS. Fig. 1c shows the acceleration of publications of such treatments since 2018, with a maximum number of 29 articles in 2022–2023. This highlights again the relevant recent interest of this technology to destroy herbicides. Fig. 1d reveals that the higher number of works corresponded to catalytic activation with a total of 56 articles including 6 articles (7.5%) for iron ions activation, 3 articles (3.8%) for Fe activation, and 47 articles (58.8%) for other materials. A relatively important number of 15 articles (18.7%) has been focused to photocatalytic activation, but ≤ 6 articles (≤ 7.5%) have been considered for thermal, UV, or electrochemical activation. All papers focused the effectiveness of the PS- and/or PMS-based AOPs in synthetic waters and wastewaters, being the effect of scavengers, inorganics anions, and NOM usually described. The treatment with real matrices, including tap water, river water, lake water, groundwater, and wastewater (WWTP) effluents has been analyzed in many cases as well. In general, conventional systems have been used and comparison with other common AOPs has been scarcely reported, except using H_2O_2.

Many activated PS and PSM processes have also been recently developed to remediate waters contaminated with other emerging organic pollutants. For instance, a total of 268 and 156 reviews and scientific papers have been published referred to using PS and PMS as oxidants of pharmaceuticals waters and wastewaters, respectively, of which 142 (53.0%) and 121 (77.6%) in the last three years (data from Scopus).

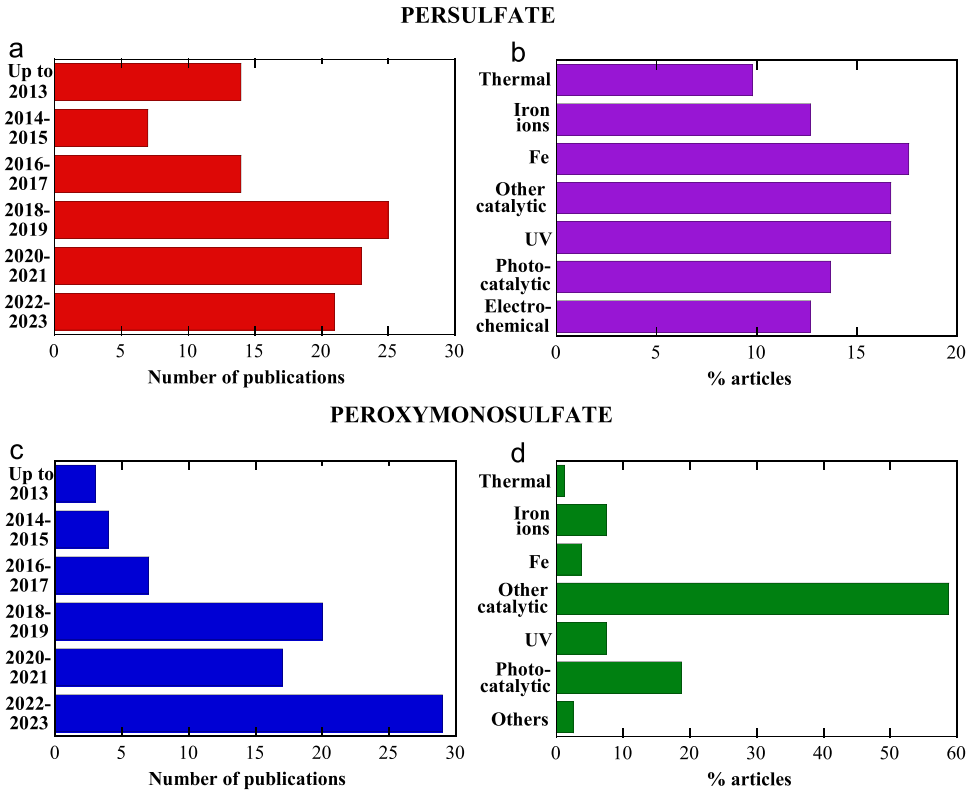

Fig. 1. Bibliometric analysis of the literature for (a,b) persulfate and (c,d) peroxymonosulfate activation to remediate herbicides from waters and wastewaters. (a,c) Number of publications by year. (b,d) Percentage of articles for the thermal, iron ions, Fe, other catalytic, UV (including with Fe^{2+}), photocatalytic, and electrochemical activations.

3. Removal of herbicides by persulfate based-processes

As can be seen in Fig. 1, PS based-processes have been the most ubiquitous $SO_4^{\bullet-}$ based-AOPs used to destroy herbicides in synthetic and real waters and wastewaters. This section is devoted to analyze the fundamentals and applications of different activation processes to enhance the oxidation power of PS, including thermal, iron ions, Fe, other catalytic materials, UV, UV with Fe^{2+}, photocatalytic, and electrochemical processes, as described below.

3.1. Thermal activation

The PS process activated by heat (PS/heat) has been checked for herbicides like clomazone, paraquat, and glyphosate [18], diuron [19], atrazine (ATZ) [20–22], clopyralid [23], 2,4-dichlorophenozyacetic acid (2,4-D) [24], simazine [21,25], and aminopyralid and picloram [26], as well as for the remediation of contaminated soils [21,27]. Table 1 lists the best results obtained for selected papers, indicating the system used and experimental remarks.

In the PS/heat process, the molecule of PS is energetically activated and homolytically decomposed into two $SO_4^{\bullet-}$radicals as follows [25]:

$$S_2O_8^{2-} + \text{heat} \rightarrow 2SO_4^{\bullet-}\ k_2 = 5{\cdot}8 \times 10^{-5}\ M^{-1}\ s^{-1}\ (\text{at } 65\ ^\circ C) \quad (1)$$

where k_2 denotes the second-order rate constant of the reaction. $SO_4^{\bullet-}$ thus formed can react with H_2O or OH^- via reactions (2) or (3) to generate $^\bullet OH$ [25], being much faster the second one in alkaline medium. Both strong oxidizing radicals can then attack the organic pollutants. However, they undergo rapid and undesirable parasitic reactions like (4)–(7) [25], where they are consumed limiting their efficiency.

$$SO_4^{\bullet-} + H_2O \rightarrow SO_4^{2-} + {}^\bullet OH + H^+\ k_2 = 200\ M^{-1}\ s^{-1} \quad (2)$$

$$SO_4^{\bullet-} + OH^- \rightarrow SO_4^{2-} + {}^\bullet OH\ k_2 = 6{\cdot}5 \times 10^7\ M^{-1}\ s^{-1} \quad (3)$$

$$2SO_4^{\bullet-} \rightarrow S_2O_8^{2-}\ k_2 = 8{\cdot}1 \times 10^8\ M^{-1}\ s^{-1} \quad (4)$$

$$SO_4^{\bullet-} + {}^\bullet OH \rightarrow HSO_5^-\ k_2 = 1{\cdot}0 \times 10^{10}\ M^{-1}\ s^{-1} \quad (5)$$

$$SO_4^{\bullet-} + S_2O_8^{2-} \rightarrow SO_4^{2-} + S_2O_8^{\bullet-} k_2 = 1{\cdot}2 \times 10^6\ M^{-1}\ s^{-1} \quad (6)$$

$$S_2O_8^{2-} + {}^\bullet OH \rightarrow S_2O_8^{\bullet-} + OH^-\ k_2 = 1{\cdot}4 \times 10^7\ M^{-1}\ s^{-1} \quad (7)$$

Table 1 shows that the systems used in these assays were either stirred tank reactors or glass vials usually immersed into a thermostatic water bath to regulate the temperature. The main drawback of these systems is the solution evaporation for > 35 °C, then being necessary their sealing to the atmosphere. Small volumes (up to 100 mL) of herbicides in synthetic solutions were degraded by PS/heat and only the effectiveness of the treatment at bench scale was evidenced, but not its viability at industrial scale. To do this, continuous flow systems with large volumes of heated effluents upon controlled PS injection should be proposed, a challenge to be developed in next future.

The studies on the s-triazines atrazine [20,22] and simazine [25], and the pyridine clopyralid [23] up to 50 μM content, and the chlorophenoxyacetic acid 2.4-D [24] at 100 mg L^{-1} disclosed an enhancement of the herbicide removal with raising the PS concentration and temperature, and with decreasing the herbicide content and pH. The herbicide concentration (c) decay with time was determined by HPLC and always obeyed a pseudo-first-order kinetics with an apparent rate constant (k_1) determined as the slope of the corresponding linear ln (c_0/c)-time plot. Variable k_1-values between 0.019 and 0.22 min^{-1} have been reported depending on the experimental conditions (see Table 1). The latter higher k_1-value was found for 100 mL of 10 μM simazine in pure water with 0.50 mM PS at pH = 7.0 and 65 °C, as shown in Fig. 2 [25], which exemplifies the above behavior. So, Fig. 2a highlights the greater degradation at lower simazine concentration since less quantity of organic matter is oxidized with a similar quantity of generated

Table 1
Selected results obtained for herbicides removal by thermal, iron ions, Fe, and other catalytic activations of persulfate.

Herbicide	System	Experimental remarks	Best results	Ref.
Thermal activation				
Atrazine	Stirred tank reactor immersed into a thermostatic water bath	50 mL of 50 μM herbicide and 0–2.0 mM PS in pure water, pH = 3.0–10.0, effect of scavengers, NOM, Cl^-, and HCO_3^-, 20–60 °C, 120 min	Faster removal at higher temperature and PS content. At pH = 7.0, total degradation in 120 min with 2.0 mM PS at 50 °C, and in 80 min with 1.0 mM PS. Slower degradation at higher pH and NOM, Cl^-, and HCO_3^- contents. $SO_4^{\bullet-}$ predominant in acid and neutral pH, $^\bullet OH$ in basic pH. 10 aromatic by-products detected by LC-MS	[20]
Atrazine	Glass vial immersed into a thermostatic water bath	100 μM herbicide and 0.1–20 mM PS in pure water, pH = 4.0–10.0, effect of scavengers, 40 °C, 60 min	Faster degradation up to 66% ($k_1 = 0.019\ min^{-1}$) with 20 mM PS at pH = 7.0. Contribution of $SO_4^{\bullet-}$ and $^\bullet OH$ as oxidants.	[22]
Clopyralid	Glass vial immersed into a thermostatic water bath	50 mL of 50 μM herbicide and 0–2.0 mM PS in pure water, pH = 3.0–10.0, effect of scavengers, 20–60 °C, 120 min	Quicker degradation at higher PS content and temperature, as well as at lower pH. Total degradation ($k_1 = 0.033\ min^{-1}$) with 2.0 mM PS, pH = 4.82, and 50 °C. $E_a = 140.0\ kJ\ mol^{-1}$. Predominance of oxidant $SO_4^{\bullet-}$. Identification or 3 heteroaromatic, 13 N-aliphatic, and 12 aliphatic acids by-products by LC-MS	[23]
2,4-D	Stirred tank reactor with a thermostatic equipment	100 mL of 100 mg L^{-1} herbicide and 3.6–27 mM PS in pure water, pH = 3.0–12.0, effect of scavengers, Cl^-, NO_3^-, and HCO_3^-, 20–70 °C, 180 min	Removal enhancement with raising PS content and temperature. and with decreasing pH. Total degradation ($k_1 = 0.075\ min^{-1}$) for 18 mM PS, pH = 3.0, and 60 °C. Negative influence of inorganic anions added. Predominance of oxidant $SO_4^{\bullet-}$.	[24]
Simazine	Stirred tank reactor immersed into a thermostatic water bath	100 mL of 2.5–50 μM herbicide and 0–0.50 mM PS in pure water, pH = 3.0–11.0, effect of Cl^-, NO_3^-, HCO_3^-, SO_4^{2-}, $H_2PO_4^-$, and humic acid, 25–75 °C, 120 min	Greater percent of herbicide decay with lower herbicide content and pH, and at higher PS content and temperature. Toral removal in 30 min ($k_1 = 0.22\ min^{-1}$) for 10 μM herbicide, 0.50 mM PS, pH = 7.0, and 65 °C. Anions and humic acid (as NOM) inhibited degradation. Predominance of oxidant $SO_4^{\bullet-}$, increasing $^\bullet OH$ in basic medium. 13 heteroaromatic derivatives identified by LC-MS.	[25]
Iron ions activation				
Atrazine	Screw-cap cylindrical glass vial with Fe^{2+}	3 mg of soil spiked with 0.3 μg herbicide with 33 mL of 3.3:3.3–16.6:16.6 mM of PS/Fe^{2+} ratio in pure water, effect of scavengers, pH = 3.0–6.2, 23 °C, 600 min	Lower pH and greater PS/Fe^{2+} ratio enhanced herbicide removal. 80% degradation ($k_1 = 2.3 \times 10^{-3}\ min^{-1}$) for 16.6:16.6 mM PS/$Fe^{2+}$ ratio at pH = 3.0. $SO_4^{\bullet-}$ as dominant oxidant. 5 heteroaromatic by-products identified by LC-MS/MS	[31]
Atrazine	Centrifuge tube with Fe^{3+} and MBQ[a]	50 mL of 0.039 mM herbicide, 0.10–0.30 mM PS, 0.05–0.20 mM Fe^{3+}, and 0.10–0.30 mM MBQ in pure water, pH = 2.0–7.0, effect of scavengers, 25 °C, 60 min	Positive action of MBQ to generate Fe^{2+}. Higher degradation with raising PS, Fe^{3+}, and MBQ doses. 60% herbicide decay with 0.25, 0.20, and 0.30 mM of such species, respectively, at pH = 3.0. Slightly lower degradation at the other pH values. Production of Fe (IV) from Fe^{2+} as oxidant. 14 heteroaromatic derivatives detected by LC-MS/MS	[33]
2,4-D	Stirred tank reactor with Fe^{2+}, H_2O_2, or NaOH	250 mL of 0.452 mM herbicide, 100 mM PS and 10 mM Fe^{2+}, 300 mM H_2O_2 (pH 5.6) or 50 mM NaOH in pure water, 20–70 °C, up to 216 h	Total degradation in 6 h with PS at 70 °C, in 48 h with PS/Fe^{2+} at 20 °C, and in 216 h with PS/H_2O_2 and PS/NaOH at 20 °C. Total TOC removal under these conditions. The cost for PS/Fe^{2+} was 1.71 US$ (g TOC)$^{-1}$.	[34]
Diuron	Stirred tank reactor with Fe^{2+}, citrate, and/or hydroxylamine	50 mL of 0.01–0.05 mM herbicide, 0.2–1.0 mM PS, 0.05–2.0 mM Fe^{3+}, and/or 0.0–1.0 mM citric acid or hydroxylamine in pure water, pH = 3.0–9.0, 240 min	Faster removal at lower pH. At pH = 7.0, 68% degradation ($k_1 = 1.23 \times 10^{-3}\ min^{-1}$) for 0.05 mM herbicide, 1.0 mM PS, and 1.0 mM Fe^{2+}, 81% degradation ($k_1 = 1.80 \times 10^{-3}\ min^{-1}$) for 0.01 mM herbicide and 0.2 mM of PS, Fe^{2+}, and citric acid, and 91% degradation ($k_1 = 4.09 \times 10^{-3}\ min^{-1}$) for 0.01 mM herbicide, 0.2 mM PS, 0.2 mM Fe^{2+}, and 0.4 mM hydroxylamine	[36]
Fe activation				
Alachlor	Stirred glass vessel with ZVI[b]	200 mL of 5 mg L^{-1} herbicide, 0.5–3.0 mM PS, and 0.5–10 mM catalyst in pure water, pH = 1.5–10.0, effect of Cl^-, NO_3^-, HCO_3^-, SO_4^{2-}, and NOM, 30–60 °C, 60 min	Degradation decreased at higher pH and increased at greater PS up to 2.0 mM and catalyst content. Overall decay in 30 min for 2.0 mM PS and 10 mM catalyst at pH = 1.5 and 3.0. Strong inhibition with Cl^-, HCO_3^-, and NOM, but little effect with NO_3^- and SO_4^{2-}. 23 aromatic derivatives found by LC-MS	[39]
Atrazine	Conical flask with a rotatory shaker with nZVI[c] /graphene	100 mL of 10 mg L^{-1} herbicide, 0.2–2.5 mM PS, and 50–200 mg L^{-1} catalyst in pure water, pH = 3.0–9.0, effect of scavengers and NOM, 15–40 °C, 60 min	Quicker abatement at 0.80 mM PS, 100–150 mg L^{-1} catalyst, pH = 3.0, and 40 °C. 92% herbicide abatement in 20 min with 39% TOC reduction for 0.50 mM PS and 100 mg L^{-1} catalyst at pH = 6.0 and 25 °C. Predominance of oxidant $SO_4^{\bullet-}$. 9 heteroaromatic by-products identified by LC-MS/MS	[42]
Atrazine	Conical flask with a rotatory shaker with nZVI/graphene like-carbon sheet	100 mL of 10 mg L^{-1} herbicide, 0.1–2.0 mM PS, and 50–200 mg L^{-1} catalyst in pure water and river water, pH = 3.0–9.0, effect of scavengers, Cl^-, and humic acid, 15–35 °C, 60 min	More rapid decay in pure water for 2.0 mM PS, 200 mg L^{-1} catalyst, pH = 3.0, and 35 °C. 88% degradation with 62% TOC removal for 0.50 mM PS, 200 mg L^{-1} catalyst, pH = 3.0, and 25 °C. Inhibitory	[43]

(*continued on next page*)

Table 1 (*continued*)

Herbicide	System	Experimental remarks	Best results	Ref.
			action of Cl^- and humic acid. Predominance of oxidant $SO_4^{\bullet-}$ in front of $^{\bullet}OH$, $O_2^{\bullet-}$, and $^1O_2$. Low reusability of the catalyst after 3 consecutive runs. 52% removal with river water. 7 heteroaromatic intermediates found by LC-MS	
Atrazine	Stirred tank reactor with 0:15 M S-nZVI/biochar	100 mL of 10 mg L^{-1} herbicide, 0.5–2.0 mM PS, and 50–250 mg L^{-1} catalyst in pure water, tap water, and river water, pH = 2.86–10.53, effect of Cl^-, CO_3^{2-}, and HCO_3^-, 15–35 °C, 60 min	In pure water, quicker abatement for 2.0 mM PS, 100 mg L^{-1} catalyst, pH = 2.86, and 30 °C. Under these conditions, total degradation in 60 min, even at 25 °C. E_a = 49.5 kJ mol^{-1}. Herbicide removal dropped down to 82% and 61% for tap and river water, respectively. Large inhibition with added anions. Excellent reusability of the catalyst after 3 consecutive runs. 4 heteroaromatic by-products detected by LC-MS	[45]
Clofibric acid	Stirred tank reactor with Fe powder	600 mL of 0.01 mM herbicide, 135–675 mg L^{-1} PS, and 14–140 mg L^{-1} catalyst in pure water, real and synthetic municipal wastewater with NH_4^+ and glucose, pH = 5.0–9.0, effect of scavengers, 21 °C, 120 min	No significant influence of pH. Herbicide removed more rapidly at greater PS and catalyst contents. In pure water, total abatement in 10 min (k_1 = 0.014 min^{-1}) for 675 mg L^{-1} PS and 140 mg L^{-1} catalyst at pH = 7.0. Slower degradation in synthetic ($k_1 = 5.4 \times 10^{-4}$ min^{-1}) and real ($k_1 = 5.4 \times 10^{-4}$ min^{-1}) municipal wastewater with 270 mg L^{-1} PS and 56 mg L^{-1} catalyst. Predominance of oxidant $SO_4^{\bullet-}$	[50]
2,4-D	Stirred tank reactor with pre-magnetized Fe-C	100 mL of 20 mg L^{-1} herbicide, 0.5–2.0 mM PS, and 125–750 mg L^{-1} catalyst in pure water, pH = 3.0–10.0, 60 min	Degradation decayed at greater pH. Maximum abatement of 98–100% with 1.5–2.0 mM PS and 500–750 mg L^{-1} catalyst. 10 aromatic by-products and 5 final carboxylic acids detected by GC-MS	[51]
Fenuron	Conical flask on thermostatic rotary shaker with ZVI	100 mL of 0.06–0.24 mM herbicide, 1.0–4.0 mM PS, and 0.25–1.25 g L^{-1} catalyst in pure water, tap water, and river water, pH = 3.0–11.0, 10–40 °C, 360 min	In pure water, total removal in 30 min (k_1 = 0.047 min^{-1}) for 0.12 mM herbicide, 2.0 mM PS, 0.50 g L^{-1} catalyst. pH = 7.0, and 25 °C. TOC reduced by 86% in 360 min. Good reusability in 3 successive runs. After 60 min, degradation: 88% for tap water and 91% for river water. $SO_4^{\bullet-}$ played a predominant oxidation role. 9 aromatic by-products identified by LC-MS/MS	[54]
Other catalytic activation				
Atrazine	Stirred tank reactor with dithionite ($S_2O_4^{2-}$)	100 mL of 1 μM herbicide, 0.05–0.50 mM PS, and 0–0.50 mM catalyst in pure water, pH = 3.0–11.0, effect of scavengers, Cl^-, HCO_3^-, and NOM, 20–50 °C, 150 min	Greater removal at higher PS content, up to 0.20 mM catalyst, smaller pH, and higher temperature. Total herbicide decay in 90 min (k_1 = 0.051 min^{-1}) with 0.50 mM PS, 0.20 mM catalyst, pH = 7.0, and 30 °C. 44% TOC reduction in 150 min. $SO_4^{\bullet-}$ predominated as oxidant. Inhibition effect of added species. 8 heteroaromatic by-products found by GC-MS	[58]
Atrazine	Stirred tank reactor with Fe_3O_4/sepiolite	100 mL of 10 mg L^{-1} herbicide, 23–184 mM PS, and 1 g L^{-1} catalyst in pure water, pH = 3.0–11.0, effect of scavengers, 30 °C, 90 min	Higher and similar degradation at pH = 3.0 and 5.0, 66% herbicide abatement ($k_1 = 4.2 \times 10^{-3}$ min^{-1}) for 46 mM PS and pH = 5.0. k_1 rose to 8.2×10^{-3} min^{-1} for 184 mM PS. Generation of $SO_4^{\bullet-}$ and $O_2^{\bullet-}$ as oxidants. Good reusability after 4 consecutive cycles	[59]
Atrazine	Stirred tank reactor with Cu^{2+}/MoS_4-LDH[d]	20 mL of 10 mg L^{-1} herbicide, 1.0–4.0 mM PS, 1.0–5.0 mg L^{-1} Cu^{2+}, and 0.05–0.20 g L^{-1} MoS_4-LHD in pure water, pH = 3.0–11.0, effect of scavengers, Cl^-, NO_3^-, HCO_3^-, CO_3^{2-}, HPO_4^-, and humic acid, 25 °C, 60 min	Herbicide more rapidly destroyed at higher PS and MoS_4-LHD content, 2.0–4.0 mg L^{-1} Cu^{2+}, and pH 7.0. Under these conditions, 85% degradation with k_1 = 0.022 min^{-1}. Strong inhibition with Cl^-, CO_3^{2-}, HPO_4^-, and humic acid, Major oxidation role of $SO_4^{\bullet-}$ than $^{\bullet}OH$. Low reusability after 5 successive steps. 9 heteroaromatic intermediates identified by LC-MS	[61]
Atrazine	Stirred tank reactor with sulfur/Fe_3O_4	100 mL of 5 μM herbicide, 0.5–4.0 mM PS, and 0.05–0.30 g L^{-1} catalyst in pure water, groundwater, and river water, pH = 4.0–9.0, effect of scavengers, 25 °C, 50 min	In pure water, faster herbicide removal at greater PS and catalyst content, and pH = 4.0. At this pH, with 1.0 mM PS and 0.10 g L^{-1} catalyst, overall decay in 20 min with k_1 = 0295 min^{-1}. Superior oxidation with $SO_4^{\bullet-}$ than $^{\bullet}OH$. Low reusability after 7 consecutive cycles. More inhibition in river water than in groundwater. 13 heteroaromatic by-products found by LC-MS	[64]
2,4-D	Stirred tank reactor with FeS	100 mL of 10 mg L^{-1} herbicide, 0.5–5.0 mM PS, and 0.10–0.50 g L^{-1} catalyst in pure water, pH = 3.0–11.0, effect of scavengers, Cl^-, NO_3^-, and HCO_3^-, 20–50 °C, 120 min	Lower degradation at greater pH. Increasing removal up to 2.5 mM PS and 0.50 g L^{-1} catalyst, and with raising temperature. Total herbicide decay with 90% TOC removal for 1.25 mM PS, 0.15 g L^{-1} catalyst, pH = 4.5, and 30 °C. E_a = 19.47 kJ mol^{-1}. Inhibitory effect: low for Cl^-, moderate for NO_3^-, and larger for HCO_3^-. More important oxidant role of $^{\bullet}OH$ than $SO_4^{\bullet-}$. Moderate reusability after 7 consecutive steps 10 aromatic derivatives and 6 final carboxylic acids detected by GC-MS	[66]
Pentachlorophenol	Florence flask in a shaker with ascorbic acid	60 mL of 200 mg L^{-1} herbicide, 40 mM PS, and 0.2–4.0 mM catalyst in pure water, pH = 2.5–12.5, effect of scavengers, 180 min	Quicker degradation at 1.0 mM catalyst. Under these conditions, 72% removal at pH = 7.2. Similar oxidant role of $^{\bullet}OH$ and $SO_4^{\bullet-}$. 9 aromatic by-products and 2 final carboxylic acids identified by GC-MS	[68]

[a] MBQ: methyl-*p*-benzoquinone.
[b] ZVI: Zero-valent iron.
[c] nZVI: Nano zero-valent iron.
[d] LDH: Layer double hydroxide.

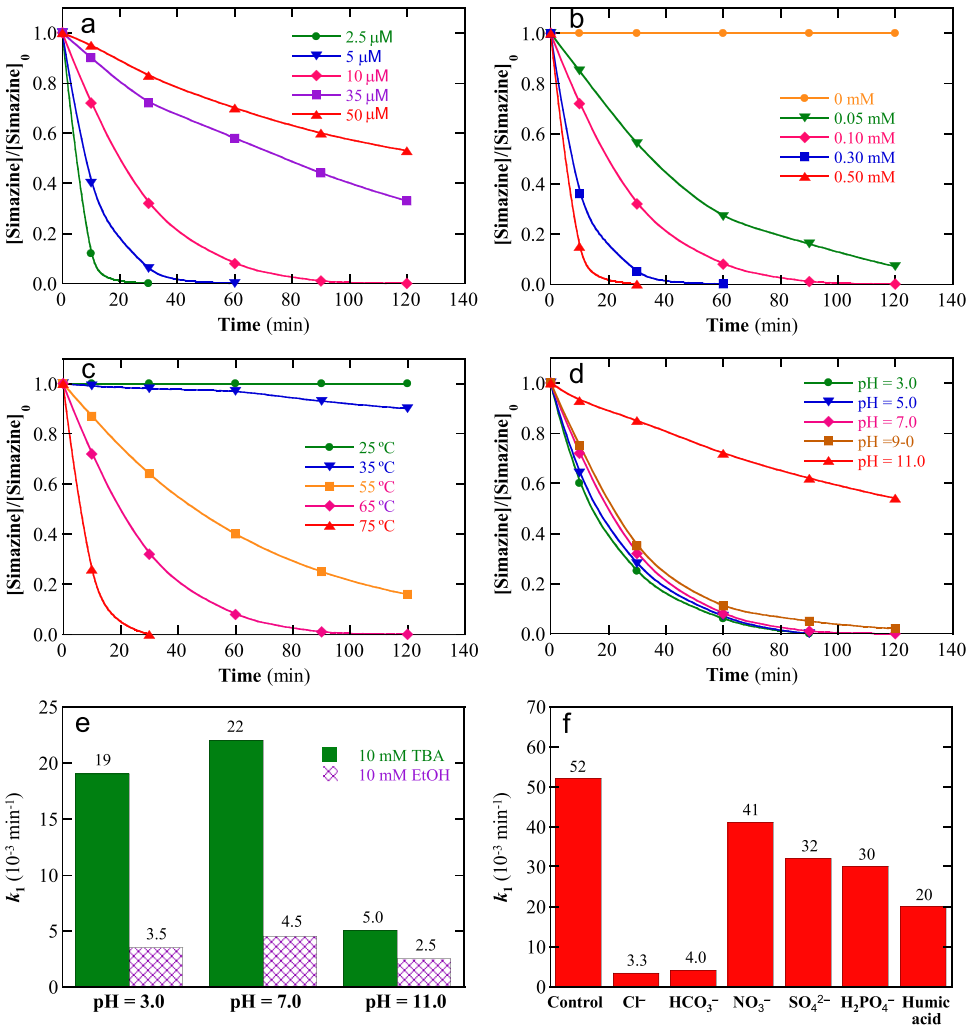

Fig. 2. Degradation of simazine upon thermal activation of PS. The assays were made with 100 mL solutions in a stirred tank reactor immersed in a thermostatic bath. Effect of: (a) herbicide content for 0.10 mM PS, pH = 7.0. and 65 °C, (b) PS concentration for 10 μM herbicide, pH = 7.0, and 65 °C, (c) temperature for 10 μM herbicide, 0.10 mM PS, and pH = 7.0, and (d) pH for 10 μM herbicide, 0.10 mM PS, and 65 °C. (e) Effect of scavengers after 120 min of treatment of the above solutions but with 10 mM PS. (f) Effect of inorganic anions (19 mM) and humic acid (10 mg L^{-1}) after 120 min of degradation of 10 μM herbicide, 0.10 mM PS, pH = 7.0, and 65 °C. Adapted from ref. [25].

oxidants, Fig. 2b and c depict the increase in degradation when PS concentration and temperature grew, respectively, due to the rise in rate of reaction (1) yielding more oxidant $SO_4^{\bullet-}$ and hence more $^{\bullet}OH$ is formed from reactions (2) or (3), accelerating the removal of the target herbicide. Fig. 2d makes evident the deceleration of herbicide degradation mainly occurs at pH = 11.0 as result of the progressive production of greater quantity of $^{\bullet}OH$ by the predominance of reaction (3) over (2), indicating a fast decay with $SO_4^{\bullet-}$. The authors determined a k_2 = 4.37 × 10^9 M^{-1} s^{-1} for the reaction of simazine with $SO_4^{\bullet-}$, greater than 9.32 × 10^8 M^{-1} s^{-1} for $^{\bullet}OH$.

The fact that $SO_4^{\bullet-}$ predominated in acidic and neutral pH, whereas $^{\bullet}OH$ prevailed in basic pH has been well-established by Ji et al. [20] for atrazine. All authors considered the effect of scavengers to clarify the role of these oxidant radicals. In the case of simazine [25]. Fig. 2e shows the change of k_1 for 10 μM herbicide, 0.50 mM PS, and 65 °C at different pH values upon addition of 10 mM ethanol (EtOH) or *tert*-butanol (TBA). It is well-known that EtOH reacts rapidly with $SO_4^{\bullet-}$ (k_2 = 1.6–7.7 × 10^7 M^{-1} s^{-1}) and $^{\bullet}OH$ (k_2 = 1.2–2.8 × 10^9 M^{-1} s^{-1}), whereas TBA only has a significant reaction with $^{\bullet}OH$ (k_2 = 3.8–7.6 × 10^8 M^{-1} s^{-1}) [25]. Fig. 2e reveals a slightly larger inhibition by the quencher EtOH than TBA, pointing to the predominance of $SO_4^{\bullet-}$ generation in all media. The greater k_1 decay at pH = 11.0 reveals the smaller production of $SO_4^{\bullet-}$, in agreement with the loss of performance depicted in Fig. 2d. The effect of different co-existing inorganic anions and humic acid (simulating NOM) has also been explored. In all cases, Fig. 2f highlights a fall of the k_1-value of the above assay at pH= 7.0 increasing in the order $Cl^- < HCO_3^- <$ humic acid $< H_2PO_4^- < SO_4^{2-} < NO_3^-$. This inhibitory effect is explained by the deactivation of $SO_4^{\bullet-}$ and $^{\bullet}OH$ to be converted into SO_4^{2-} and OH^-, respectively, by their oxidation via electron transfer of such species. For instance, Cl^- can deactivate both oxidizing radicals to generate $Cl^{\bullet}$ according to reactions (8) and (9), respectively [20,21]. This weaker oxidant can then produce $Cl_2^{\bullet-}$ from reaction (10) or the active chlorine Cl_2 from reaction (11) that evolves to the more powerful hypochlorous acid (HClO) in acidic medium by reaction (12) [20].

$$SO_4^{\bullet-} + Cl^- \rightarrow SO_4^{2-} + Cl^{\bullet} \quad (8)$$

$$^{\bullet}OH + Cl^- \rightarrow OH^- + Cl^{\bullet} \quad (9)$$

$$Cl^{\bullet} + Cl^- \rightarrow Cl_2^{\bullet-} \quad (10)$$

$$2Cl_2^{\bullet-} \rightarrow Cl_2 + 2Cl^- \quad (11)$$

$$Cl_2 + H_2O \rightarrow HClO + Cl^- + H^+ \quad (12)$$

Similarly, $HCO_3^{\bullet-}$ is transformed into $HCO_3^{\bullet}$ by both $SO_4^{\bullet-}$ and $^{\bullet}OH$ with $k_2 \approx 10^6$ M^{-1} s^{-1} from reactions (13) and (14), respectively [20]:

$$SO_4^{\bullet-} + HCO_3^{-} \rightarrow SO_4^{2-} + HCO_3^{\bullet} \quad (13)$$

$$^{\bullet}OH + HCO_3^{-} \rightarrow OH^{-} + HCO_3^{\bullet} \quad (14)$$

This behavior suggests a drop in the oxidation power of the PS/heat process with real wastewaters containing the above anions and humic acid. Additionally, the by-products produced were detected in some cases by LC-MS (see Table 1).

3.2. Iron ions activation

The activation of PS by iron ions has been confirmed for the removal of amicarbazone [28], atrazine [29–33], 2,4-D [34], diuron [35-37] , and propachlor [38]. The electron-transfer reaction between PS and Fe^{2+} yields Fe^{3+} and $SO_4^{\bullet-}$ via reaction (15) [34], which can then form $^{\bullet}OH$ from reactions (2) or (3).

$$S_2O_8^{2-} + Fe^{2+} \rightarrow Fe^{3+} + SO_4^{\bullet-} + SO_4^{2-} \; k_2 = 20 \; M^{-1} \; s^{-1} \quad (15)$$

In an interesting work of Chen et al. [31], 3 mg of soil were spiked with 0.3 μg of atrazine and further suspended in 33 mL of pure water with different PS/Fe^{2+} ratios using a screw-cap cylindrical glass vial. The assays were made at pH= 3.0–6.2 and 23 °C for 600 min. The herbicide removal was enhanced at lower pH, where Fe^{2+} predominated over Fe^{3+}, and with greater oxidant content. The best degradation of 80% with $k_1 = 2.3 \times 10^{-3}$ min^{-1} was found for 16.6:16.6 mM PS/Fe^{2+} ratio at pH = 3.0 (see Table 1). The use of EtOH and TBA as scavengers revealed that $SO_4^{\bullet-}$ was the dominant oxidant radical. The authors identified 5 heteroaromatic by-products by LC-MS/MS.

An et al. [33] enhanced the oxidation power of PS activated with iron ions using the catalytic action of the methylhydroquinone (MHQ)/methylbenzoquinone (MBQ) redox pair. Fig. 3a shows a schematic diagram of the formation of the oxidant radicals under these conditions, in which the MHQ/MBQ and Fe(III)/Fe(II) pairs are continuously cycled. The oxidation of MHQ to MBQ takes place with the reduction of Fe(III) to Fe (II). The latter ion then regenerates Fe(III) when it is oxidized by PS and generates $SO_4^{\bullet-}$ and $^{\bullet}OH$ from reactions (2) or (3), and (8). The authors also proposed the generation of a strong non-radical oxidant as Fe(IV) from Fe(II). The trials were made with a centrifuge tube filled with 50 mL of 0.039 mM herbicide in pure water at 25 °C for 60 min. The effect of 0.10–0.30 mM PS, 0.05–0.20 mM Fe^{3+}, and 0.10–0.30 mM MBQ, as well as of pH = 2.0–7.0, on the herbicide degradation was studied. Higher atrazine concentration decay was determined with raising PS, Fe(III), and MBQ doses. Fig. 3b depicts the comparative percentage of herbicide degradation with time for different treatments using 0.20 mM of PS and/or MBQ, 0.05 mM Fe(III) or Fe(II), at pH 3.0. A poor degradation was achieved after 60 min of applying PS alone or combined with Fe(III) or MBQ, which was upgraded up to a 24% for PS/Fe(II) and much more largely, up to near 60%, for the combined PS/Fe(III)/MBQ (see also Table 1). The positive action of MBQ in the latter process respect to PS/Fe(II) within the pH interval 2.0–7.0 can be

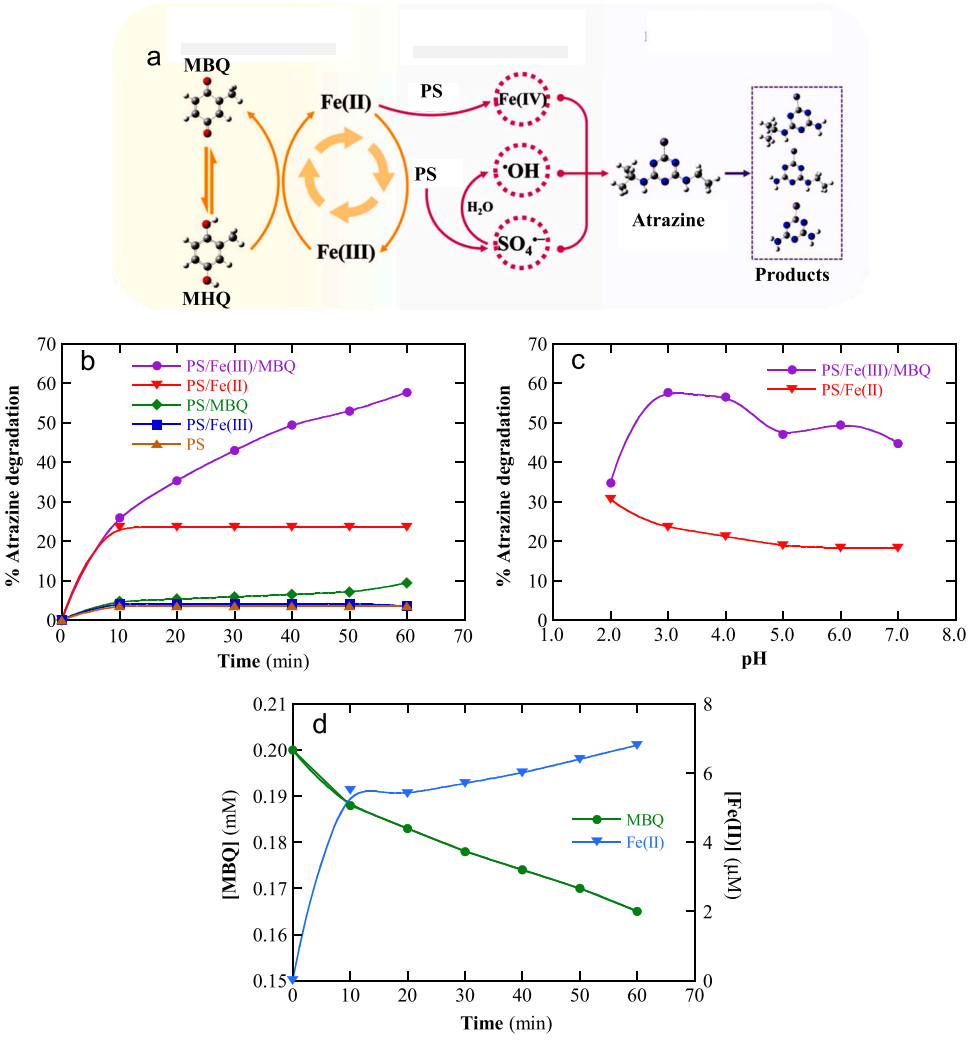

Fig. 3. (a) Mechanism proposed for the generation of radical oxidants for the PS//Fe(III)/MBQ system during atrazine removal. MBQ means methyl-*p*-benzoquinone and MHQ, methylhydroquinone. The trials were carried out with a centrifuge tube filled with 50 mL of 0.039 mM (8.5 mg L^{-1}) atrazine at 25 °C. (b) Percentage of herbicide degradation with time for different treatments with 0.20 mM PS and/or MBQ, 0.05 mM Fe(III) or Fe(II), at pH 3.0. (c) Effect of pH on the percentage of atrazine degradation after 60 min of the MBQ/Fe(III)/PS and Fe(II)/PS processes upon the above conditions. (d) Change of MBQ and Fe(II) concentrations for the MBQ/Fe(III)/PS assay at pH = 3.0. Adapted from ref. [33].

observed in Fig. 3c, being optimal at pH = 3.0. Fig. 3d discloses the fast generation of a low Fe(II) content of 5.5 μM at the beginning of the PS/Fe(III)/MBQ process that slightly increased to 6.8 μM at 60 min of treatment. This demonstrates the effectiveness of the MHQ/MBQ to continuously catalyze the Fe(III)/Fe(II) cycle, although the MBQ concentration dropped from 0.20 to 0.17 mM due to their removal with the produced oxidizing agents. The LC-MS/MS analysis of the treated solution allowed the identification of 14 primary heteroaromatic derivatives of atrazine, and the proposed reaction sequence is depicted in Fig. 4, where the products formed are designed by their abbreviation. The sequence is initiated by four pathways in which the target molecule is oxidized to CVIT and CEFT by olefination, CDIT by alkylic oxidation, and OEIT by dechlorination/hydroxylation. The two former intermediates are then transformed into the most important intermediates DEA, DEIA, and DIA via dealkylation. The other 7 by-products are originated from further dealkylation, deamination, hydroxylation, de-ethoxylation, alkylic oxidation, alkylic hydroxylation, and/or dechlorination processes of the above compounds.

Liang et al. [34] compared the removal of 2,4-D by PS/Fe^{2+} with other activation procedures of PS including heat, H_2O_2, and OH^- (as NaOH). The study was performed in a stirred tank reactor with 250 mL of 0.452 mM herbicide in pure water with 100 mM PS and 10 mM Fe^{2+}, 300 mM H_2O_2 (pH = 5.6) or 50 mM NaOH at 20 and 70 °C. The quicker degradation was obtained for PS/heat at 70 °C where 2,4-D disappeared in 6 h. The other processes performed at 20 °C were much slower. So, total degradation was reached after 48 h with PS/Fe^{2+} and in 216 h with PS/ H_2O_2 and PS/NaOH (see Table 1). After such reaction times, total TOC removal was achieved as well. It was found a high cost of 1.71 US$ $(g\ TOC)^{-1}$ for PS/Fe^{2+}. Unfortunately, the cost for the better PS/heat process at 70 °C was not determined, avoiding the comparative suitability with respect to PS/Fe^{2+}.

Other possibilities to enhance the oxidation power of PS/Fe^{2+} have been explored by Tan et al. [36] by adding citric acid as chelating agent or hydroxylamine to accelerate the reduction of Fe^{3+} to Fe^{2+}. The addition of citric acid is not recommended in practice because it presupposes an increasing of the organic matter that is more difficulty mineralized. The authors carried out the experiments with a stirred tank reactor containing 50 mL of 0.01–0.05 mM of the urea diuron in pure water at room temperature. They added 0.2–1.0 mM PS, 0.05–2.0 mM Fe^{3+}, and/or 0.0–1.0 mM citric acid or hydroxylamine at pH = 3.0–9.0,

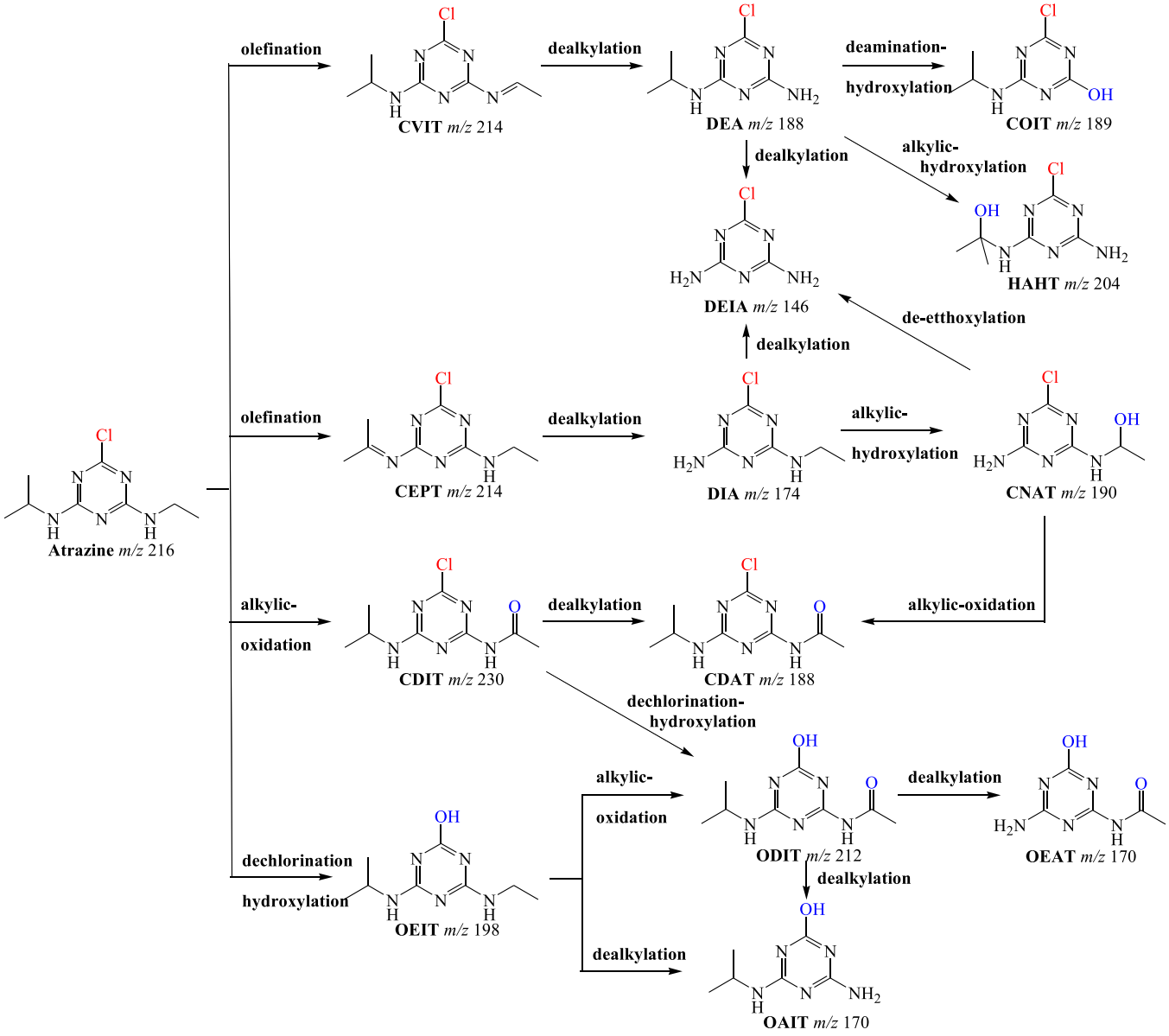

Fig. 4. Reaction sequence proposed for atrazine degradation with $SO_4^{\bullet-}$ and $^{\bullet}OH$ oxidizing radicals. Adapted from ref. [33].

prolonging the reaction during 240 min Table 1 shows that at pH = 7.0, the diuron abatement raised in the order: PS/Fe^{2+} ($k_1 = 1.23 \times 10^{-3}$ min^{-1}) < PS/Fe^{2+}/citric acid ($k_1 = 1.80 \times 10^{-3}$ min^{-1}) < PS/Fe^{2+}/hydroxylamine ($k_1 = 4.09 \times 10^{-3}$ min^{-1}). This interesting finding of the PS/Fe^{2+}/hydroxylamine process needs more research for other herbicides at neutral pH to confirm if actually, its acceleration of Fe^{2+} regeneration yields superior performance than PS/Fe^{2+}, which can be useful in practice to treat little volumes of real wastewaters.

3.3. Fe activation

Fe, also known as zero-valent iron (Fe^0, ZVI) or nanoparticles ZVI (nZVI), has been used in suspension for activating PS to remediate herbicides in aqueous media. This procedure has been tested for alachlor [39,40], amicarbazone [41], atrazine [42–48], bentazon [49], clofibric acid [50], 2,4-D [51], diuron [52,53], fenuron [54], and isoproturon [55]. When pure Fe is used, its surface is directly oxidized by PS to generate soluble Fe^{2+} from reaction (16) [49], which is subsequently converted into Fe^{3+} by PS originating $SO_4^{\bullet-}$ from reaction (15). This ion can then yield $^{\bullet}OH$ by reactions (2) or (3).

$$S_2O_8^{2-} + Fe^0 \rightarrow Fe^{2+} + 2SO_4^{2-} \quad (16)$$

When Fe is supported on a carbonaceous material, a more complex mechanism for generating oxidants is proposed. As an example, Fig. 5a schematizes the processes proposed for S-nZVI deposited onto biochar [45]. Apart from the radical oxidants $SO_4^{\bullet-}$ and $^{\bullet}OH$ generated, another ROS like $O_2^{\bullet-}$ is formed from reduction of soluble O_2 at the carbon matrix.

Table 1 shows that the above works detected the intermediates formed from the herbicides by LC-MS, LC-MS/MS, and GC-MS analysis of degraded suspensions. This table also reveals that high amounts of Fe are required when it acted alone as catalyst, being more effective at low pH where dissolved Fe^{2+} became more effective to produce $SO_4^{\bullet-}$ as main oxidant. In the case of the chloroacetanilide alachlor, 200 mL of 5 mg L^{-1} of this herbicide with 0.5–3.0 mM PS and 0.5–10 mM catalyst in pure water were treated at pH = 1.5–10.0 using a stirred tank reactor [39]. The quicker alachlor abatement was obtained up to 2.0 mM PS and catalyst at pH 1.5 and 3.0 with total removal in only 30 min (see Table 1). It was observed a strong inhibition after adding Cl^-, HCO_3^-, and NOM by their preferential consumption of $SO_4^{\bullet-}$ preventing its attack over the herbicide. In contrast, a little effect was observed for less aggressive ions like NO_3^- and SO_4^{2-}, as stated above. Xie et al. [50] reported a little influence of pH between 5.0 and 9.0 for the treatment of 600 mL of 0.01 mM clofibric acid with Fe powder in pure water with a stirred tank reactor. At pH = 7.0, a very rapid destruction in 10 min of the herbicide with $k_1 = 0.014$ min^{-1} for 675 mg L^{-1} PS and 140 mg L^{-1} catalyst was found, thus demonstrating its large effectiveness at neutral conditions, much higher than using a synthetic wastewater (with NH_4^+ and glucose) and a real WWTP effluent as aqueous matrices (see Table 1). The same positive behavior has been described for the phenyl urea fenuron by Hayat et al. [54] when 100 mL of suspensions of this herbicide with ZVI were treated with a conical flask on thermostatic rotary shaker. A concentration of 0.12 mM fenuron in pure water at pH = 7.0 and 25 °C was completely abated in only 30 min with k_1

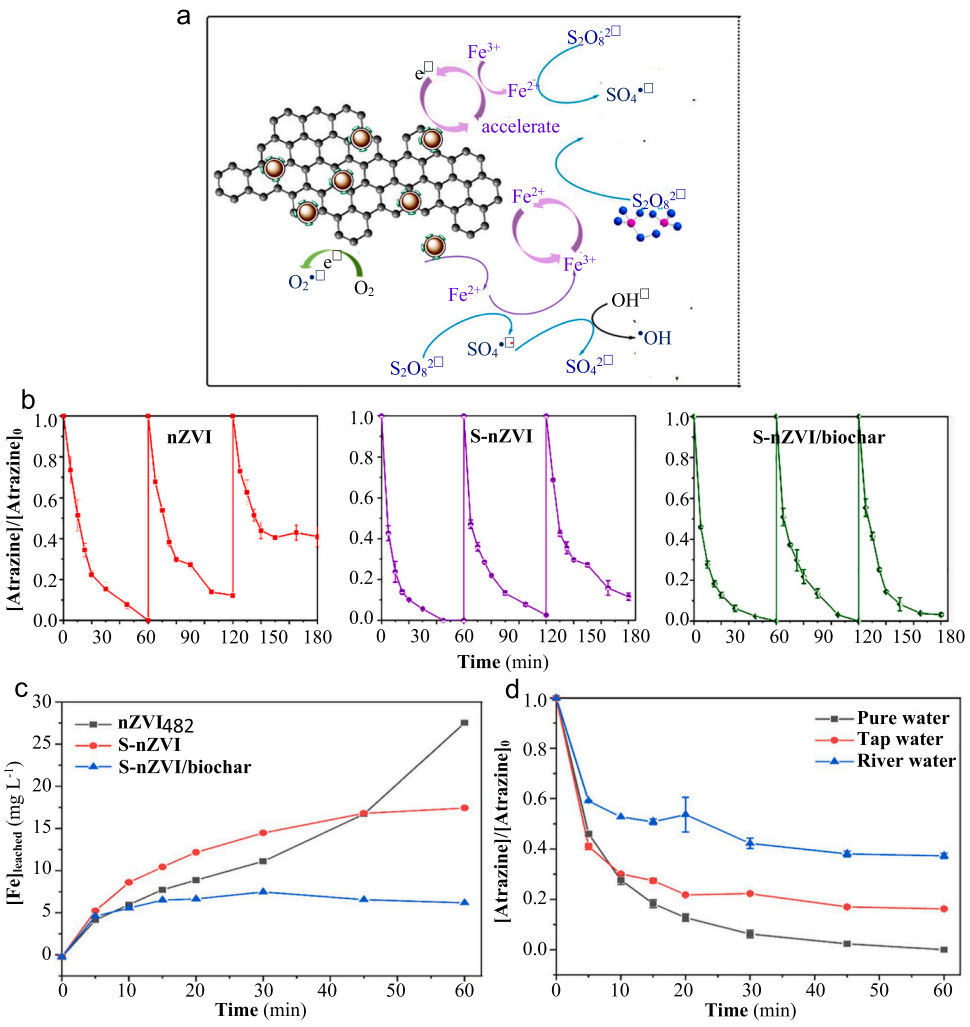

Fig. 5. (a) Mechanism proposed for the production of radical oxidants for the S-nZVI/biochar system during atrazine degradation. (b) Change of normalized herbicide concentration with time for 3 consecutive treatments of 100 mL of 10 mg L^{-1} atrazine in pure water with 1.0 mM PS and 100 mg L^{-1} of catalyst (nZVI, S-nZVI, and S-nZVI/biochar) at pH = 2.86 and 30 °C using a stirred tank reactor. (c) Concentration of Fe leached from the catalysts in the above assays. (d) Comparative normalized atrazine concentration vs. time for is degradation with S-nZVI/biochar upon the above conditions in pure water, tap water, and river water. Adapted from ref. [45].

$= 0.047\ min^{-1}$ for 2.0 mM PS and 0.50 g L^{-1} catalyst, whereas 83% of TOC was reduced in 360 min (see Table 1). It is interesting to note that the catalyst showed a good reusability after 3 consecutive cycles. The negative influence of the components of the aqueous matrix was confirmed again by determining that under the same conditions, the herbicide was removed by 88% with tap water and 91% with river water in 60 min

Good results have been reported with Fe/carbonaceous materials as catalysts as well. The treatment with pre-magnetized Fe-C has been explored in a stirred tank reactor filled with 100 mL of 20 mg L^{-1} 2,4-D in pure water at pH = 3.0–10.0 lasting 60 min [51]. The herbicide degradation was faster at pH = 3.0 and 98–100% abatement was reached with 1.5–2.0 mM PS and 500–750 mg L^{-1} catalyst (see Table 1). More relevant findings have been described for atrazine. Wu et al. [42] found that 10 mg L^{-1} of this herbicide in a 100 mL suspension were rapidly abated up to a 92% in 20 min with 39% TOC removal using 0.50 mM PS and 100 mg L^{-1} nZVI/graphene as catalyst at pH = 6.0 and 25 °C (see Table 1). The use of scavengers pointed to the predominance of $SO_4^{\bullet-}$ as oxidizing agent. This has been confirmed with composites of nZVI/graphene-like carbon sheet [43] and 0.15 M S-nZVI/biochar [45]. These studies detected the presence of ROS like $^{\bullet}OH$, $O_2^{\bullet-}$, and $^1O_2$ (formed from the attack of $^{\bullet}OH$ on $O_2^{\bullet-}$) and from EPR spectra, as shown in Fig. 5a. Jiang et al. [45] prepared a 0.15 M S-nZVI/biochar composite to obtain a larger reusability as compared to nZVI and S-nZVI, as can be seen in Fig. 5b for 3 consecutive cycles of 100 mL of 10 mg L^{-1} atrazine in pure water treated with 1.0 mM PS and 100 mg L^{-1} of each catalyst at pH = 2.86 and 30 °C using a stirred tank reactor. Under these conditions, total herbicide decay was achieved after the first 60 min of all the catalysts, but only the composite maintained its catalytic performance in the successive steps. The superior stability of 0.15 M S-nZVI/biochar was ascribed to the lower leaching of Fe^{2+} to the solution (see Fig. 5c). For this composite, the herbicide removal was studied between 15 and 35 °C determining an activation energy (E_a) of 49.5 kJ mol^{-1}. Fig. 5d presents the comparative treatments carried out with natural waters under the above conditions. At 60 min, the atrazine abatement decreased in the sequence: pure water (100%) > tap water (82%) > river water (61%). This trend can be related to the increasing presence of anions and NOM that react with the oxidizing agents and decelerate their attack over atrazine. This was confirmed from the inhibition effect found for common anions such as Cl^-, CO_3^{2-}, and HCO_3^-. The use of new Fe composites to activate PS should be more largely studied in the next future to improve their catalytic action and stability for practical use.

3.4. Other catalytic materials

Several herbicides have been removed by PS activated with other catalytic materials including atrazine with CuS [56], ascorbic acid [57], dithionite [58], Fe_3O_4/sepiolite [59], magnetic clay [60], Cu^{2+}/MoS_4-layer double dihydroxide (LDH) [61], hydrochar [62], MoS_2 @SiO_2 [63] and sulfur/Fe_3O_4 [64], 4-chlorophenol with a 3D porous carbon [65], 2,4-D with FeS [66] and hematite (α-Fe_2O_3) [67], and pentachlorophenol with ascorbic acid [68] and dithionite [69]. Electron-transfer reactions were involved in the catalytic action of these homogeneous (homo-) and heterogeneous (hetero-) materials. For hetero-catalysts with heavy metals (Me), the activation process can mainly proceed by: (i) heterogeneous reaction with a surface metallic cation ($\equiv Me^{n+}$) yielding its surface the oxidized cation ($\equiv Me^{(n+1)+}$) and $SO_4^{\bullet-}$ by reaction (17) and (ii) homogeneous reaction with the leached metallic cation (Me^{n+}) to give its soluble oxidized cation ($Me^{(n+1)+}$) and $SO_4^{\bullet-}$ by reaction (18) [57,64]. $SO_4^{\bullet-}$ can further yield $^{\bullet}OH$ via homogeneous reactions (2) or (3). The $Me^{(n+1)+}$/Me^{n+} cycle can be accelerated by other components into the outer layer of the composite. An example is shown in Fig. 6a for the mechanism proposed for the generation of oxidant radicals for the sulfur/Fe_3O_4 system [64], where species like $\equiv S^{2-}$ and $\equiv S_2^{2-}$ reduce leached Fe^{3+} to Fe^{2+} accelerating the $SO_4^{\bullet-}$ generation from reaction (15). The high conductivity of

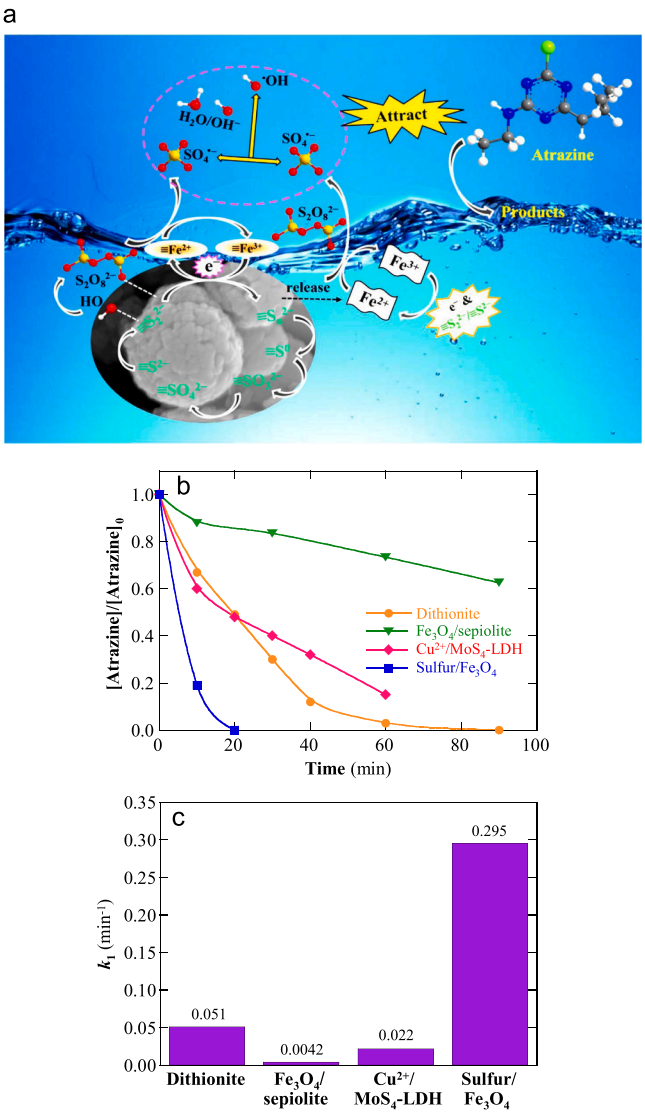

Fig. 6. Mechanism proposed for the generation of radical oxidants for the sulfur/Fe_3O_4 system during atrazine removal (adapted from ref. [64]). Variation of normalized atrazine concentration with time for atrazine degradation with activated PS by different catalysts: dithionite, Fe_3O_4/sepiolite, Cu^{2+}/MoS_4-LDH, and sulfur/Fe_3O_4 under the conditions given in Table 1 (adapted from ref. [58,59,61,64]). (c) Pseudo-first-order rate constant determined for the above assays.

the carbonaceous material of the composite can also produce active electrophilic sites that can reduce soluble species like O_2 to form $O_2^{\bullet-}$, as shown in Fig. 5a.

$$S_2O_8^{2-} + \equiv Me^{n+} \rightarrow \equiv Me^{(n+1)+} + SO_4^{\bullet-} + SO_4^{2-} \quad (17)$$

$$S_2O_8^{2-} + Me^{n+} \rightarrow Me^{(n+1)+} + SO_4^{\bullet-} + SO_4^{2-} \quad (18)$$

In contrast, homo-catalysts reduce directly PS to produce $SO_4^{\bullet-}$ in the solution. A typical example is ascorbic acid ($C_6O_8H_6$) that transforms PS into $SO_4^{\bullet-}$ and SO_4^{2-} while it is oxidized to dehydroascorbic acid [57]. Another well-known catalyst is dithionite ($S_2O_4^{2-}$) that reacts according to the complex reaction (19) [58]:

$$2S_2O_8^{2-} + 2S_2O_4^{2-} + H_2O \rightarrow 2HSO_4^- + S_2O_3^{2-} + 2SO_3^{\bullet-} + 2SO_4^{\bullet-} \quad (19)$$

Atrazine has been the more used herbicide to check the effectiveness of catalytic materials in synthetic solutions. The relevant results given in Table 1 for homo- [58] and hetero-catalysts [59,61,64] make evident a

growth of its degradation rate at higher PS and catalyst contents, low pH values, and increasing temperature. The predominance of $SO_4^{\bullet-}$ as oxidant and the strong inhibition with the addition of Cl^-, NO_3^-, HCO_3^-, CO_3^{2-}, HPO_4^-, and humic acid was reported in all cases, along with the detection of several intermediates from GC-MS and LC-MS that agree with those shown in Fig. 4. Fig. 6b presents the comparative normalized atrazine concentration with time under the best conditions listed in Table 1 for the above catalysts. The quicker overall removal was achieved in 20 min for the sulfur/Fe_3O_4 hetero-catalyst, followed by the dithionite homo-catalyst that required near 90 min. A pseudo-first-order reaction for atrazine decay was always determined and the k_1-value increased in the order: Fe_3O_4/sepiolite ($0.0042\ min^{-1}$) < Cu^{2+}/MoS_4-LDH ($0.022\ min^{-1}$) < dithionite ($0.051\ min^{-1}$) < sulfur/Fe_3O_4 ($0.295\ min^{-1}$), as depicted in Fig. 6c. However, a good reusability after consecutive cycles for the hetero-catalysts was only found for the lesser potent Fe_3O_4/sepiolite system [59], probably because the active sites of its surface were less inhibited by the precipitation of lower amount of by-products formed. Further research of new hetero-catalysts should be focused to develop reusable materials, a requirement for their possible application in practice.

An interesting work has been described for 2,4-D removal using a stirred tank reactor with 100 mL of 10 mg L^{-1} herbicide in pure water with FeS as hetero-catalyst at pH = 3.0–11.0 and 20–50 ºC during 120 min [66]. The herbicide abatement raised up to 2.5 mM PS and 0.50 g L^{-1} FeS, at lower pH and high temperature. Total decay with an excellent 90% TOC reduction was reported for 1.25 mM PS, 0.15 g L^{-1} hetero-catalyst, pH = 4.5, and 30 ºC (see Table 1). An E_a = 19.47 kJ mol^{-1} was found for 2.4-D reaction. Addition of anions yielded different inhibitory effect to those described in previous works, being low for Cl^-, moderate for NO_3^-, and larger for HCO_3^-. The low Cl^- influence could be due that the fact that the oxidant role of $^{\bullet}OH$ became more important than $SO_4^{\bullet-}$, conversely to previous activation processes where $SO_4^{\bullet-}$ prevailed. It is noticeable that the hetero-catalyst presented a moderate reusability after 7 consecutive steps. For pentachlorophenol treated by PS/ ascorbic acid [68], a similar oxidant role of $^{\bullet}OH$ and $SO_4^{\bullet-}$ was detected with scavengers like methanol and TBA. A 72% herbicide decay was determined after 180 min of treatment of 60 mL of 200 mg L^{-1} pentachlorophenol in pure water with 40 mM PS and 1.0 mM catalyst at pH = 7.2 (see Table 1).

3.5. UV activation

The molecule of PS can be energetically activated by exposition to an UV light to be decomposed into two $SO_4^{\bullet-}$radicals by reaction (20) [70]:

$$S_2O_8^{2-} + h\nu \rightarrow 2SO_4^{\bullet-} \quad (20)$$

This process has been studied for atrazine [70–73], isoproturon and chlorotoluron [74], and trifularin [75]. Table 2 summarizes selected results for these works. It is noticeable that reaction (20) only takes place under UVC irradiation, where the light absorption of PS increased progressively with decreasing λ from 280 to 200 nm, having a molar absorption coefficient of 21.1 $M^{-1}\ cm^{-1}$ and a quantum yield of 0.7 mol $Einstein^{-1}$ at λ = 254 nm [76].

Fig. 7a shows the larger effectiveness of the combined PS/UV process respect to the single PS and UV ones for the degradation of 250 mL of 0.1 mg L^{-1} atrazine and/or 2.0 mg L^{-1} PS in pure water at pH = 7.0 filling a stirred tank reactor under an external UV light. This demonstrates the production of $SO_4^{\bullet-}$ from reaction (20) followed by that of $^{\bullet}OH$ from reactions (2) or (3) for PS/UV. The effect of the herbicide concentration, PS dose, and pH on the percentage of atrazine degradation in the above PS treatment can be observed in Fig. 7b, c and d, respectively. The best conditions were just obtained under the conditions of Fig. 7a with 97% degradation at 120 min and $k_1 = 3.4 \times 10^{-2}\ min^{-1}$ (see Table 2). The gradual drop of the percentage of atrazine degradation from 0.1 to 10.0 mg L^{-1} depicted in Fig. 7b can be explained by the slower attack of a similar amount of generated $SO_4^{\bullet-}$ and $^{\bullet}OH$ over higher quantity of organic matter. The maximum degradation for 2.0 mg L^{-1} PS revealed in Fig. 7c can be justified by a gradual production of the oxidizing agent up to such content, whereupon it progressively decreased due to the larger acceleration of parasitic reactions like (4) to (7) by the presence of an excess of PS. Fig. 7d makes evident a maximum loss of herbicide at pH = 7.0 where the above parasitic reactions were slower. The decay at alkaline pH = 10.0 can be also accelerated by the consumption of $SO_4^{\bullet-}$ with OH^- to give SO_4^{2-} and $^{\bullet}OH$ from reaction (3).

Fig. 7e shows the effect of 2 mg L^{-1} of the scavengers TBA (for $^{\bullet}OH$) and methanol (for $SO_4^{\bullet-}$ and $^{\bullet}OH$) over the normalized atrazine concentration upon the conditions of Fig. 7a. The larger inhibition observed for methanol confirms the generation of both oxidizing species. A large deceleration of the herbicide removal was also found by adding humic acid as component of natural waters due to its competitive oxidation with it and its by-products. The authors identified 6 primary hetero-aromatic intermediates by LC-MS/MS.

Another study on atrazine degradation was made with a flow plant with a quartz tube photoreactor upon sunlight [72]. The use of free and renewable unlight with λ > 300 nm is preferable to an UV light because it offers a more cost-effective process avoiding the electric consumption of the artificial lamp, then being more attractive for industrial purposes. The flow system treated 1 L of 5.18 μM herbicide and 0.78 mM PS in pure water and lake water at natural pH lasting 60 min. While direct photolysis was very inefficient with only 12% of degradation, an excellent atrazine decay was found for pure water and even slightly superior of 96% for lake water, indicating that some components of the natural water promoted the degradation of the herbicide (see Table 2).

An interesting work by comparing the PS/UVC and the photocatalytic ZnO/UVC processes of trifularin (2,6-dinitro-*N*,*N*-dipropyl-4-(trifluoromethyl)benzenamine) has been published by Sadeghi et al. [75]. The tests performed with 250 mL of 1.2 mg L^{-1} herbicide and 60 μM PS or 100 mg L^{-1} ZnO in pure water at pH = 9.0 for 60 min using a stirred tank reactor upon an external 6 W UVC light disclosed a degradation of 98% for PS/UVC and slightly lower of 92% for ZnO/UVC. However, the cost for the former process was estimated of 43.95 kWh kg^{-1}, much greater than 20.41 kWh kg^{-1}, determined for the latter one (see Table 2). This means that the relative high price of PS can be a handicap for its application in practice under the economical point of view.

3.6. UV activation with Fe^{2+}

Some authors have checked the coupling of PS/Fe^{2+} with UV light to remove amicarbazone [77], atrazine [78–81], and tebuthiuron [82]. Graça et al. [77] studied the behavior of the triazolone amicarbazone (see chemical structure in Fig. 8a) using the system of Fig. 8b consisting of a stirred tank reactor illuminated with an external 60 W UVA light with λ = 320–400 nm in a closed container to prevent the irradiation loss. Fig. 8c shows the normalized herbicide concentration decay with time for the PS, PS/Fe(II), PS/UVA, and the combined PS/Fe(II)/UVA treatments of 100 mL of 41.4 μM herbicide in pure water with 2.5 mM PS and 0.134 mM Fe^{2+} at free pH. A much faster and overall herbicide abatement at 60 min with $k_1 = 0.044\ min^{-1}$ can be observed for the combined process (see also Table 2), which can be explained by the synergistic activation of PS with Fe(II) from reaction (15) and with UVA light from reaction (20). Apart from these reactions, the Fe(II) activation can be accelerated by the regeneration of this ion with more $^{\bullet}OH$ production by the photo-Fenton reaction (21) of the $Fe(OH)^{2+}$ species originated in the medium from Fe^{3+} produced by reaction (15) [5,6]:

$$Fe(OH)^{2+} + h\nu \rightarrow Fe^{2+} + {}^{\bullet}OH \quad (21)$$

Based on this reaction, the authors analyzed the performance of the PS/Fe(III)/UVA process for the above solution by replacing Fe^{3+} by

Table 2
Selected results reported for herbicides removal by UV, photocatalytic, and electrochemical activations of persulfate.

Herbicide	System	Experimental remarks	Best results	Ref.
UV activation				
Atrazine	Stirred tank reactor under external UV light	250 mL of 0.1–10.0 mg L^{-1} herbicide and 0–15 mg L^{-1} PS in pure water, pH = 4.0–10.0, effect of scavengers and humic acid, 120 min	More rapid destruction at lower herbicide concentration. 97% and 66% degradation for 0.1 mg L^{-1} ($k_1 = 3.4 \times 10^{-2}$ min^{-1}) and 5 mg L^{-1} ($k_1 = 8.6 \times 10^{-3}$ min^{-1}) with 2 mg L^{-1} PS at pH = 7.0. 42% TOC reduction. Oxidation by $^{\bullet}OH$ and $SO_4^{\bullet-}$. Inhibition by humic acid. 6 heteroaromatic by-products found by LC-MS/MS	[70]
Atrazine	Flow plant with a quartz tube photoreactor upon sunlight	1 L of 5.18 μM herbicide and 0.78 mM PS in pure water and lake water, natural pH, 60 min	Degradation: 12% by direct photolysis, 94% in pure water, 96% in lake water. Organic components of the latter water promoted degradation	[72]
Trifularin	Stirred tank reactor upon external 6 W UVC light	250 mL of 0.4–1.2 mg L^{-1} herbicide and 20–60 μM PS or 50–150 mg L^{-1} ZnO in pure water, pH = 9.0, 60 min	Faster degradation of 98% and 92% for 1.2 mg L^{-1} herbicide with 60 μM PS and 100 mg L^{-1} ZnO. Cost: 43.95 and 20.41 kWh kg^{-1}, respectively	[75]
UV activation with Fe^{2+}				
Amicarbazone	Stirred tank reactor with Fe^{2+} under external 60 W UVA light	100 mL of 41.4 μM herbicide, 2.5 mM PS, and 0.134 mM Fe^{2+} or Fe^{3+} in pure water, free pH, effect of chelating oxalate, citrate, and tartrate, 20 °C, 60 min	Overall herbicide abatement with Fe^{2+} (k_1 = 0.044 min^{-1}) and 92% with Fe^{3+}. Total removal in 20 min for 1 Fe/III): 3 oxalate and 1 Fe(III):2 citrate, and 30 min for 1 Fe(III):tartrate	[77]
Atrazine	Stirred glass dish with Fe^{2+} upon external UV light from a KrCl excilamp at λ = 222 nm	50 mL of 4 mg L^{-1} herbicide, 3.5 mM PS, and 1.0 mM Fe^{2+} in pure water, river water, and WWTP effluent, pH = 3.5 and 5.5, effect of scavengers, 120 min	More rapid removal at pH = 3.5. Total degradation: pure water (11 min) < natural water (20 min) < WWTP (> 20 min). $SO_4^{\bullet-}$ predominated over $^{\bullet}OH$	[79]
Photocatalytic activation				
Alachlor	Flow plant with a tubular photoreactor with TiO_2 P25[a] upon 38 W UVC light	10 L of 10–124 mg L^{-1} herbicide, 595–2381 mg L^{-1} PS, and 50 mg L^{-1} photocatalyst in pure water, pH 3.0, 25 °C, 500 min	Greater herbicide decay with lowering its content and increasing PS concentration. Total degradation in 45 min and total mineralization in 85 min for 50 mg L^{-1} herbicide and 2381 mg L^{-1} PS. Evolution of Cl^-, NH_4^+, and NO_3^- released. 2 aromatics and 1 heteroaromatic derivatives detected by GC-MS	[83]
Atrazine	Stirred tank reactor with Ag_3VO_4/Bi_2MoO_6/diatomite under 150 W Xe lamp (visible light at λ = 420 nm)	100 mL of 2.5–12.5 mg L^{-1} herbicide, 0–1.2 mM PS, and 20–100 mg L^{-1} photocatalyst in pure water, tap water, and river water, effect of scavengers, Cl^-, NO_3^-, SO_4^{2-}, and CO_3^{2-}, pH = 3.0–11.0, 60 min	In pure water, higher degradation with decreasing herbicide content and pH, and with increasing PS concentration and up to 80 mg L^{-1} photocatalyst. 97% decay for 2.5 mg L^{-1} herbicide, 1.0 mM PS, 80 mg L^{-1} photocatalyst, and pH = 3.0. Larger inhibition with CO_3^{2-} than the other anions. Oxidation by $^{\bullet}OH$, $SO_4^{\bullet-}$, $O_2^{\bullet-}$, and holes. Low reusability after 5 consecutive cycles. Degradation dropped down to 74% for tap water and 57% for river water. 13 heteroaromatics by-products and 2 final carboxylic acids found by LC-MS/MS	[87]
Diuron	Stirred tank reactor with Ag|AgCl/MIL-88 (Fe)|g-C_3N_4 upon external 93.4 W LED light (λ = 531.5 nm)	150 mL of 10 mg L^{-1} herbicide, 1.0 mM PS, and 1.0 g L^{-1} photocatalyst in pure water, natural pH, 25 °C, 120 min	Total degradation in 30 min with 31% TOC decay in 120 min. Only 13% herbicide removal with PS/Vis in 120 min. Slightly better behavior using H_2O_2 as oxidant	[91]
Paraquat	Stirred tank reactor with anatase under inner 150 W UVC light	400 mL of 30 mg L^{-1} herbicide, 150–485 mg L^{-1} PS, and 16–184 mg L^{-1} photocatalyst in pure water, pH = 2.3–10.7, 60 min	Optimization performed with response surface methodology. 77% degradation (k_1 = 0.0299 min^{-1}) with 32% TOC removal in 40 min for optimum 400 mg L^{-1} PS and 150 mg L^{-1} photocatalyst at pH = 6.3. Energy cost at 60 min = 482 kWh m^{-3}	[84]
Electrochemical activation				
Atrazine	Stirred undivided tank reactor with BDD anode and SS[b] cathode	100 mL of 5 μM herbicide, 0.25–5.0 mM PS, and 2.0 mM Na_2SO_4 in pure water, effect of scavengers, Cl^-, NO_3^-, HCO_3^-, and $H_2PO_4^-$, pH = 4.0–10.0, j[c] = 1.0–9.0 mA cm^{-2}, 25 °C, 30 min	Increase of herbicide removal with raising PS concentration and j, and with decreasing pH. 78% degradation (k_1 = 0.050 min^{-1}) with 1.0 mM PS, pH = 4.0, and j = 5.0 mA cm^{-2}. With 1.0 mM anions, k_1 rose to 0.069 min^{-1} using Cl^-, but it decreased as: HCO_3^- > $H_2PO_4^-$ > NO_3^-. Oxidation with $^{\bullet}OH$, $SO_4^{\bullet-}$, and non-radical species. 10 heteroaromatic by-products detected by LC-MS	[96]
Atrazine	Stirred undivided tank reactor with Ti|RuO_2-IrO_2 anode, SS cathode, and $CuFeO_4$ NPs as catalyst	400 mL of 46 μM herbicide, 0–4.5 mM PS, 0–4.0 g L^{-1} catalyst, and 20 mM Na_2SO_4 in pure water, effect of Cl^-, NO_3^-, HCO_3^-, and $H_2PO_4^-$, pH = 3.0–11.0, j = 0–24 mA cm^{-2}, 30 °C, 30 min	Increasing PS concentration, up to 3.0 g L^{-1} catalyst, and j, and lowering pH favored degradation. Total herbicide removal at > 4.0 mM PS, 0.30 g L^{-1} catalyst, pH= 6.3, and j > 8 mA cm^{-2}. Acceleration with Cl^-, inhibition with the other ions added. Larger oxidation role played by $SO_4^{\bullet-}$ than $^{\bullet}OH$. Moderate reusability of the catalyst after 5 consecutive runs. 13 heteroaromatic derivatives found by LC-MS	[97]
Atrazine	Stirred undivided tank reactor with blue TiO_2 nanotubes or Al-doped blue TiO_2 nanotubes anode and SS cathode	100 mL of 5 μM herbicide, 0–5.0 mM PS, and 20 mM $NaClO_4$ in pure water, effect of scavengers, Cl^-, ClO_4^-, HCO_3^-, SO_4^{2-}, and humic acid, pH = 2.8–11.0, j = 0–10 mA cm^{-2}, 25 °C, 180 min Experiment with an actual soil washing wastewater with 8.05 mg L^{-1} herbicide and 25.96 mg L^{-1} TOC	For Al-doped blue TiO_2 nanotubes, more rapid degradation at higher PS content up to 5 mA cm^{-2} and at pH = 9.0. Under these conditions with 1.0 mM PS, total degradation in 60 min with k_1 = 0.048 min^{-1} and 52% TOC reduction in 180 min. Cl^- strongly accelerated degradation and at less extent, SO_4^{2-}. Inhibition with humic acid < HCO_3^-.	[100]

(*continued on next page*)

Table 2 (*continued*)

Herbicide	System	Experimental remarks	Best results	Ref.
		using 5.0 mM PS, pH = 6.3, and j = 5 mA cm^{-2} for 120 min	$SO_4^{\bullet-}$ as the main oxidant. Large stability of the anode after 20 cycles. For the real wastewater, overall herbicide removal, similar to BDD anode. In contrast, 20% TOC reduction for the checked anode < 42% for BDD	
2,4-D	Stirred undivided tank reactor with graphene anode, Ti cathode, under inner 16 W UVC lamp, and nZVI as catalyst	500 mL of 25–125 mg L^{-1} herbicide, 0–125–0.625 mg L^{-1} PS, 0.025–0.125 mg L^{-1} catalyst, and Na_2SO_4 in pure water, effect of scavengers, pH = 1.0–5.0, I[d] = 0.25–1.25 A, 100 min	Optimization by response surface methodology: 92% removal for 50.05 mg L^{-1} herbicide, 0.49 mg L^{-1} PS, 0.10 mg L^{-1} catalyst, pH = 3.47, and I = 1.0 A in 80 min, with k_1 = 0.0194 min^{-1}. COD and TOC were reduced by 78% and 63%, respectively. Faster degradation due to the combination of electrolysis and UVC irradiation. Formation of $SO_4^{\bullet-}$ and $^{\bullet}OH$ as oxidants. 9 aromatic derivatives and 6 final carboxylic acids detected by GC-MS	[102]

[a] TiO_2 P25 = TiO_2 from Degussa with 75% anatase + 25% rutile.
[b] SS:Sainless steel.
[c] j = current density.
[d] I = current.

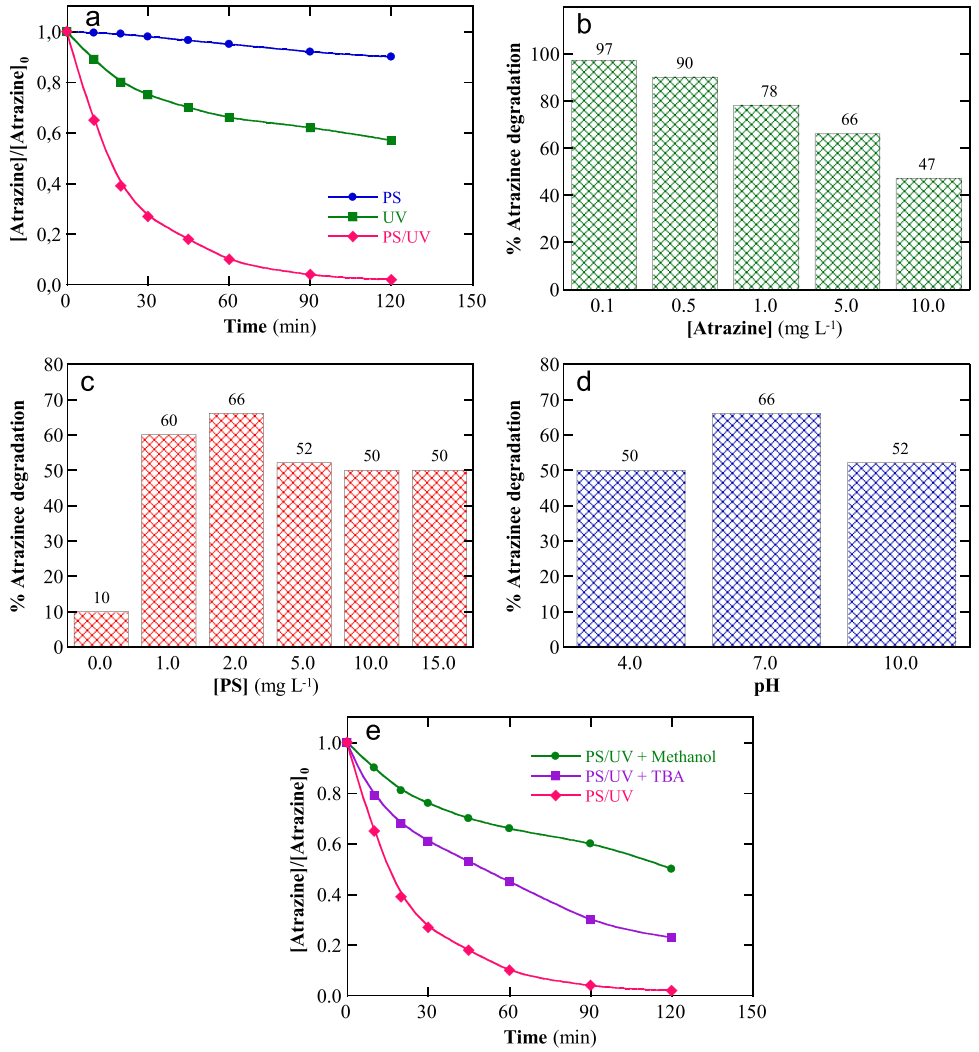

Fig. 7. (a) Time course of normalized atrazine concentration during different treatments of 250 mL of 0.1 mg L^{-1} herbicide and 2.0 mg L^{-1} PS in pure water at pH = 7.0 using a stirred tank reactor upon an external UV light. Effect of: (b) atrazine concentration for 2.0 mg L^{-1} PS at pH = 7.0, (c) PS concentration for 5.0 mg L^{-1} atrazine at pH = 7.0, (d) pH for 5.0 mg L^{-1} atrazine and 2.0 mg L^{-1} PS, and (e) scavengers (2.0 mg L^{-1}) over the PS/UV assays of graphic a. Adapted from ref. [70].

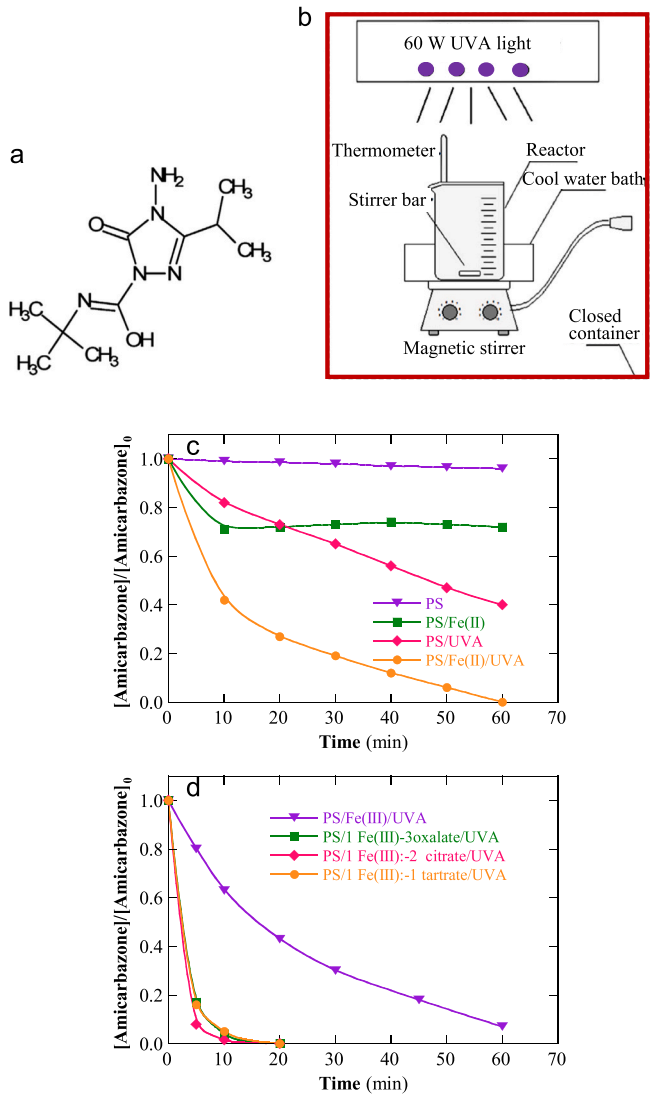

Fig. 8. (a) Chemical structure of the herbicide amicarbazone. (b) Sketch of the experimental photolytic system used for the degradation of amicarbazone solutions under external 60 W UVA light. Normalized herbicide concentration vs. time for: (c) different treatments of 100 mL of 41.4 μM herbicide, 2.5 mM PS, and 0.134 mM Fe^{2+} in pure water at free pH and 20 ºC, and (d) under the same conditions but with 0.134 mM Fe^{3+} and optimum ratios of several chelating agents (oxalate, citrate, and tartrate). Adapted from ref. [79].

Fe^{2+}. A slower herbicide degradation up to 92% was found, as shown in Fig. 8d, which can be attributed to the lower amount of Fe^{2+}in solution, thus activating less PS. Trials with chelating carboxylates like oxalate, citrate, and tartrate were further made to confirm if these complexes were a good source of Fe^{2+} because they can be easily photodecomposed by the general reaction (22) [5,6]:

$$Fe(OOC\text{-}R)^{2+} + h\nu \rightarrow Fe^{2+} + CO_2 + R^{\bullet} \quad (22)$$

Fig. 8d highlights the very fast amocarbazine abatement achieved in only 20 min for the better molar ratios of (1;3), (1:2), and (1;1) between PS and oxalate, citrate, and tartrate, respectively, largely improving the PS/Fe(II)/UVA process. Despite these excellent findings, the addition of organic compounds to the treated effluent is not advisable because of the hard mineralization of more organic matter, lowering down the process efficiency.

Good degradation results were obtained for the PS/Fe(II)/UV process of atrazine as well. For instance, Popova et al. [79] reported a very rapid remediation of 50 mL of 4 mg L^{-1} of this herbicide with 3.5 mM PS and 1.0 mM Fe^{2+} at pH = 3.5 filling a stirred glass dish exposed to an external UV light from a KrCl excilamp at λ = 222 nm. Note that an UVC light (λ = 190–285 nm) can photolyze the herbicide contributing to its removal. The treatment was carried out with different aqueous matrices and total degradation was achieved in 11 min for pure water < 20 min for river water < WWTP effluent (> 20 min) (see Table 2), according to the attack of less oxidizing agents due to their consumption by inhibiting species (e.g., inorganic anions, NOM, and other organics) in the medium, as pointed out above. The use of scavengers allowed establishing the predominance of $SO_4^{\bullet-}$ over $^{\bullet}OH$ as oxidizing agent.

3.7. Photocatalytic activation

Photocatalysis (PC) consists of the illumination of a semiconductor immersed into the polluted solution to promote the pass of an electron e_{CB}^- of its valence band (VB) to its conduction band (CB) originating a hole h_{VB}^+ in the VB by reaction (23) [83–85]. The energy of the incident photons has to be higher or equal to the band gap energy (E_{bg}) of the semiconductor to separate the charges giving rise to the e_{CB}^-/h_{VB}^+ pair. The h_{VB}^+ can then directly oxidize the organics or react with water or OH^- to produce oxidant $^{\bullet}OH$ by reactions (24) or (25), respectively. For its part, the e_{CB}^- can reduce species like O_2 to $O_2^{\bullet-}$, H_2O_2 to $^{\bullet}OH$, and $S_2O_8^{2-}$ to $SO_4^{\bullet-}$ from reactions (26)–(28), respectively. The main drawback of the process is the rapid recombination of h_{VB}^+ and e_{CB}^- by reaction (29) with the consequent loss of PC efficiency.

$$\text{Semiconductor} + h\nu \rightarrow h_{VB}^+ + e_{CB}^- \quad (23)$$

$$h_{VB}^+ + H_2O \rightarrow {}^{\bullet}OH + H^+ \quad (24)$$

$$h_{VB}^+ + OH^- \rightarrow {}^{\bullet}OH \quad (25)$$

$$O_2 + e_{CB}^- \rightarrow O_2^{\bullet-} \quad (26)$$

$$H_2O_2 + e_{CB}^- \rightarrow {}^{\bullet}OH + OH^- \quad (27)$$

$$S_2O_8^{2-} + e_{CB}^- \rightarrow SO_4^{\bullet-} + SO_4^{2-} \quad (28)$$

$$h_{VB}^+ + e_{CB}^- \rightarrow \text{semiconductor} + \text{heat} \quad (29)$$

The hybrid PS/PC process has been reported by several herbicides like alachlor [83], atrazine [86,87], 4-chloro-2-methylphenoxyacetic acid [88], chlorotoluron [89], dicamba [90], diuron [91], imazapyr [92], metribuzin [93], and paraquat [84]. Other works have been devoted to the treatment of many herbicides [94,95].

The most typical photocatalyst is TiO_2 or its anatase form with an E_{bg} value close to 3.2 eV, being photoexcited under UVA light. The study of P é rez et al. [83] was performed with a flow plant with a tubular photoreactor with TiO_2 P25 upon 38 W UVC light. It operated with 10 L of 10–124 mg L^{-1} of alachlor in pure water with 595–2381 mg L^{-1} of PS and 50 mg L^{-1} of photocatalyst at pH 3.0 and 25 ºC. Quicker herbicide decay was obtained for lower alachor content and greater PS dose, being determined a total degradation in 45 min with total mineralization in 85 min for 50 mg L^{-1} herbicide and 2381 mg L^{-1} PS (see Table 2). This excellent result confirms the high oxidation power of the oxidizing agents alongside the parallel photolysis of organics provided by the PS/PC treatment with TiO_2/UVC. This behavior has also been reported by Ghavi et al. [84] when treated 400 mL of 30 mg L^{-1} of the viologen paraquat filling a stirred tank reactor with anatase under inner 150 W UVC light. The process was optimized by response surface methodology and found optimal for 400 mg L^{-1} PS and 150 mg L^{-1} photocatalyst at pH = 6.3 yielding 77% degradation with k_1 = 0.0299 min^{-1} and 32% TOC removal in 40 min, although the energy cost was as high as 482 kWh m^{-3} in 60 min due to the high electric power of the UVC lamp (see Table 2).

Recently, complex semiconductor composites have been synthesized to be photoactivated with visible light aiming to using the free sunlight as energy source. So, Chen et al. [87] prepared an Ag_3VO_4/Bi_2MoO_6/-diatomite photocatalyst to be photoexcited with a 150 W Xe lamp with a

cut-off providing visible light at $\lambda = 420$ nm. A content of 20–100 mg L^{-1} of this material was suspended in 100 mL of 2.5–12.5 mg L^{-1} atrazine in several aqueous matrices and treated with 0–1.2 mM PS at pH = 3.0–11.0 lasting 60 min. In pure water, a quicker 97% degradation was found for 2.5 mg L^{-1} herbicide, 1.0 mM PS, and 80 mg L^{-1} photocatalyst at pH = 3.0 (see Table 2). Lower percent of atrazine removal was determined with raising the herbicide content and pH and with decreasing the PS and photocatalyst concentrations. The degradation upon the above conditions dropped down to 74% for tap water and 57% for river water, by the increasing inhibitory effect of their components, as stated above. This phenomenon was corroborated by the large inhibition of the process when adding CO_3^{2-}, much greater than other anions like Cl^-, NO_3^-, and SO_4^{2-}. The use of scavengers revealed the action of $^{\bullet}OH$, $SO_4^{\bullet-}$, $O_2^{\bullet-}$, and holes. Despite these good findings, the photocatalyst presented a low reusability after 5 consecutive cycles, probably by the deposition of by-products at this surface.

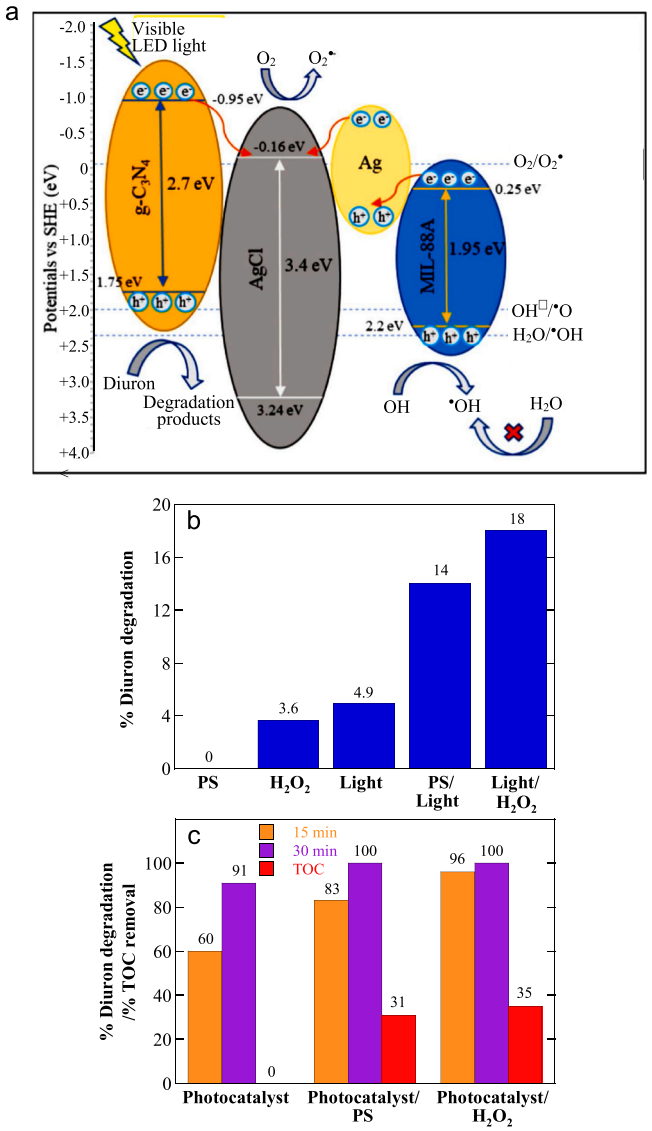

Fig. 9. (a) Schematic diagram of the charge transfer mechanism of the Ag|AgCl/MIL-88 (Fe)|g-C_3N_4 photocatalyst used for diuron removal in a stirred tank reactor upon external 93.4 W visible LED light. (b) Percentage of degradation after 120 min of different treatments of 150 mL of 10 mg L^{-1} herbicide with 1.0 mM PS or 1.0 mM H_2O_2 in pure water at natural pH and 25 °C, (c) Percent of degradation at 15 and 30 min and percent of TOC removal at 120 min for photocatalytic processes under the above conditions with 1.0 g L^{-1} photocatalyst. Adapted from ref. [91].

This makes difficult its applicability since stable photocatalysts are required in practice.

Fig. 9a schematizes the diagram proposed for the charge transfer mechanism of the Ag|AgCl/MIL-88 (Fe)|g-C_3N_4 photocatalyst synthesized by Akgün et al. [91] for visible LED light photoexcitation at $\lambda = 531.5$ nm. The E_{bg}-values of the three semiconductors are given, showing that the oxidation of the pollutant diuron with holes takes place at the VB of g-C_3N_4 and the formation of $^{\bullet}OH$ at the VB of MIL-88 and $O_2^{\bullet-}$ at the CB of AgCl. On the latter site, H_2O_2 or $S_2O_8^{2-}$ can be reduced as well. The photocatalytic power of this composite was checked by degrading 150 mL of 10 mg L^{-1} diuron with 1.0 mM PS or 1.0 mM H_2O_2 in pure water at natural pH and 25 °C using a stirred tank reactor upon a 93.4 W visible LED light. Fig. 9b depicts the increasing percentage of diuron degradation after 120 min of several treatments without photocatalyst in the sequence: PS < H_2O_2 < light < PS/light < light/H_2O_2, demonstrating the photoactivity of the herbicide and the superior oxidation ability of H_2O_2than PS. However, much more rapid degradation was achieved by adding 1.0 g L^{-1} of photocatalyst, as shown in Fig. 9c. Total herbicide decay can be observed in 30 min, more rapidly achieved by H_2O_2 than PS, meaning a more powerful oxidation with $^{\bullet}OH$ formed from H_2O_2 reduction by reaction (27) than $SO_4^{\bullet-}$ generated from PS by reaction (28). Following this trend, higher TOC removal was more destroyed with H_2O_2 as well (see Fig. 9c). Stability studies showed the photoreduction of the AgCl component to Ag, pointing to a low reusability of the photocatalyst.

3.8. Electrochemical activation

The electrochemical activation of PS has been tested for atrazine [96–100], 2,4-D [101–103], diuron [104], and oxyfluorfen [105] in pure water. The anode (M) and the cathode of the electrolytic cell play the main role of this hybrid process. The process begins when a current (I) is applied to the electrodes and water is anodically oxidized originating the physisorbed hydroxyl radical at the anode surface, symbolized as M($^{\bullet}OH$), from reaction (30) [15,96]. This radical then reacts with PS to produce $SO_4^{\bullet-}$ from reaction (31). On the other hand, PS can also be reduced at the cathode to generate $SO_4^{\bullet-}$ by reaction (32) and this radical can be additionally formed from SO_4^{2-} oxidation by reaction (33).

$$M + H_2O \rightarrow M(^{\bullet}OH) + H^+ + e^- \quad (30)$$

$$S_2O_8^{2-} + M(^{\bullet}OH) \rightarrow M + HSO_4^- + SO_4^{\bullet-} + \tfrac{1}{2}O_2 \quad (31)$$

$$S_2O_8^{2-} + e^- \rightarrow SO_4^{2-\cdot} + SO_4^{\bullet-} \quad (32)$$

$$SO_4^{2-} \rightarrow SO_4^{\bullet-} + e^- \quad (33)$$

Electrochemical activation uses simple electrolytic systems, easily affordable, with a low electric energy input as compared to that needed for UV lamps, making the removal of herbicides much more cost-effective. Atrazine has been the most herbicide studied with this procedure using stirred undivided tank reactors to profit of the oxidants formed at both, the anode and cathode. Boron-doped diamond (BDD) anode is the most powerful anode known with greater generation of physisorbed BDD($^{\bullet}OH$) than other ones. Bu et al. [96] reported the PS activation with this anode coupled to a stainless-steel (SS) cathode for treating 100 mL of 5 μM atrazine in pure water with 0.25–5.0 mM PS and 2.0 mM Na_2SO_4 as supporting electrolyte. The assays were made at pH = 4.0–10.0 and 25 °C by applying a low current density (j) of 1.0–9.0 mA cm^{-2} during a short time of 30 min. $SO_4^{\bullet-}$,$^{\bullet}OH$, and non-radical species were detected as generated oxidants by means of scavengers. The herbicide removal was enhanced with the production of more quantities of such oxidants with raising PS concentration and j, and with lowering pH. The best results were found with 1.0 mM PS, pH = 4.0, and $j = 5.0$ mA cm^{-2} yielding 78% degradation with $k_1 = 0.050$ min^{-1} (see Table 2). Addition of 1.0 mM Cl^- accelerated the herbicide removal to $k_1 = 0.069$ min^{-1} because of the production of

another oxidant like active chlorine (HClO) at the anode, but other anions decelerated the process by consumption of PS in the order: HCO_3^- > $H_2PO_4^-$ > NO_3^-. The authors also identified 10 primary heteroaromatic by-products by LC-MS. Li et al. [97] considered a less potent anode like Ti|RuO_2-IrO_2, *a* SS cathode, and added $CuFeO_4$ nanoparticles (NPs) to accelerate the PS decomposition. The treatment was focused to 400 mL of a synthetic suspension with 46 μM herbicide, 0–4.5 mM PS, 0–4.0 g L^{-1} catalyst, and 20 mM Na_2SO_4 in pure water at pH = 3.0–11.0, j = 0–24 mA cm^{-2}, and 30 °C, lasting 30 min. Overall atrazine removal was determined at > 4.0 mM PS, 0.30 g L^{-1} catalyst, pH= 6.3, and j > 8 mA cm^{-2} (see Table 2). Again, a positive effect was found by adding Cl^- to the suspension due to active chlorine formation, whereas an inhibitory effect was observed for other anions like NO_3^-, HCO_3^-, and $H_2PO_4^-$. They reported a predominance of $SO_4^{\bullet-}$ over $^\bullet$OH as oxidant, a moderate reusability of the catalyst after 5 consecutive runs, and the detection of 13 heteroaromatic derivatives by LC-MS.

An interesting work of Zhou et al. [100] compared the performance of blue TiO_2 nanotubes and Al-doped blue TiO_2 nanotubes anodes and a SS cathode. Electrolyses were first carried out with 100 mL of 5 μM atrazine in 20 mM $NaClO_4$ with 0–5.0 mM PS, pH = 2.8–11.0, 25 °C, and j = 0–10 mA cm^{-2}. Fig. 10a reveals that herbicide was completely abated with 1.0 mM PS at pH = 9.0 and j = 5.0 mA cm^{-2} (so-called control) in 60 min for the Al-doped blue TiO_2 nanotubes, whereas Fig. 10b highlights a slower abatement up to 77% for the blue TiO_2 nanotubes. For the former anode, a greater TOC reduction of 52% was determined after 180 min of electrolysis (see Table 2). Fig. 10a and b also shows the effect of several scavengers (methanol for all radicals, furfuryl acid (FFA) for all radicals and non-radical $^1O_2$, and TBA for $^\bullet$OH) on the normalized atrazine decay. As can be observed, TBA showed a lesser inhibitory effect for the Al-doped blue TiO_2 nanotubes, pointing to a smaller generation of $^\bullet$OH. This was confirmed from the EPR spectra with DMPO for both anodes depicted in Fig. 10c, where both adducts of DMPO-$SO_4^{\bullet-}$ and DMPO-$^\bullet$OH were detected for the Al-doped blue TiO_2 nanotubes, whereas the second one only appeared for the other anode. Since similar percentage of radical and non-radical oxidants were formed in both cases (see Fig. 10d), one can conclude that the Al-doped blue TiO_2 nanotubes has higher oxidation power because of the generation of $SO_4^{\bullet-}$, a fact that did not occur with the blue TiO_2 nanotubes. Fig. 10e illustrates the production of oxidants at the surface of both anodes, remarking the PS activation to $SO_4^{\bullet-}$ over the Al sites of the former one. Using this anode, the addition of Cl^- strongly accelerated the degradation process, and SO_4^{2-}, at less extent. In contrast, it was found an increasing inhibition with: humic acid < HCO_3^-. $SO_4^{\bullet-}$ was the main oxidant. It is noticeable that the anode showed a large stability after 20 electrolytic cycles. From these positive finding, an actual soil washing wastewater with 8.05 mg L^{-1} atrazine and 25.96 mg L^{-1} TOC was treated under the conditions given in Table 2 with Al-doped blue TiO_2 nanotubes and BDD anodes. Although total herbicide degradation at similar rate was obtained for both anodes in 120 min, TOC more rapidly decayed with BDD (42% vs. 20%) showing its higher power to

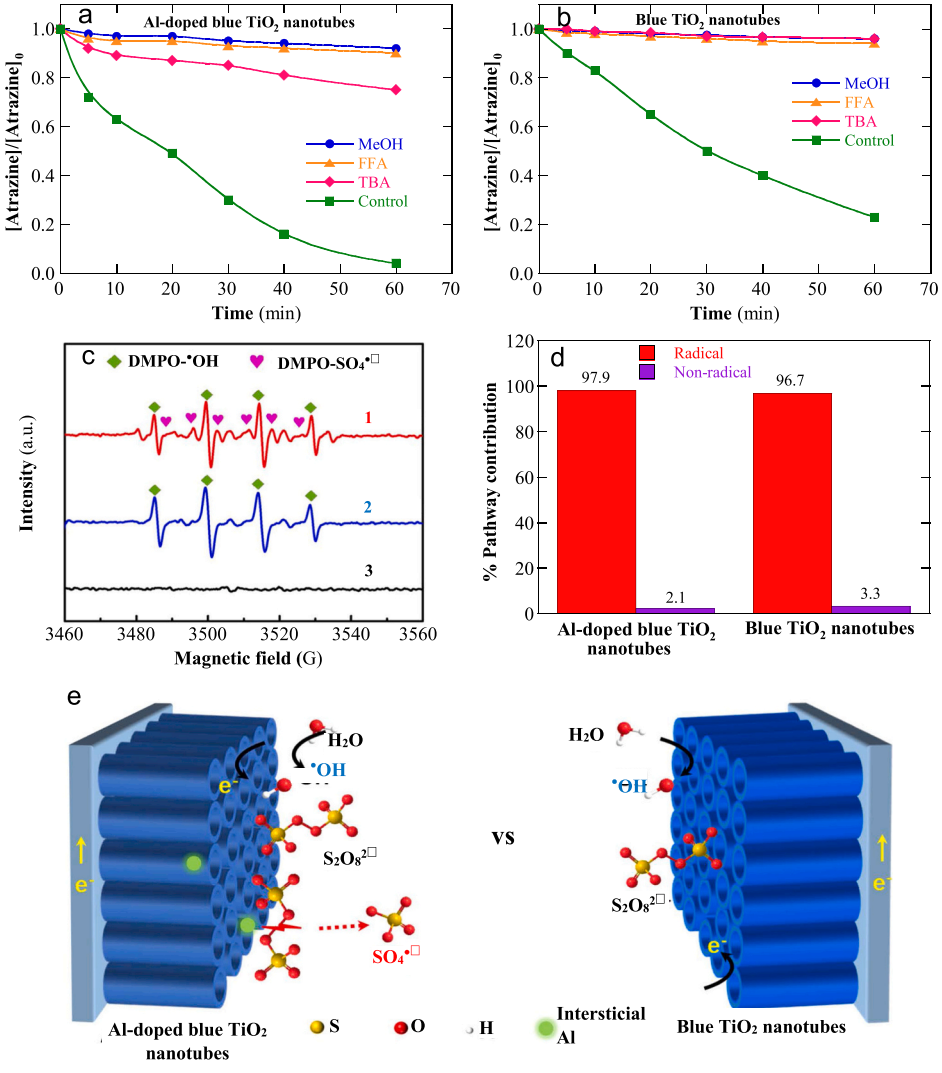

Fig. 10. Normalized atrazine concentration vs. time for the electrochemical degradation of 100 mL of 5 μM herbicide in 20 mM $NaClO_4$ with 1.0 mM PS and 100 mM of scavenger (methanol, furfuryl alcohol (FFA), and *t*-butanol (TTBA) at pH = 9.0 and 25 °C using a stirred tank reactor with (a) an Al-doped blue TiO_2 nanotubes or (b) blue TiO_2 nanotubes anode and a stainless-steel cathode at current density of 5 mA cm^{-2}. (c) EPR spectra obtained with addition of DMPO to the: (1) electrolysis with Al-doped blue TiO_2 nanotubes, (2) electrolysis with blue TiO_2 nanotubes, and (3) with the former electrode without electrolysis, (d) Percent of contribution of the radical and non-radical pathways to the above processes. (e) Schematic illustration of the generation of oxidant radicals in both anodes. Adapted from ref. [100].

activate PS.

A more complex PS/electrochemical/UVC/nZVI process has been reported by Mehralipour and Kermani [102] by electrolyzing 500 mL of 25–125 mg L^{-1} 2,4-D in pure water containing 0–125–0.625 mg L^{-1} PS, 0.025–0.125 mg L^{-1} nZVI as catalyst, and Na_2SO_4 at pH = 1.0–5.0. The trials were wade with a stirred undivided tank reactor equipped with a graphene anode, a Ti cathode, and an inner 16 W UVC lamp by applying an I = 0.25–1.25 A. The process was analyzed by response surface methodology and was found optimal with 92% removal for 50.05 mg L^{-1} herbicide, 0.49 mg L^{-1} PS, 0.10 mg L^{-1} catalyst, pH = 3.47, and I = 1.0 A in 80 min, with $k_1 = 0.0194$ min^{-1}. At 100 min, COD and TOC were reduced by 78% and 63%, respectively. It was found the formation of $SO_4^{\bullet-}$ and $^{\bullet}OH$ as oxidants using scavengers and 9 aromatic derivatives and 6 final carboxylic acids were detected by GC-MS. The UVC irradiation helped to remove the photoactive organics present in the suspension.

4. Removal of herbicides by peroxymonosulfate-based processes

The oxidant $SO_4^{\bullet-}$ can also be generated from the activation of PMS. Over the last three years, many solid metallic catalysts have been synthesized and used to treat herbicides in synthetic waters and real wastewaters by this procedure, as can be seen in Fig. 1d and Table 3. Activation by iron ion, Fe, photocatalysis, and other methods have been developed as well. This section is devoted to analyze the best results reported by all these techniques.

4.1. Catalytic activation

Atrazine has been again the most herbicide studied for PMS activated with catalysts. The works have used compounds with Co [106–119], Cu [120–123], and Fe [124–129], as well as drinking water treatment residuals [130,131], kaolinite [132], magnetic N-doped graphitic carbon [133], and molybdenite [134]. Fig. 11 presents several mechanisms proposed for the generation $SO_4^{\bullet-}$ and $^{\bullet}OH$ from PMS under catalytic activation for atrazine removal. Other works have considered the treatment of dicamba with hydrochar-montmorillonite [135], 2,4-D with $CuFe_2O_4$ NPs/O_3 [136]. Fe-MoS_2 [137], and $NiFe_2O_4$ or B-$NiFe_2O_x$ [138], diuron with coated Fe_3O_4 [139], glyphosate with Co composites [140–142] and $Fe_3Ce_1O_x$ [143], 2-methyl-4-chlorophenoxyacetic acid with CuZn-MIL101 [144], metolachlor [145,146], pentachlorophenol [147,148] and quinclorac [149] with Co composites, 2,4,6-trichlorophenol with Fe_3S_4 [150], and tritosulfuron with chloride [151]. The surface of a solid metallic catalyst contains active sites with linked metallic ion ($\equiv Me^{n+}$) that reduces PMS to form the surface oxidized form of the ion ($\equiv Me^{(n+1)+}$), $SO_4^{\bullet-}$, and $^{\bullet}OH$ as follows [114,123]:

$$6\ Me^{n+} + HSO_5^- \rightarrow 6\ Me^{(n+1)+} + SO_4^{\bullet-} + {}^{\bullet}OH \quad (34)$$

Reaction (34) takes place for the surface $\equiv Co^{2+}$, $\equiv Fe^{2+}$, and $\equiv Cu^{+}$ ions to produce $\equiv Co^{3+}$, $\equiv Fe^{3+}$, and $\equiv Cu^{2+}$ ions, respectively. This is highlighted in Fig. 11a for Co_3O_4/TiO_2 NPs [114], Fig. 11b for $CoFe_2O_4$ NPs [108], Fig. 11c for CoMgAl-LDOs [109], Fig. 11d for $LaCoO_3/Al_2O_3$ [112], Fig. 11e for CuO-Fe_2O_3/5% MXene [123], and Fig. 11f for $LaFe_{0.9}Co_{0.1}O_3$ [129]. $SO_4^{\bullet-}$ generated from reaction (34) can then produce more $^{\bullet}OH$ from reactions (2) or (3). Other oxidants can be produced as well. For instance, in the case of the $\equiv Co^{3+}/\equiv Co^{2+}$ pair, the $\equiv Co^{2+}$ can be regenerated from the attack of PMS over $^{+}/\equiv Co^{3+}$ yielding the peroxymonosulfate radical ($SO_5^{\bullet-}$) by reaction (35) [152]:

$$\equiv Co^{3+} + HSO_5^- \rightarrow \equiv Co^{2+} + SO_5^{\bullet-} + H^+ \quad (35)$$

However, $SO_5^{\bullet-}$ is a very weak oxidant ($E^{o}(SO_5^{\bullet-}/SO_4^{2-})$ = 1.1 V [153]), reason for which its oxidation over the organic pollutants is disregarded.$SO_4^{\bullet-}$ and $^{\bullet}OH$ are the effective oxidants in most PMS-based AOPs.

Table 3 shows that 30–300 mL of suspensions of up to 30 mM atrazine were rapidly remediated in pure water, usually at near neutral pH with the different catalysts tested containing Co, Fe, and/or Cu. Glass vials and more usually, stirred tank reactors were used in the trials. As expected, higher percent of degradation was always obtained with decreasing the herbicide content and with increasing the PMS and catalyst doses and temperature by the same reasons as argued for the PS-based AOPs in Section 3. In some cases, maximum loss of atrazine was achieved at given PMS and catalyst concentrations, whereupon the degradation process was decelerated by the large acceleration of parasitic reaction like reactions (4)–(7). It was confirmed the predominance of $SO_4^{\bullet-}$ over $^{\bullet}OH$ as oxidant by means of scavengers and the large inhibition of the degradation process in the presence of anions like HCO_3^-, CO_3^{2-}, and HPO_4^{2-}, as well as humic acid, due to the consumption of oxidants by these species. However, the atrazine removal was slightly inhibited with Cl^- and NO_3^-, bur in some cases, it was even accelerated with low contents of Cl^- because of the generation of active chlorine from reactions (11) and (12) and strong oxidants like $Cl^{\bullet}$ from reactions (8) and (9) and $Cl_2^{\bullet-}$ from reaction (10) [109,112,129]. This behavior explained the superior oxidation ability of the PMS-based processes in pure water than in real waters and wastewaters that contain high contents of such species. In general, the catalysts tested presented a low reusability due to the leaching of its metallic components, which represents a drawback for their practical application. Only in the case of $LaFe_{0.9}Co_{0.1}O_3$, good reusability was found after 5 consecutive cycles of treating 2.50 mg L^{-1} herbicide in pure water with 100 mg L^{-1} PMS and 300 mg L^{-1} catalyst at pH = 6.9 and 30 °C for 30 min, maintaining the overall atrazine decay. It is noticeable that the primary heteroaromatic derivatives were always identified by LC-MS or LC-MS/MS, being in agreement with those given in Fig. 4.

Fig. 12a shows the variation of the normalized atrazine concentration with time for the treatment of 200 mL of 5 mg L^{-1} herbicide in pure water with 0.3 mM PMS and/or 0.20 g L^{-1} of Co_3O_4/TiO_2 NPS as catalyst at pH = 6.7, and 30 °C lasting 60 min. An 82% degradation was determined for the PMS/catalyst process, whereas the PMS or the catalysts alone only yielded the loss of about 7–8% of herbicide. This makes evident the high oxidation power of $SO_4^{\bullet-}$ and $^{\bullet}OH$ oxidants formed in the combined treatment. Nevertheless, the catalyst showed a low reusability, as can be seen in Fig. 12b for the gradual decay of herbicide removal during four consecutive cycles from 83% to 71% owing to the surface corrosion leaching Co and the deposition of by-products on the active sites. Fig. 12c and d show the progressive rise of the pseudo-first-order rate constant for atrazine removal with increasing the content of the catalyst from 0.02 to 0.30 g L^{-1} and PMS up to 0.6 mM, as expected by the continuous acceleration of reaction (34) by the presence of more reactants. In contrast, Fig. 12e discloses that the PS/catalyst was active in the pH interval of 5.0–9.0, with a maximum $k_1 = 0.0463$ min^{-1} at pH = 9.0 (see Table 3). The authors related the strong inhibition at pH = 3.0 to the protonation of the oxidants decreasing their oxidation power, whereas at pH = 11.0, the conversion of HSO_5^- into its inactive deprotonated from SO_5^{2-} (with pK_a = 9.4), avoiding the formation of oxidant radicals. The former argument disagrees with the results of other authors who found a large degradation rate at pH = 3.0, indicating that this was conditioned by the nature of the catalyst. Fig. 12f highlights a surprising effect of HCO_3^- ion when it is added to the suspension upon the conditions of Fig. 12a. While 1.0 mM of HCO_3^-, NO_3^-, and $HPO_4^{\bullet-}$ caused a clear inhibition of the atrazine abatement because they reacted with $SO_4^{\bullet-}$ and $^{\bullet}OH$ decreasing their content to attack the herbicide, the presence of 0.1 mM HCO_3^- largely accelerated its degradation. This was ascribed to the concomitant increase of pH up to 8.5, where atrazine was more largely destroyed (see Fig. 12e).

Another interesting work of Ali et al. [128] reported the characteristics of PMS activated with MoS_4-Fe-LDH. The trials were carried out by suspending 0.10–0.25 g L^{-1} of this catalyst in 30 mL of pure water containing 10 mg L^{-1} herbicide and 0.5–3.0 mM PMS at pH = 3.0–11.0 and 30 °C during 40 min Fig. 13a depicts the positive influence of adding

Table 3
Selected results obtained for herbicides removal by catalytic activation of peroxymonosulfate.

Herbicide	System	Experimental remarks	Best results	Ref.
Atrazine	Glass vial with Co_3O_4	30 mL of 20 μM herbicide, 2.0 mM PMS, and 0.4 g L^{-1} catalyst in pure water, lake water, and groundwater, pH = 3.0–10.0, effect of scavengers, 25 °C, 15 min	Degradation: 99% with Co_3O_4 > 68% with 0.06 mg L^{-1} Co^{2+} at optimum pH = 6.0. Co was dissolved up to pH 6.0. Increasing $^{\bullet}OH$ in front of $SO_4^{\bullet-}$ at greater pH. Low reusability of catalyst in 9 cycles. k_1 (min^{-1}): 0.068 for pure water > 0.042 for groundwater > 0.024 for lake water. Evolution of 7 heteroaromatic by-products by LC-MS/MS	[107]
Atrazine	Stirred tank reactor with magnetic $CoFe_2O_4$ NPs[a]	200 mL of 5–30 mM herbicide, 0–1.0 mM PMS, and 0–0.6 g L^{-1} catalyst in pure water, pH = 3.0–11.0, effect of scavengers, NO_3^-, HCO_3^-, and HPO_4^{2-}, 30 min	The degradation rate was enhanced with decreasing herbicide content and with raising PMS dose and up to 0.5 g L^{-1} catalyst. Little effect of pH. Total degradation for < 10 mM herbicide, > 0.8 mM PMS, and > 0.3 g L^{-1} catalyst, with 27% TOC reduction. Greater k_1 = 0.198 min^{-1}. Low inhibition with NO_3^-, upgraded with HCO_3^- and HPO_4^{2-}. $SO_4^{\bullet-}$ as main oxidant. Scarce reusability after 5 successive cycles. 6 heteroaromatic derivatives detected by LC-MS	[108]
Atrazine	Stirred tank reactor with CoMgAl-LDOs[b]	300 mL of 5–10 mg L^{-1} herbicide, 0–0.6 mM PMS, and 0–150 mg L^{-1} catalyst in pure water, pH = 3.0–11.0, effect of scavengers, Cl^-, NO_3^-, HCO_3^-, and HPO_4^{2-}, 30 °C, 15 min	Total degradation for < 10 mg L^{-1} herbicide, > 0.4 mM PMS, 75–100 mg L^{-1} catalyst, and neutral pH. Acceleration with Cl^-, low inhibition with NO_3^-, and large inhibition with HCO_3^- and HPO_4^{2-}. $SO_4^{\bullet-}$ predominated over $^{\bullet}OH$ as oxidant. Co leaching and scarce reusability after 4 consecutive runs. 9 heteroaromatic intermediates identified by LC-MS	[109]
Atrazine	Stirred tank reactor with magnetic $CoFe_2O_4$/water treatment residues	200 mL of 10 μM herbicide, 0.15–0.30 mM PMS, and 0.01–0.04 g L^{-1} catalyst in pure water, tap water, surface water, and groundwater, pH = 3.15–10.12, effect of scavengers, 30 °C, 120 min	In pure water, total herbicide removal in 20 min for > 0.25 mM PMS, > 0.03 g L^{-1} catalyst, and pH = 4.01. Predominance of $SO_4^{\bullet-}$ over $^{\bullet}OH$ as oxidant. Degradation in 120 min: 87% for surface water and groundwater, and 69% for tap water, 14 heteroaromatic by-products identified by LC-MS	[111]
Atrazine	Stirred tank reactor with $LaCoO_3/Al_2O_3$	200 mL of 2.5–10 mg L^{-1} herbicide, 0–200 mg L^{-1} PMS, and 0–200 mg L^{-1} catalyst in pure water, pH = 3.0–11.0, effect of scavengers, Cl^-, CO_3^{2-}, HCO_3^-, and $H_2PO_4^-$, 30 °C, 30 min	Overall herbicide decay for < 5 mg L^{-1} herbicide, > 100 mg L^{-1} PMS, > 100 mg L^{-1} catalyst, and pH 5.0–7.0, Greater k_1 = 0.21 min^{-1}. $SO_4^{\bullet-}$ predominated over $^{\bullet}OH$ as oxidant. Large inhibition with CO_3^{2-}, HCO_3^-, and HPO_4^{2-}, although > 5 mM Cl^- accelerated the degradation. Low reusability after 3 cycles. 6 heteroaromatic by-products found by LC-MS/MS	[112]
Atrazine	Stirred tank reactor with Co_3O_4/TiO_2 NPs	200 mL of 5 mg L^{-1} herbicide, 0–0.6 mM PMS, and 0.02–0.30 g L^{-1} catalyst in pure water, pH = 3.0–11.0, effect of scavengers, NO_3^-, HCO_3^-, and HPO_4^{2-}, 30 °C, 60 min	Quicker degradation at higher PMS and catalyst doses, and at pH 9.0. With 0.3 mM PMS and 0.2 g L^{-1} catalyst at this pH, k_1 = 0.0463 min^{-1}. Process inhibited at pH = 3.0 and 11.0. Acceleration with 0.1 mM HCO_3^-, but strong inhibition at higher anion content. Low inhibition with NO_3^-, upgraded with HPO_4^{2-}. Predominance of oxidant $SO_4^{\bullet-}$. Low reusability in 4 consecutive steps. 9 heteroaromatic intermediates found by LC-MS	[114]
Atrazine	Stirred tank reactor with Co/biochar	100 mL of 10 μM herbicide, 100 mM PMS, and 0.1 g L^{-1} catalyst in pure water, pH = 2.0–10.0, effect of scavengers, Cl^-, NO_3^-, HCO_3^-, and $H_2PO_4^-$, 15–35 °C, 10 min	Total herbicide abatement in the pH range 4.0–8.0, more rapid with increasing temperature. Oxidants: $SO_4^{\bullet-}$ (main), $^{\bullet}OH$, and $O_2^{\bullet-}$. Little influence of Cl^- and NO_3^-, large inhibition with HCO_3^- and $H_2PO_4^-$. Low reusability after 3 consecutive runs. 27 heteroaromatic intermediates detected by LC-MS	[116]
Atrazine	Stirred tank reactor with CuO-Fe_2O_3/5% MXene	100 mL of 10 mg L^{-1} herbicide, 4–10 M ratio of PMS, and 5–30 mg L^{-1} catalyst in pure water, pH = 2.0–12.0, effect of scavengers, Cl^-, NO_3^-, CO_3^{2-}, SO_4^{2-}, $H_2PO_4^-$, and humic acid, 15–35 °C, 60 min	Overall removal for 8 M ratio of PMS, > 10 mg L^{-1} catalyst, and pH 6.4–10.0, with higher k_1 = 0.10 min^{-1}. Oxidants: $SO_4^{\bullet-}$ (main), $^{\bullet}OH$, and $^1O_2$. Inhibitory effect of all the species added. 14 heteroaromatic derivatives identified by LC-MS	[123]
Atrazine	Stirred tank reactor with MoS_4-Fe-LDH	30 mL of 10 mg L^{-1} herbicide, 0.5–3.0 mM PMS, and 0.10–0.25 g L^{-1} catalyst in pure water and real effluents, pH = 3.0–11.0, effect of scavengers, Cl^-, NO_3^-, HCO_3^-, CO_3^{2-}, HPO_4^{2-}, and humic acid, 30 °C, 40 min	Herbicide completely removed with 1.0 mM PMS and 0.15 g L^{-1} catalyst at pH = 3.0–7.0, with k_1 = 0.1173 min^{-1}. $SO_4^{\bullet-}$ predominated over $^{\bullet}OH$ as oxidant. Inhibitory effect of all species added. Degradation: pure water > tap water > lake water > industrial wastewater. 9 heteroaromatic by-products detected by LC-MS	[128]
Atrazine	Stirred tank reactor with $LaFeO_3$ or $LaFe_{0.9}Co_{0.1}O_3$	200 mL of 2.50 mg L^{-1} herbicide, 0–150 mg L^{-1} PMS, and 0–400 mg L^{-1} catalyst in pure water, tap water, and lake water, pH = 3.0–11.0, effect of scavengers, Cl^-, NO_3^-, CO_3^{2-}, and HCO_3^-, 30 °C, 30 min	For $LaFe_{0.9}Co_{0.1}O_3$, total degradation for 100 mg L^{-1} PMS, 300 mg L^{-1} catalyst, and pH = 6.9. Lower oxidation with $^{\bullet}OH$ than with $SO_4^{\bullet-}$. Slight acceleration with Cl^-, little inhibition with NO_3^-, and large inhibition with CO_3^{2-} and HCO_3^-. Good reusability after 5 successive runs. Degradation: pure water > tap water > lake water. 7 heteroaromatic derivatives found by LC-MS/MS	[129]
Dicamba	Stirred tank reactor with hydrochar-montmorillonite	Suspensions with 10 mg L^{-1} herbicide, 0.5–4.0 mM PMS, and 0.6–3.0 g L^{-1} catalyst in pure water, well	In pure water, total removal in 180 min for 2.0 mM PMS and 3.0 g L^{-1} catalyst at pH = 2.52. Oxidants: $SO_4^{\bullet-}$ (main), $^{\bullet}OH$, and $O_2^{\bullet-}$. Degradation: pure water > well	[135]

(*continued on next page*)

Table 3 (*continued*)

Herbicide	System	Experimental remarks	Best results	Ref.
		water, and lake water, pH = 2.52–9.15, effect of scavengers, 25 °C, 240 min	water > lake water. 8 aromatic derivatives and 2 final carboxylic acids identified by LC-MS	
2,4-D	Sealed flask on a shaker with $CuFe_2O_4$ NPs[a]/O_3	200 mL of 5–50 mg L^{-1} herbicide, 1.0 and 2.0 mM PMS, 0.10 and 0.20 g L^{-1} catalyst, and 4–20 mg L^{-1} O_3 in pure water, tap water, river water, and WWTP effluent, pH = 3.0–10.0, effect of scavengers, Cl^-, NO_3^-, NO_2^-, SO_4^{2-}, and HCO_3^-, 10–45 °C, 60 min	In pure water, 2,4-D completely disappeared with 20 mg L^{-1} herbicide, 2.0 mM PMS, 0.20 g L^{-1} catalyst, and 16 mg L^{-1} O_3 at optimum pH = 6.0 and 25 °C. 67% of TOC removal with 50 mg L^{-1} herbicide. Higher contribution of $SO_4^{\bullet-}$ than $^{\bullet}OH$ as oxidant. Inhibition with all the species added. Moderate reusability after 5 consecutive cycles. Degradation: pure water > tap water > river water > WWTP effluent. 5 aromatic by-products and 2 final carboxylic acids detected by LC-MS	[136]
2,4-D	Stirred tank reactor with $NiFe_2O_4$ or B-$NiFe_2O_x$	250 mL of 0.05–1.0 mg L^{-1} herbicide, 5–80 mg L^{-1} PMS, and 10–150 mg L^{-1} catalyst in pure water, pH = 3.2–9.9, effect of scavengers, Cl^-, NO_3^-, SO_4^{2-}, and HCO_3^-, 25 °C, 15 min	Overall decay for 0.5 mg L^{-1} herbicide, 80 mg L^{-1} PMS, and 50 mg L^{-1} B-$NiFe_2O_x$ at optimum pH = 7.0, with k_1 = 0.215 min^{-1}. Very slow reduction with $NiFe_2O_4$. Oxidants: $SO_4^{\bullet-}$ (pre-eminent), $^{\bullet}OH$, and $O_2^{\bullet-}$. Inhibition with all the species added. 20 aromatic intermediates and 3 final carboxylic acids found by LC-MS	[138]
Glyphosate	Stirred tank reactor with CuCoFe-LHD	100 mL of 100 mg L^{-1} herbicide, 0–400 mg L^{-1} PMS, and 0–200 mg L^{-1} catalyst in pure water, pH = 3.5–13.0, effect of scavengers, 25 °C, 6 min	Total degradation under optimum conditions of 200 mg L^{-1} PMS, 100 mg L^{-1} catalyst, and pH = 11.0. Oxidation in the order: $SO_4^{\bullet-}$ > $O_2^{\bullet-}$ > $^1O_2$ > $^{\bullet}OH$. Moderate reusability after 5 consecutive steps	[140]
Glyphosate	Stirred tank reactor with Co_3O_4/g-C_3N_4	100 mL of 10–100 mg L^{-1} herbicide, 0–300 mg L^{-1} PMS, and 0–500 mg L^{-1} catalyst in pure water, pH = 3.5–11.0, effect of scavengers, Cl^-, NO_3^-, SO_4^{2-}, and HCO_3^-, 0–45 °C, 10 min	94% degradation and 88% mineralization for 50 mg L^{-1} herbicide, 200 mg L^{-1} PMS, 50 mg L^{-1} catalyst, and pH = 11.0 at 25 °C. Oxidants: $^1O_2$ > $O_2^{\bullet-}$ > $SO_4^{\bullet-}$ > $^{\bullet}OH$. Decomposition: SO_4^{2-} < NO_3^- < Cl^- < HCO_3^-. 2 heteroaliphatic by-products detected by LC-MS	[141]
Glyphosate	Stirred tank reactor with $NiCo_2S_4$/Co_9S_8/NiS	100 mL of 0.1–1.0 mM herbicide, 1.5–4.5 mM PMS, and 150–300 mg L^{-1} catalyst in pure water, pH = 3.0–11.0, effect of scavengers, Cl^-, NO_3^-, SO_4^{2-}, and CO_3^{2-}, 15–45 °C, 55 min	82% degradation and 46% TOC removal for 0.1 mM herbicide, 3.5 mM PMS, and 200 mg L^{-1} catalyst at pH = 3.9 and 28 °C, with k_1 = 0.035 min^{-1}. E_a = 38.7 kJ mol^{-1}. Oxidants: $^{\bullet}OH$ (main), $SO_4^{\bullet-}$, $O_2^{\bullet-}$, and $^1O_2$. Decomposition: SO_4^{2-} < NO_3^- < HCO_3^- < Cl^-. Good reusability after 4 successive steps. 8 heteroaliphatic by-products and 2 carboxylic acids identified by LC-MS	[142]
Metolachlor	Conical flask on a rotary shaker with $CoFe_2O_4$ NPs[a]/N-biochar	50 mL of 10 mg L^{-1} herbicide, 0.1–3.0 mM PMS, and 200 mg L^{-1} catalyst in pure water, river water, groundwater, and wastewater, pH = 3.0–11.0, effect of scavengers, 28 °C, 40 min	In pure water, total degradation with 0.5 mM PMS and 200 mg L^{-1} catalyst at optimum pH = 9.0, with k_1 = 0.10 min^{-1}. Oxidants: $SO_4^{\bullet-}$ (main), $^{\bullet}OH$, and $^1O_2$. Degradation: pure water > river water > groundwater > wastewater. 11 aromatic derivatives detected by LC-MS	[145]
Pentachlorophenol	Quartz cuvette under stirring with CoS/rGO[c]	Suspensions with 0.4 mM herbicide, 0.01–0.3 mM PMS, and 500 mg L^{-1} catalyst, pH = 3.0–10.0, effect of scavengers, Cl^-, SO_4^{2-}, CO_3^{2-}, $H_2PO_4^-$, and humic acid, 25 °C, 10 min	Overall herbicide abatement and 89% mineralization with 0.05 mM PMS and 250 mg L^{-1} catalyst at pH= 6.4, with k_1 = 0.405 min^{-1}. $SO_4^{\bullet-}$ and $^{\bullet}OH$ as oxidants. Inhibitory effect of all the species added. Excellent reusability after 8 consecutive runs	[148]
2,4,6-Trichlorophenol	Stirred tank reactor with Fe_3S_4/humic acid	50 mL of 20 mg L^{-1} herbicide, 1.0 mM PMS, and 200 mg L^{-1} catalyst in pure water, pH = 3.0–11.0, effect of scavengers, 25 °C, 60 min	Total degradation at optimum pH = 5.3, with k_1 = 0.015 min^{-1}. $SO_4^{\bullet-}$ (dominant) and $^{\bullet}OH$ as oxidants. 5 aromatic intermediates found by LC-MS	[150]

[a] NPs: nanoparticles.
[b] LDOs: Layer double oxides.
[c] rGO: Reduced graphene oxide.

more catalyst to the suspensions by the larger production of oxidants, whereas Fig. 13b makes evident that the maximum k_1-value was achieved with 1.0 mM PMS. The slight decay in k_1 with raising PMS from 1.0 to 3.0 mM is indicative of a larger consumption of more amounts of oxidants by their parasitic reactions, as pointed out above. These parasitic reactions are more significant with MoS_4-Fe-LDH than previously using Co_3O_4/TiO_2 NPS because the k_1-values are one magnitude order-fold higher and hence, much more amount of $SO_4^{\bullet-}$ and $^{\bullet}OH$ are generated. Fig. 13c reveals a slight decrease in atrazine removal from pH 3.0–7.0, a greater decay at pH = 9.0, and a strong inhibition at pH = 11.0 (see Table 3). This can be explained from the pH of point zero-charge of the catalyst = 6.4. The negatively charged PMS is attracted by the positive surface in acidic medium, favoring the production of oxidants, whereas the repulsion of PMS at the negative surface in alkaline media, along with the formation of inactive SO_5^{2-} at pH > 9.4, inhibits their generation. The identification of the generated oxidants by EPR with the spectra characteristics of DMPO-$SO_4^{\bullet-}$ and DMPO-$^{\bullet}OH$ recorded using 1.0 mM PMS and 0.15 g L^{-1} catalyst at pH = 3.0 are shown in Fig. 13d. Fig. 13e presents the change of the normalized herbicide content with time under the above conditions (control) and with a high 5 mM concentration of several common anions. As can be seen, the inhibitory effect of such anions decreased in the order; HCO_3^- > CO_3^{2-} > HPO_4^{2-} > Cl^- > NO_3^-. The presence of these anions alongside competitive organic pollutants like NOM explains that atrazine was more slowly removed in the order: pure water > tap water > lake water > industrial wastewater, as shown in Fig. 13f.

Dicamba has been effectively degraded with PMS/hydrochar-montmorillonite [135]. Total herbicide abatement was found for suspensions with 10 mg L^{-1} herbicide, 2.0 mM PMS, and 3.0 g L^{-1} catalyst in pure water at pH = 2.52 (see Table 2). $SO_4^{\bullet-}$ (main), $^{\bullet}OH$, and $O_2^{\bullet-}$ were detected as oxidants by scavengers. The presence of inhibitors in real waters caused a drop of dicamba removal in well water, at larger extent than lake water. Intermediates were identified by LC-MS.

Jaafarzadeh et al. [136] presented an interesting work dealing with

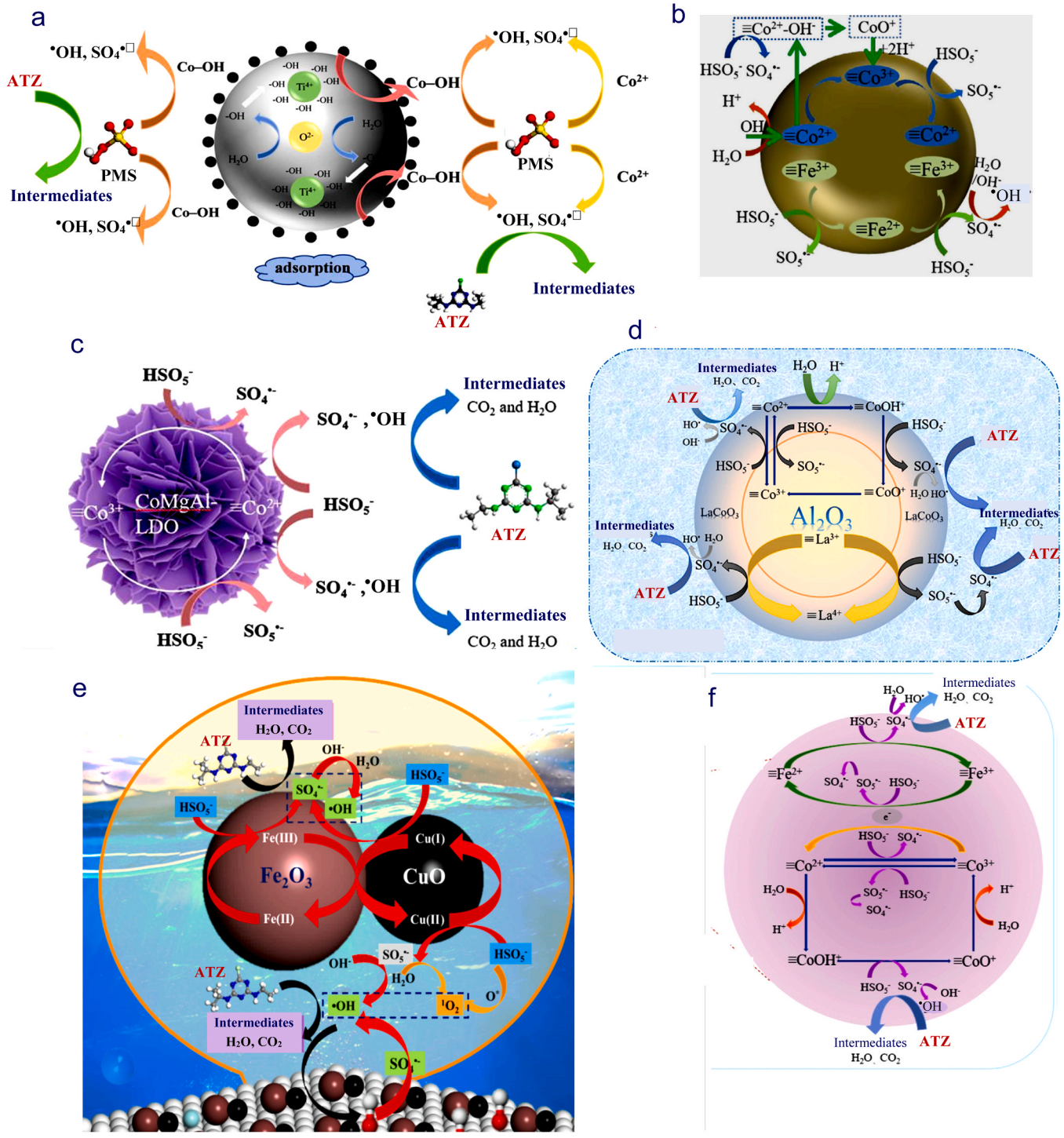

Fig. 11. Mechanisms proposed for the generation of $SO4^{\bullet-}$- and $^{\bullet}OH$ oxidants from PMSunder catalytic activation to remove atrazine (ATZ). Catalyst: (a) Co3O4/TiO2NPs (adapted from ref. [114]),(b) CoFe2O4 NPs (adapted from ref. [108]), (c) CoMgAl-LDOs(adapted from ref. [109]), (d)LaCoO3/Al2O3 (adapted from ref. [112]), (e) CuO-Fe2O3/5%MXene (adapted from ref. [123]), and (f) LaFe0.9Co0.1O3 (adapted fromref. [129]).

the treatment of 200 mL of 2,4-D suspensions with PMS activated with $CuFe_2O_4$ NPs/O_3. Fig. 14a shows the generation of $SO_4^{\bullet-}$ (with $^{\bullet}OH$) and $SO_5^{\bullet-}$ by the surface $\equiv Fe^{3+}/\equiv Fe^{2+}$ and $\equiv Cu^{3+}/\equiv Cu^{2+}$ pairs, which was enhanced by the production of $SO_4^{\bullet-}$, $^{\bullet}OH$, $O_2^{\bullet-}$, and $^1O_2$ upon the catalytic action of O_3. Fig. 14b depicts the percentage of 2,4-degradation achieved after 60 min of different treatments of 200 mL of 20 mg L^{-1} herbicide with 2.0 mM PMS and 16 mg L^{-1} O_3 at pH = 6.0 and 25 °C using a sealed flask on a shaker. Overall herbicide removal was attained in the presence of 0.20 g L^{-1} catalyst (see also Table 3) in front of 44% degradation achieved by PMS/O_3, confirming the positive role of the active sites of the catalyst. The low degradation improvement when adding 0.52 mg L^{-1} Fe^{3+} and 0.11 mg L^{-1} Cu^{2+} indicate the superior heterogeneous formation of oxidants with the surface $\equiv Fe^{3+}/\equiv Fe^{2+}$ and $\equiv Cu^{3+}/\equiv Cu^{2+}$ pairs of the catalyst. This trend was also verified for the percent of TOC and dechlorination removals shown in Fig. 14c, where greater values of 67% and 43% were obtained with the catalyst, respectively, because of its higher oxidation power. Higher contribution of $SO_4^{\bullet-}$ than $^{\bullet}OH$ as the stronger oxidant was determined with

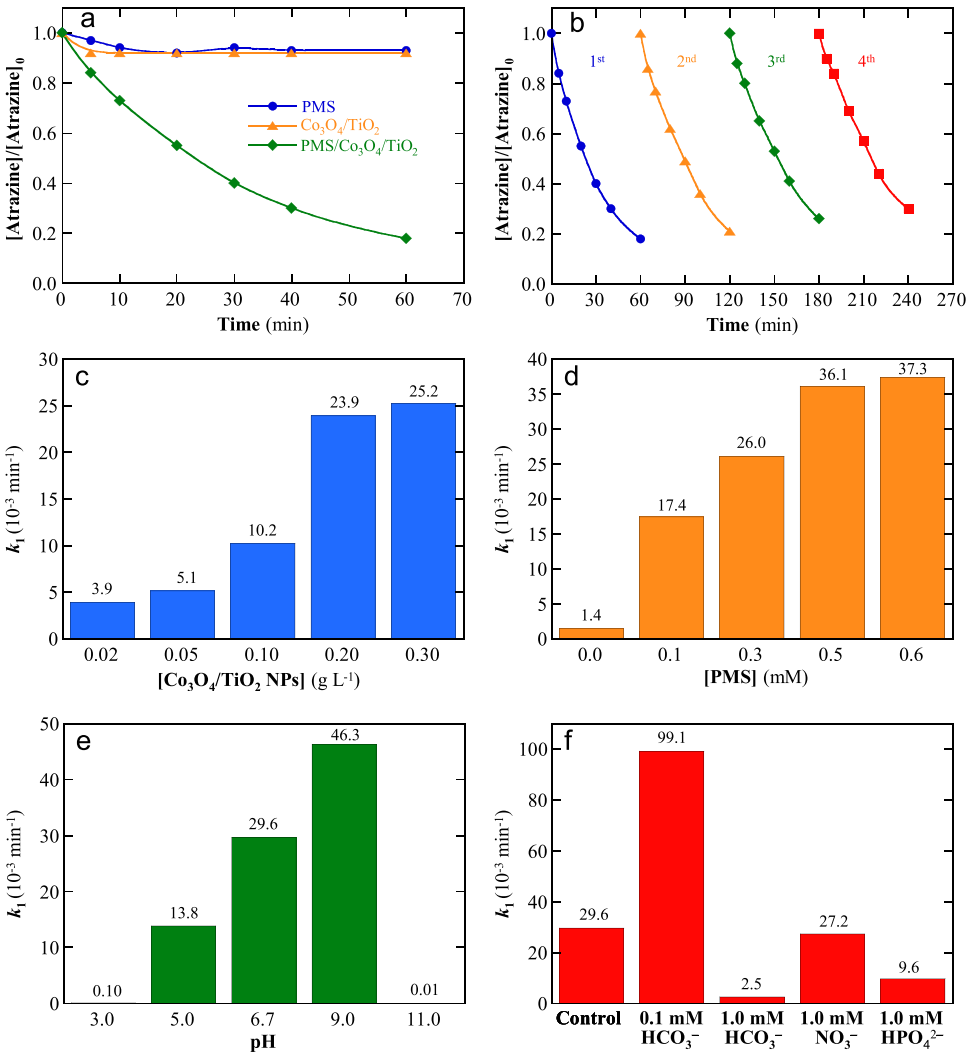

Fig. 12. (a) Change of normalized atrazine concentration with time upon application of PMS or Co_3O_4/TiO_2 NPs alone and their combination to 200 mL of 5 mg L^{-1} herbicide in pure water with a stirred tank reactor. Conditions: 0.3 mM PMS, 0.20 g L^{-1} catalyst, pH = 6.7, and 30 °C. (b) Time course of normalized herbicide content during four consecutive cycles of the above combined process. Influence over the pseudo-first-order rate constant for 5 mg L^{-1} atrazine removal of: (c) catalyst content for 0.3 mM PMS at pH = 6.7, (d) PMS content for 0.20 g L^{-1} catalyst at pH = 6.7, (e) pH for 0.3 mM PMS and 0.20 g L^{-1} catalyst, and (f) the addition of 0.1 mM HCO_3^- or 1.0 mM HCO_3^-, NO_3^-, or HPO_4^{2-} for 0.3 mM PMS and 0.20 g L^{-1} catalyst at pH = 6.7. Adapted from ref. [114].

scavengers. Fig. 14d highlights that the better $k_1 = 0.0949$ min^{-1} for the catalyzed process was attained at 25 °C, whereas k_1 dropped down to 0.091 min^{-1} at 45 °C. This negative effect can be ascribed to the concomitant volatilization of more O_3 at higher temperature, thus losing the ability of produce more oxidants. The authors confirmed the inhibition of the percent of 2,4-D degradation in the presence of anions such as Cl^-, NO_3^-, NO_2^-, SO_4^{2-}, and HCO_3^-, and this justified the decay of this parameter in different aqueous matrices in the sequence: pure water > tap water > river water > agriculture water > WWTP effluent, presented in Fig. 14e.

Zuo et al. [138] showed the great ability of B-$NiFe_2O_x$ compared to that of $NiFe_2O_4$ to activate PMS for 2,4-D degradation. The former catalyst allowed that PMS mainly yielded $SO_4^{\bullet-}$ that predominated over $^{\bullet}OH$ and $O_2^{\bullet-}$. In only 15 min, overall removal of 0.5 mg L^{-1} herbicide was reached in 250 mL of suspensions with 80 mg L^{-1} PMS, and 50 mg L^{-1} B-$NiFe_2O$ at optimum pH = 7.0 with $k_1 = 0.215$ min^{-1} (see Table 3). From the 20 aromatic intermediates and 3 carboxylic acids identified by LC-MS, they proposed the reaction sequence for 2,4-D mineralization shown in Fig. 15. It is initiated by 4 pathways involving decarboxylation/hydroxylation, deacetylation, dechlorination/hydroxylation, and dechlorination of the target molecule producing 2,4-dichlorophenoxyethanol, 2,4-dichlorophenol, 2-chloro.4. hydroxyphenoxyacetic acid, and 2-chlorophenoxyacetic acid, respectively. These compounds evolve to the other 16 aromatics detected and the cleavage of their benzenic moieties leads to the short-linear succinic acid, which is subsequently oxidized to the ultimate oxalic and formic acids that are directly transformed into CO_2.

Several works have described the destruction of the organophosphorus glyphosate by PMS activation with several catalysts [140–142]. Using the composite $NiCo_2S_4/Co_9S_8$/NiS [142], 82% degradation with $k_1 = 0.035$ min^{-1} and 46% TOC removal were obtained after 55 min of treatment of 100 mL of 0.1 mM herbicide in pure water with 3.5 mM PMS and 200 mg L^{-1} of such catalyst at pH = 3.9 and 28 °C using a stirred tank reactor (see Table 3). A good reusability of the catalyst was found after 4 successive steps, pointing to its application in practice. The study carried out between 15 and 45 °C allowed determining a low E_a = 38.7 kJ mol^{-1} and the use of scavengers revealed a surprising behavior since the main oxidant was $^{\bullet}OH$, being $SO_4^{\bullet-}$, $O_2^{\bullet-}$, and $^1O_2$ present at less extent. Fig. 16a schematizes the generation of these oxidants by the charge transfer between the surface $\equiv Co^{2+}$ and $\equiv Ni^{2+}$ of the catalyst and PMS. The formation of $O_2^{\bullet-}$ and $^1O_2$ was confirmed by the EPR spectra with DMPO (see Fig. 16b) and TEMP (see Fig. 16c), respectively. From the LC-MS analysis of the treated suspensions, 8 heteroaliphatic by-products and 2 carboxylic acids were identified by LC-MS. The proposed reaction sequence for glyphosate mineralization of Fig. 16d shows the evolution of the compounds with the 4 oxidizing agents, releasing the heteroatoms as H_3PO_4, NH_4^+, and NO_3^-.

The PMS activation with solid catalysts has been analyzed for other herbicides like metolachlor [145], pentachlorophenol [148], and 2,4,6-trichlorophenol [150]. In all cases, optimum conditions were determined for achieving their total removal with a major contribution of oxidant $SO_4^{\bullet-}$ over $^{\bullet}OH$ (see Table 3). A good reusability was only

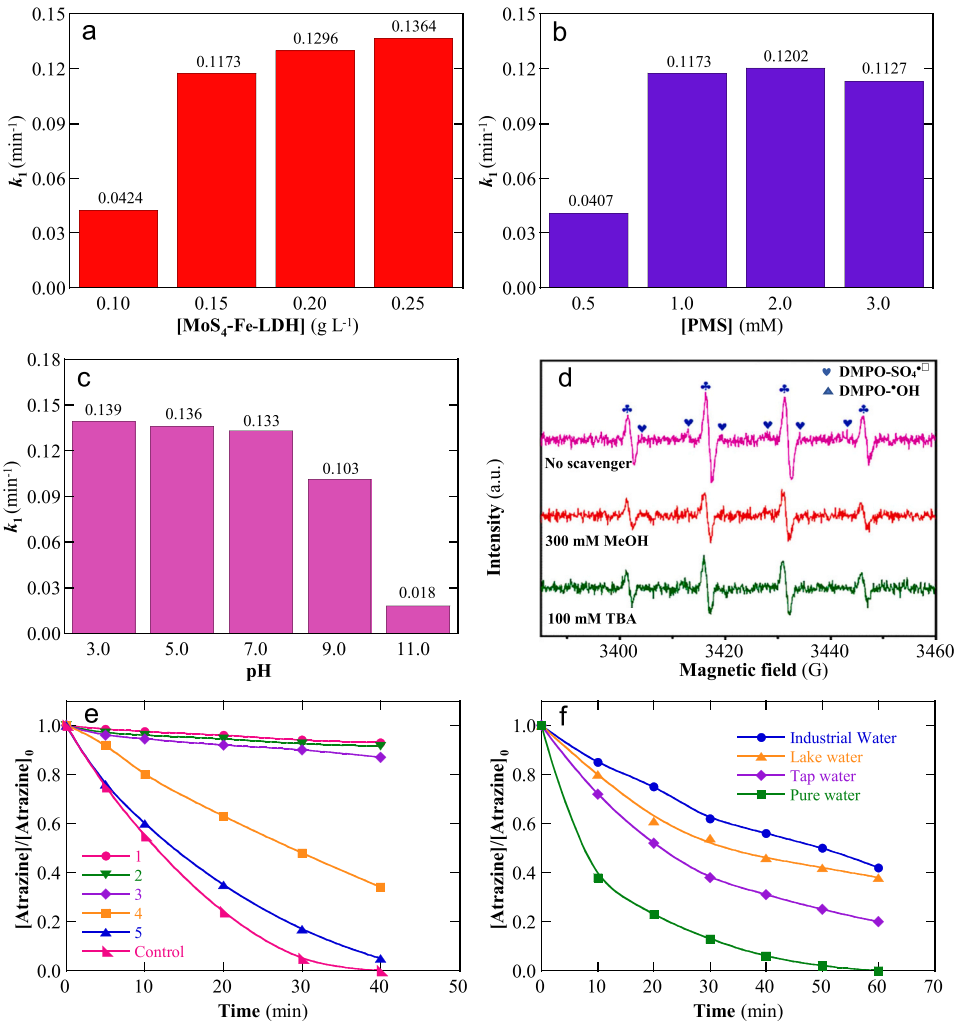

Fig. 13. Degradation of 30 mL of 10 mg L^{-1} atrazine by 0.5–3.0 mM PMS activated with 0.10–0.25 g L^{-1} MoS_4-Fe-LDH catalyst in pure water at pH = 3.0–11.0 and 30 °C with a stirred tank reactor. Effect of: (a) catalyst concentration, (b) PMS concentration, and (c) pH on the pseudo-first-order rate constant for herbicide removal. (d) EPR spectra of DMPO-$SO_4^{\bullet-}$ and DMPO-$^{\bullet}$OH obtained for 1.0 mM PMS and 0.15 g L^{-1} catalyst at pH = 3.0 in the absence and presence of scavengers. (e) Time course of normalized herbicide removal under the latter conditions with addition of 5 mM of; (1) HCO_3^-, (2) CO_3^{2-}, (3) HPO_4^{2-}, (4) Cl^-, and (5) NO_3^-. (f) Effect of the aqueous matrix over the normalized atrazine content decay using 1.0 mM PMS and 0.15 g L^{-1} catalyst at pH = 7.0. Adapted from ref. [128].

described for CoS/reduced graphene oxide (rGO) when treating 0.4 mM pentachlorophenol in pure water with 0.05 mM PMS and 250 mg L^{-1} catalyst at pH= 6.4 and 25 °C in only 10 min. A high k_1 = 0.405 min^{-1} was obtained with a fast TOC decay of 89% at this time, demonstrating the high power of the catalyst for PMS activation. Most of these works were completed by identifying the by-products formed by LC-MS.

On the other hand, the treatment of atrazine solutions with PMS activated with ion ions has been reported [152–155]. Li et al. [155] used *p*-benzoquinone to enhance the Fe^{2+} regeneration from added Fe^{3+} accelerating its reaction with PMS to be converted into $SO_4^{\bullet-}$ and $^{\bullet}$OH to promote atrazine removal. The mechanism for this system is similar to that explained for Fig. 3a, but using PMS instead of PS. For 50 mL of 0.050 mM herbicide in pure water with 0.25 mM PMS and 0.20 mM Fe^{3+} at 30 °C filling a plastic centrifuge tube with a water bath shaker at 150 rpm, atrazine was completely degraded in 20 min in the presence of 0.50 mM *p*-benzoquinone, whereas at that time without this compound, only a 10% of the herbicide was removed. This demonstrated the effectiveness of the hydroquinone/*p*-benzoquinone redox pair to enhance the Fe^{3+}/Fe^{2+} one. Nevertheless, a 60% of the initial *p*-benzoquinone content remained in the solution, which represents a drawback for the process because the solutions contained higher amount of organic matter that is more hardly removed and mineralized.

The PMS/Fe system was also applied for the treatment of atrazine suspensions [156–159]. Li et al. [158] prepared Fe-15%carbon composites from water treatment residuals and well-proven the Fe oxidation to Fe^{2+} to transform PMS into $SO_4^{\bullet-}$ and $^{\bullet}$OH. The degradation process was slow because 120 min were needed to remove a 92% of 0.050 mM herbicide under the optimum conditions of 0.25 mM PMS, 0.06 g L^{-1} Fe-15% C, and initial pH 3.58. To improve the treatment, *p*-benzoquinone was also added to accelerate atrazine abatement from Fe^{2+} regeneration by Fe^{3+} reduction. The presence of 0.25–0.50 mM of *p*-benzoquinone in the above system led to overall degradation in a short time of 20 min

4.2. Photocatalytic activation

Like in the case of catalytic activation, atrazine degradation has been the most widely studied by PMS activated by photocatalysis. Photocatalysts such as activated carbon/graphitic carbon nitride [160], Bi_2MoO_6 [161,162], Co_3O_4/g-C_3N_4 [163], MIL-53(Fe/Co)/CeO_2 [164], PDI/g-C_3N_4/TiO/Ti_3C_2 [165], TiO_2/$LaFeO_3$ [166], C_3N_5/C_3N_4 [167], TiO_{2-x}/g-C_3N_4/CNFe [168], and S-BUC-21(Fe) [169] have been recently checked for this purpose. The removal of monuron with N-TiO_2 [170] and other herbicides with TiO_2/$LaCoO_3$ [171] has been reported as well. Table 4 summarizes relevant results of these works remarking the nature and power of the light irradiated.

Most photocatalysts were photoexcited with expensive visible artificial lamps aiming to profit the free and renewable sunlight. The use of solar irradiation should then be checked in the next future to explore this procedure. Shen et al. [161] reported the treatment of 150 mL suspensions of atrazine with Bi_2MoO_6 nanosheets using a stirred tank reactor illuminated with an external 300 W Xe lamp with a cut-off emitting $\lambda \geq 415$ nm. Overall abatement of 2.5 mg L^{-1} herbicide with 0.8 mM PMS and 0.6 g L^{-1} photocatalyst at optimum pH = 9.0 was obtained in

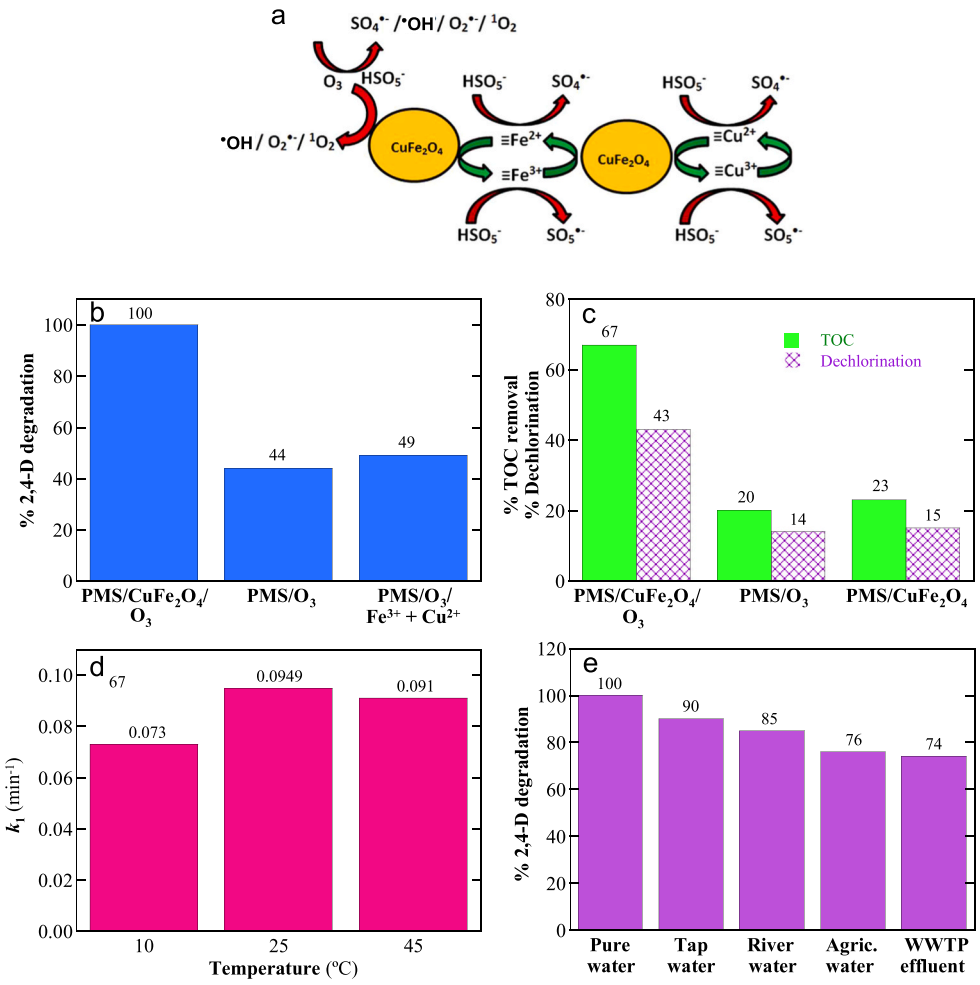

Fig. 14. (a) Proposed generation of oxidants in the PMS/$CuFe_2O_4$ NPs/O_3 system. (b) Percentage of 2,4-D degradation obtained after 60 min of different treatments of 200 mL of 20 mg L^{-1} herbicide at pH = 6.0 and 25 °C using a sealed flask on a shaker. Conditions: 2.0 mM PMS, 0.20 g L^{-1} catalyst, 16 mg L^{-1} O_3, 0.52 mg L^{-1} Fe^{3+}, and 0.11 mg L^{-1} Cu^{2+}. (c) Percentage of TOC removal and dichlorination found for several systems under the above conditions. (d) Effect of temperature on the pseudo-first-order rate constant of 2,4-D degradation for the PMS/$CuFe_2O_4$ NPs/O_3 process. (e) Influence of the aqueous matrix on the percent of herbicide degradation upon the same conditions. Adapted from ref. [136].

60 min. $SO_4^{\bullet-}$, $^{\bullet}OH$, and $O_2^{\bullet-}$ were detected as oxidants and an excellent reusability of the catalyst was found after 5 consecutive cycles (see Table 4), To enhance the oxidation power of the system, the same authors investigated the behavior of Bi_2MoO_6 powders and Fe^{3+} as co-catalysts [162]. The schematic illustration of the mechanism proposed for the generation of the above oxidants is presented in Fig. 17a. The oxidation of H_2O/OH^- by the holes at the VB of the catalyst originates $^{\bullet}OH$ from reactions (24) and (25), whereas the e^-_{CB} at the CB reduced the O_2 to $O_2^{\bullet-}$ from reaction (26) as well as the PMS to $SO_4^{\bullet-}$ and $^{\bullet}OH$. In the reaction medium, Fe^{2+} can be produced from the photolysis of $Fe(OH)^{2+}$ by the photo-Fenton reaction (21). Fe^{2+} then reacts with PMS to yield $SO_4^{\bullet-}$ alongside $^{\bullet}OH$ that can dimerize to H_2O_2. Finally, all the generated oxidants attack atrazine and its by-products. Fig. 17b highlights the superiority of the PMS/Bi_2MoO_6/Fe^{3+}/Vis process over simpler arrangements, yielding total herbicide abatement after 20 min of treating 150 mL of 2.5 mg L^{-1} herbicide in pure water with 0.8 mM PMS, 0.6 g L^{-1} photocatalyst, and 2.0 mg L^{-1} Fe^{3+} at pH 3.0 and 25 °C (see also Table 4). The coupling of Fe^{3+} catalyst largely enhanced the oxidation power of the PMS/Bi_2MoO_6/Vis considered in [161]. Fig. 17c reveals that less Fe^{2+} content is accumulated in the medium in the presence of PMS, as expected by its consumption by that oxidant. The effect of 5 mg L^{-1} of anions and 10 mg L^{-1} of humic acid on the change of normalized atrazine content with time for the above test is shown in Fig. 17d. The process was accelerated with this low Cl^- concentration, which was ascribeded to the deceleration of the recombination of the photogenerated e^-_{CB}/h^+_{VB} pair by the interaction of h^+_{VB} with the anion and the extra generation of the oxidant active chlorine (HClO) from Cl^- oxidation by PMS. It can also be observed a slower acceleration with humic acid because it is a natural photosensitizer that transfers electrons to the VB of Bi_2MoO_6, enhancing the production of oxidizing agents. In contrast, the presence of NO_3^- only showed a little influence because of its low reactivity with $SO_4^{\bullet-}$ and $^{\bullet}OH$, whereas CO_3^{2-} strongly inhibited the process due to its quick reaction with such radicals. This can explain Fig. 17e where the typical inhibition of the process from pure water using tap water < river water is shown, since it can be ascribed to the increasing presence of carbonate ion in these natural waters.

Good degradations can be observed in Table 4 for atrazine with PMS activated with other photocatalysts under visible light, with similar characteristics to those described above. Co_3O_4/g-C_3N_4 and TiO_2/$LaFeO_3$ were very stable with a good reusability during consecutive oxidation cycles [163,166]. When an UVA LED light of λ = 365 nm was applied to irradiate a metal organic framework (MOF) like S-BUC-21 (Fe) particles in a stirred tank reactor [169], a rapid and complete destruction of 10 mg L^{-1} herbicide in pure water with 0.4 mM PMS and 300 mg L^{-1} at pH = 5.6 in 20 min was obtained with a very high k_1 = 0.521 min^{-1} (see Table 4). Under these conditions, it was determined the pre-eminence of $SO_4^{\bullet-}$ and $^1O_2$ as oxidants, with smaller participation of $^{\bullet}OH$ and $O_2^{\bullet-}$, and an excellent reusability after 5 consecutive runs. The performance of this MOF photocatalyst was then much better than those reported in other works with photocatalysts under visible light, pointing to its development in the next future.

Abdelhaleem and Chu [170] presented a study on the degradation of the phenylurea monuron in a stirred tank reactor with a non-metallic photocatalyst like N-TiO_2 submitted to a visible LED light with λ = 420–700 nm. A suspension of 100 mL with 5 μM herbicide was treated with 2 mM PMS and 3.0 g L^{-1} of photocatalyst at optimum pH

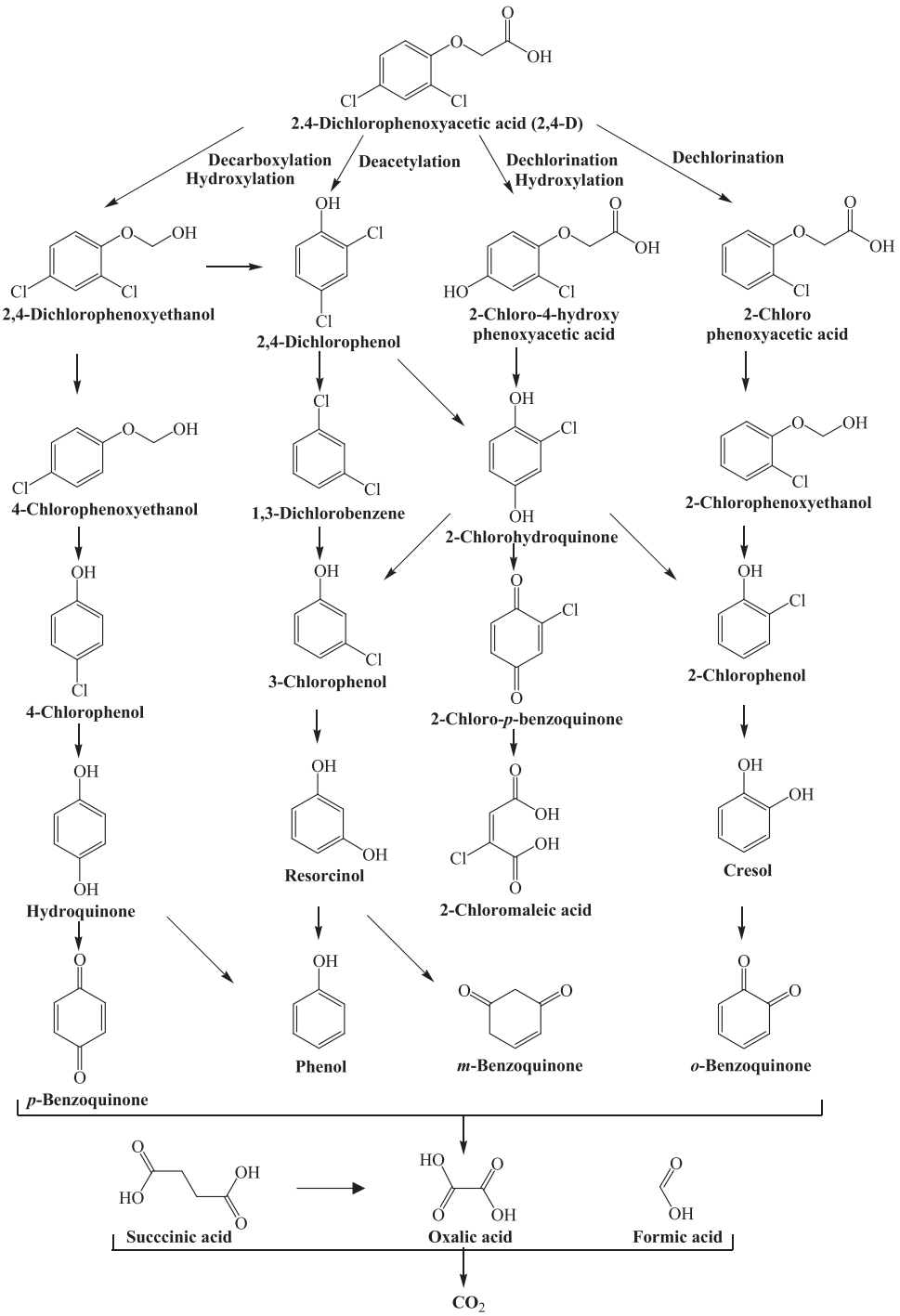

Fig. 15. Reaction sequence proposed for the mineralization of 2,4-D with $SO_4^{\bullet-}$ and $^{\bullet}OH$ oxidizing radicals. Adapted from ref. [138].

= 10.9 and the herbicide wa scompletely degraded in 30 min with k_1 = 0.075 min^{-1} (see Table 4). In contrast the system was unable to rapidly mineralize the herbicide and only 80% of TOC reduction was attained with 12 mM PMS in 720 min. Formation of the predominant oxidant $SO_4^{\bullet-}$ along with $^{\bullet}OH$ was detected with scavengers and surprisingly, no apparent influence of NO_3^-, SO_4^{2-}, and HCO_3^- was found, but with inhibition with Cl^- and $H_2PO_4^-$. The low effect of HCO_3^- suggests its interaction with the holes of the photocatalyst increasing the process efficiency by decelerating the recombination of the $e_{CB}^-//h_{VB}^+$ pair from reaction (29) that compensates its consumption of oxidants. Moreover, 20 aromatic by-products were detected by LC-MS.

4.3. Other activation processes

Few papers [172–175] have focused the degradation of herbicides with PMS activated by different procedures to those described above with catalytic and photocatalytic treatments (see Fig. 1d). Yin et al. [172] explored the effective degradation of pentachlorophenol with a PMS/heat system in a stirred tank reactor with a thermostatic water bath. Faster degradation of 5 μM herbicide was obtained by increasing the PMS dose up to 0.4 mM, the temperature from 25 to 60 ºC, and the pH from 3.0 and 9.0. Total abatement was found operating with the above maximum parameters during 60 min. A high E_a = 105.60 kJ mol^{-1} was determined for pentachlorophenol degradation.

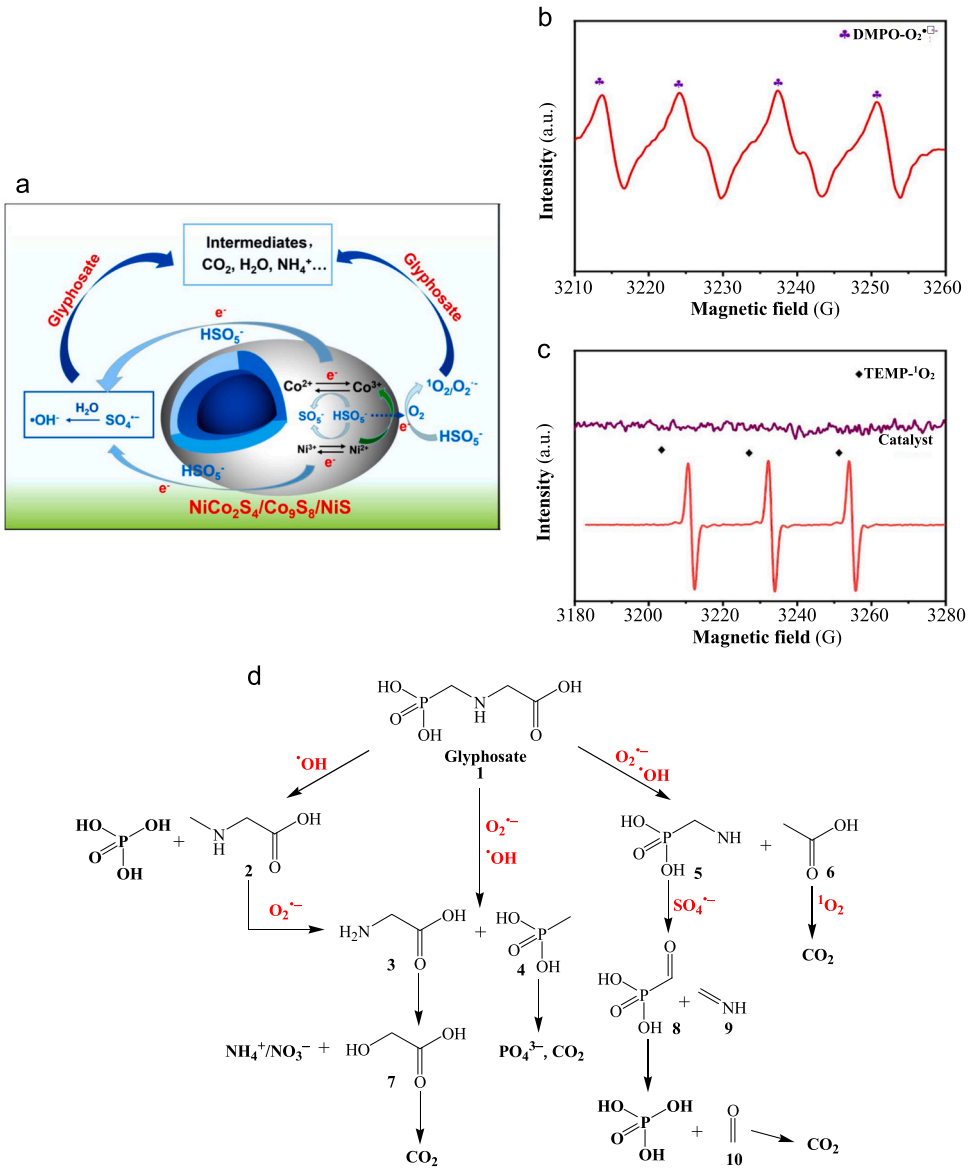

Fig. 16. (a) Mechanism proposed for the production of oxidizing species during the treatment of 100 mL of 0.1 mM glyphosate, 3.5 mM PMS, and 200 mg L^{-1} $NiCo_2S_4/Co_9S_8/NiS$ catalyst in pure water at pH = 3.9 and 28 °C using a stirred tank reactor. EPR spectra of: (b) $O_2^{\bullet-}$ and (c) $^1O_2$ captured by DMPO and TEMP, respectively. (d) Reaction sequence proposed for the mineralization of glyphosate by activated PMS. Adapted from ref. [142].

As expected, TOC was reduced more slowly by 61% in 120 min. The use of scavengers and EPR analysis showed the predominance of $SO_4^{\bullet-}$ as oxidant with smaller contribution of $^{\bullet}OH$. A total of 10 by-products was identified by LC-MS.

Herbicides like alachlor, atrazine, and simazine have been degraded in a secondary WWTP effluent by PMS/UVA [174]. The experiments were performed with 1 L of the effluent of pH 7.6 spiked with 100 μg L^{-1} of each herbicide with 0.10 mM PMS illuminated with 4 UVA LED lamps (λ_{max} = 385 nm) providing 390 W m^{-2} irradiation. After 60 min of treatment, good abatements of 74% for alachlor, 62% for atrazine, and 76% for simazine were found, whereas the application of UVA alone yielded a smaller degradation of 10%, 36%, and 12%. Atrazine was the herbicide more photoactive, but the more slowly attacked with $SO_4^{\bullet-}$ and $^{\bullet}OH$ formed from PMS photoactivation.

5. Comparative treatment with persulfate and peroxymonosulfate

The comparative treatment of herbicides with activated PS and PMS has been assessed in several articles, and in some cases, with additional comparison with AOPs based in the decomposition of H_2O_2 to $^{\bullet}OH$. Activation has been made with iron ions for atrazine [176] and 2,4-D [177]. nZVI/biochar for atrazine [178], catalysis for 2,4-D with nano--Fe_2O_3 [179] and atrazine with Co(II) [180], UV for alachor [181], ametryn [182], atrazine [183,184], and tebuthiuron [185], UV with Fe^{2+} for desethyl-atrazine (DEA) and desisopropyl-atrazine (DIA) [186], photocatalysis for atrazine [187], and electrolysis for pentachlorophenol [188].

It is remarkable the work of Diao et al. [178] who suspended 10 g of 23.6 mg atrazine kg^{-1} of contaminated soil in 200 mL of pure water with 2.0 g L^{-1} of nZVI/biochar and 4.0 mM PMS, PS, or H_2O_2 at pH = 6.93. After 240 min of these treatments, 96%, 74%, and 31% of the herbicide were removed with k_1-values of 0.0121, 0.0054, and 0.0016 min^{-1}, respectively. The mineralization process followed the same trend, attaining values of 48%, 41%, and 15%. The low activity of H_2O_2 was related to the fact that it inhibits the active centers of the nZVI/biochar catalyst probably because the generated $^{\bullet}OH$ corrodes its surface. In contrast, the catalyst activated PMS at larger extent than PS

Table 4
Selected results found for herbicides removal by photocatalytic activation of peroxymonosulfate.

Herbicide	System	Experimental remarks	Best results	Ref.
Atrazine	Stirred tank reactor with Bi_2MoO_6 nanosheets upon external 300 W Xe lamp (cut-off emitting $\lambda \geq 415$ nm)	150 mL of 1.25–10 mg L^{-1} herbicide, 0.2–0.8 mM PMS, and 0–1.0 g L^{-1} photocatalyst in pure water, pH = 3.0–11–0, effect of scavengers, Cl^-, NO_3^-, CO_3^{2-}, and humic acid, 25 °C, 60 min	Total removal for 2.5 mg L^{-1} herbicide, 0.8 mM PMS, and 0.6 g L^{-1} photocatalyst at optimum pH = 9.0. Oxidants: $SO_4^{\bullet-}$,$^{\bullet}OH$, and $O_2^{\bullet-}$. Greater decontamination with Cl^-, little effect of NO_3^- and humic acid,' large inhibition with CO_3^{2-}. Excellent reusability after 5 successive cycles. 8 heteroaromatic derivatives identified by LC-MS/MS	[161]
Atrazine	Stirred tank reactor with Fe^{3+} and Bi_2MoO_6 powder upon external 300 W Xe lamp (cut-off emitting $\lambda \geq 415$ nm)	150 mL of 1.25–10 mg L^{-1} herbicide, 0–2.0 mM PMS, 0–1.0 g L^{-1} photocatalyst, and 0–6.0 mg L^{-1} Fe^{3+} in pure water, tap water, and river water, pH = 3.0 or free pH, effect of scavengers, Cl^-, NO_3^-, CO_3^{2-}, and humic acid, 25 °C, 20 min	In pure water, overall degradation for 2.5 mg L^{-1} herbicide, 0.8 mM PMS, 0.6 g L^{-1} photocatalyst, and 2.0 mg L^{-1} Fe^{3+} at optimum pH = 3.0, with k_1 = 0.213 min^{-1}. Oxidants: $SO_4^{\bullet-}$,$^{\bullet}OH$, and $O_2^{\bullet-}$. Greater decontamination with Cl^- and humic acid, little effect of NO_3^-,' large inhibition with CO_3^{2-}. Excellent reusability after 5 successive cycles. Degradation: pure water > tap water > river water	[162]
Atrazine	Stirred tank reactor with Co_3O_4/g-C_3N_4 upon external 300 W Xe lamp (cut-off emitting $\lambda \geq 400$ nm)	100 mL of 50 μM herbicide, 1.0 mM PMS, and 500 mg L^{-1} photocatalyst in pure water, pH = 7.0, effect of scavengers, Cl^-, NO_3^-, SO_4^{2-}, and CO_3^{2-}, 35 min	Complete degradation of the herbicide. Oxidants: $SO_4^{\bullet-}$ and$^{\bullet}OH$. Little effect of NO_3^- and SO_4^{2-}, slower removal with Cl^- and large inhibition with CO_3^{2-}. Co leaching and excellent reusability after 5 successive steps	[163]
Atrazine	Quartz tube with TiO_2/$LaFeO_3$ upon external 200 W LED light (λ = 410–760 nm)	50 mL of 2.5 mg L^{-1} herbicide, 0–0.4 mM PMS, and 0–500 mg L^{-1} photocatalyst in pure water, pH = 3.0–11.0, effect of scavengers, Cl^-, NO_3^-, HCO_3^-, and humic acid, 30 °C, 120 min	Total herbicide abatement in 90 min and 37% TOC reduction in 120 min with 0.3 mM PMS and 400 mg L^{-1} photocatalyst at pH = 7.0, with k_1 = 0.0296 min^{-1}. Oxidants: $SO_4^{\bullet-}$,$^{\bullet}OH$,$^1O_2$, and $O_2^{\bullet-}$. Small inhibition with Cl^-, NO_3^-, and humic acid, large inhibition with HCO_3^-. Excellent reusability after 7 cycles. 9 heteroaromatic derivatives found by LC-MS	[166]
Atrazine	Stirred tank reactor with C_3N_5/C_3N_4 upon external 300 W Xe lamp (cut-off emitting $\lambda \geq 420$ nm)	50 mL of 10 mg L^{-1} herbicide, 200 mg L^{-1} PMS, and 400 mg L^{-1} photocatalyst in pure water, pH = 3.0–11.0, effect of scavengers, Cl^-, NO_3^-, HCO_3^-, CO_3^{2-}, and humic acid, 60 min	97% degradation at pH = 3.0, with k_1 = 0.556 min^{-1}. Oxidants: $SO_4^{\bullet-}$,$^{\bullet}OH$,$^1O_2$, and holes. Acceleration with Cl^-, little effect with NO_3^-, CO_3^{2-}, and humic acid, large inhibition with HCO_3^-. 13 heteroaromatic by-products detected by LC-MS	[167]
Atrazine	Stirred tank reactor with S-BUC-21 (Fe) particles upon external 10 W UVA LED light (λ = 369 nm)	50 mL of 10 mg L^{-1} herbicide, 0.4 mM PMS, and 300 mg L^{-1} photocatalyst in pure water, pH = 3.5–9.5, effect of scavengers, 20 min	Overall herbicide decay at optimum pH = 5.56, with k_1 = 0.521 min^{-1}. Oxidants: pre-eminently $SO_4^{\bullet-}$ and$^1O_2$, smaller participation of$^{\bullet}OH$ and $O_2^{\bullet-}$. Excellent reusability after 5 consecutive runs.	[169]
Monuron	Stirred glass reactor with N-TiO_2 upon external visible LED light (λ = 420–700 nm)	100 mL of 5 μM herbicide, 0.25–12 mM PMS, and 0.2–3.0 g L^{-1} photocatalyst in pure water, pH = 2.5–11.6, effect of scavengers, Cl^-, NO_3^-, SO_4^{2-}, HCO_3^-, and $H_2PO_4^-$, 30 min	Total removal with 2 mM PMS and 3.0 g L^{-1} at optimum pH = 10.9, with k_1 = 0.075 min^{-1}. 80% TOC abatement with 12 mM PMS in 720 min. Oxidants: $SO_4^{\bullet-}$ (main) and$^{\bullet}OH$. No apparent influence of NO_3^-, SO_4^{2-}, and HCO_3^-, inhibition with Cl^- and $H_2PO_4^-$. 20 aromatic by-products detected by LC-MS	[170]

causing a higher production of $SO_4^{\bullet-}$ and $^{\bullet}OH$. A similar behavior has been described for the removal of 2,4-D with nano-Fe_2O_3 [179]. Suspensions of 200 mL of 20 mg L^{-1} of this herbicide in pure water were treated with 3.0 mM of each oxidant and 0.6 g L^{-1} of catalyst at pH = 6.0 and 25–27 °C using flasks shaken at 300 rpm. After 60 min, the percentage of 2,4-D removal was 80% for PMS, slightly higher than 76%

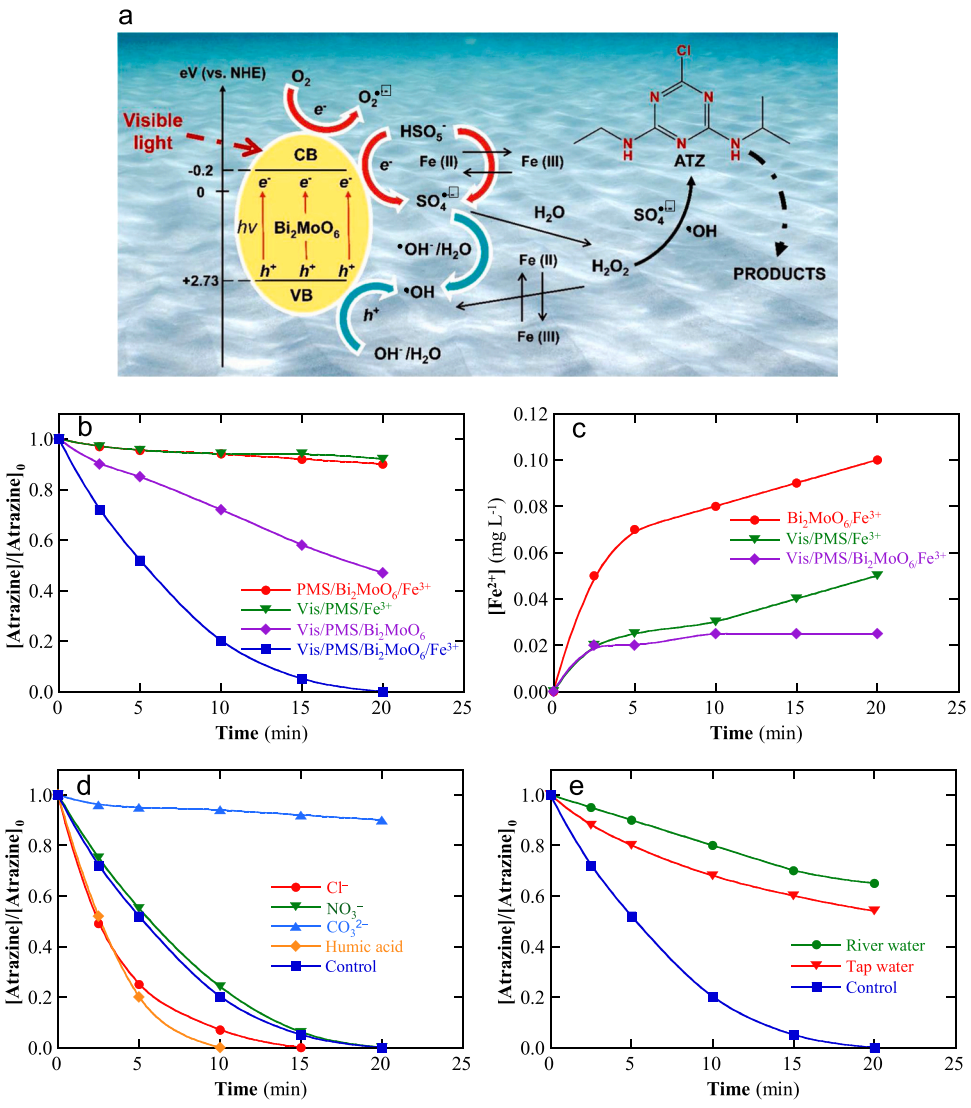

Fig. 17. (a) Proposed mechanism for the activation of PMS with Bi_2MoO_6 photocatalyst in the presence of soluble Fe^{3+}. (b) Variation of normalized atrazine concentration with time for different systems applied to the degradation of 150 mL of 2.5 mg L^{-1} herbicide, 0.8 mM PMS, 0.6 g L^{-1} photocatalyst, and 2.0 mg L^{-1} Fe^{3+} in pure water at pH 3.0 and 25 °C using a stirred tank reactor exposed to a 300 W Xe lamp (cut-off emitting at $\lambda \geq 415$ nm). (c) Evolution of generated Fe^{2+} in the above assays. (d) Influence of the addition of 5 mM of Cl^-, NO_3^-, or CO_3^{2-}, or 10 mg L^{-1} of humic acid, (e) Effect of the water matrix over the process. Adapted from ref. [162].

found for PS. However, only 42% of the herbicide was abated using H_2O_2, suggesting again an inhibition by corrosion of the catalyst surface.

Jazic et al. [181] explored the treatment of 100 μg L^{-1} alachlor spiked in surface water and groundwater with 0.30 mM of each oxidant at pH 3.0–9.5 filling a quartz stirred tank reactor with an inner 1.5 mW cm^{-2} UVC lamp at $\lambda = 253.7$ nm. For pH = 5.0, the pseudo-first-order rate constants for such real waters were 1.3×10^{-3} and 1.4×10^{-3} cm^2 J^{-1} for PMS/UVC < 1.7×10^{-3} and 1.6×10^{-3} cm^2 J^{-1} for UVC/H_2O_2 < 2.0×10^{-3} and 1.9×10^{-3} cm^2 J^{-1} for PS/UVC, respectively. Conversely, the two former processes were strongly decelerated at pH = 9.5, whereas the latter one was strongly improved giving apparent rate constants of 2.3×10^{-3} and 1.9×10^{-3} cm^2 J^{-1}. This phenomenon at pH = 9.5 can be explained by the fast conversion of $SO_4^{\bullet-}$ to $^{\bullet}OH$ that accelerates the PMS decomposition. The quicker degradation with surface water in front of groundwater is pre-eminently due to its low TOC content (3.14 vs. 6.88 mg L^{-1}) since the degradation of their organic components competed with that of alachlor. Other work of Gonçalves et al. [185] studied the behavior of 500 mL of 0.5 mg L^{-1} of the urea tebuthiuron in pure water with 0.050 mM of PS, PMS, or H_2O_2 at pH 6.8 filling a stirred amber glass photoreactor illuminated with a 16 W UVC light. Fig. 18a depicts that the photoactivity of the herbicide caused its reduction by 75% in 30 min. At that time, total degradation was achieved with UVC/H_2O_2, whereas a shorter time of 20 min was required for its complete disappearance at similar rate for PS/UVC and PMS/UVC. The quicker herbicide oxidation with PS and PMS led to their quicker consumption, as can be seen in Fig. 18b. The study was extended to a WWTP effluent spiked with 0.1 mg L^{-1} tebuthiuron and 2.206 mM of each oxidant at pH = 6.8. Fig. 18c highlights a small photolysis of the herbicide, only a 20% in 30 min, indicating that the irradiated light was mostly adsorbed by the organic components of the WWTP. A slower process was found for PMS/UVC as well, needing about 30 min for total herbicide abatement, whereas the UVC/H_2O_2 treatment was slightly quicker and the PS/UVC was strongly enhanced yielding overall degradation in only 15 min. The competitive attack of oxidants over the herbicide and the organics of the WWTP can justify the drop of its abatement by PMS/UVC. A slightly faster activation of H_2O_2, at larger extent by some photoexcited by-products in the WWTP, can account for by the acceleration observed for these oxidants. The nature of the oxidizing radicals was ascertained by adding scavengers like 2-`propanol (only react with $^{\bullet}OH$) and methoxybenzene (react with $SO_4^{\bullet-}$ and $^{\bullet}OH$) to the assays of Fig. 18a. From the results of Fig. 18d, one can infer that $^{\bullet}OH$ was formed with all oxidants, but at higher proportion with PMS than PS. $SO_4^{\bullet-}$ was then produced at larger extent with PS.

Khan et al. [186] presented a remarkable work dealing with the degradation of DEA and DIA, two derivatives of atrazine (see their chemical structure in Fig. 4). Firstly, the trials were carried out with 1.0 mg L^{-1} of each *s*-triazine in pure water at pH = 7.4 using a stirred tank photoreactor exposed to a 0.1 mW cm^{-2} UVC light. Fig. 19a and b

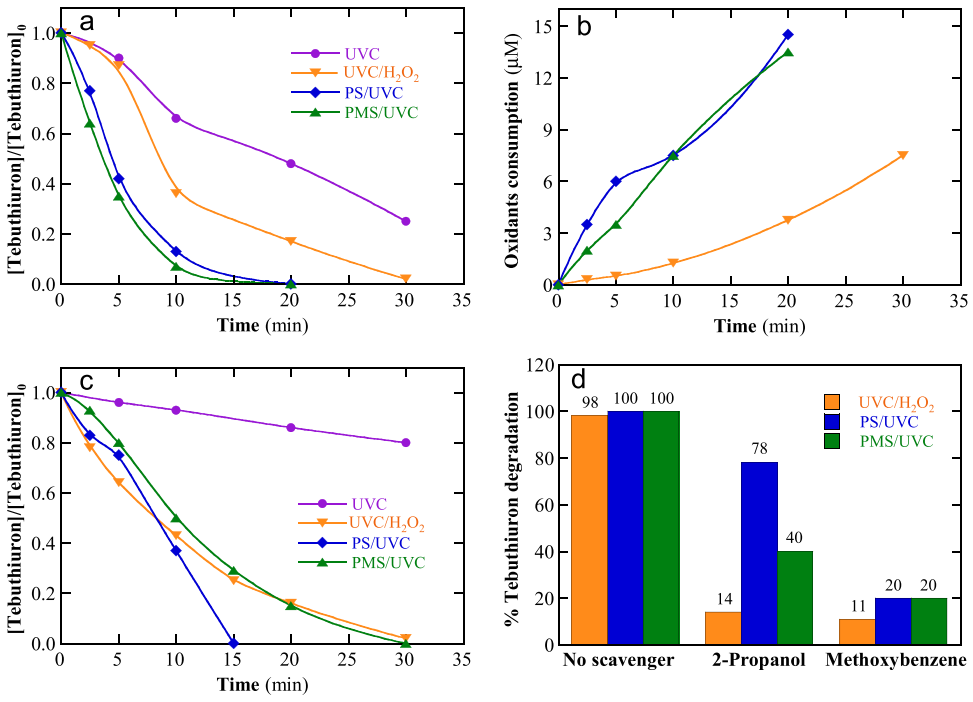

Fig. 18. (a) Normalized tebuthiuron concentration vs. time for the degradation of 500 mL of 0.5 mg L^{-1} of herbicide in pure water with 0.050 mM of H_2O_2, PS, or PMS at pH 6.8 using a stirred amber glass photoreactor illuminated with a 16 W UVC light. (b) Evolution of oxidants consumption upon the above conditions. (c) Change of normalized herbicide concentration with time in a WWTP effluent spiked with 0.1 mg L^{-1} tebuthiuron and 2.206 mM of each oxidant at pH = 6.8. (d) Effect of 10 mM of 2-propanol or methoxybenzene as scavengers after 30 min of the above trials. Adapted from ref. [185].

show the percentage of DEA and DIA degraded for different oxidant doses after consumption of 500 mJ cm^{-2} UVC fluence, respectively. In both cases, more herbicide was degraded in the sequence: PMS/UVC < UVC/H_2O_2 < PS/UVC, with higher removal with increasing the oxidant content due to the formation of greater quantity of oxidizing radicals. DIA was more quickly removed than DEA. Further study was centered to clarify the effect of adding 0.50 mg L^{-1} Fe^{2+} to both s-triazine solutions with low concentrations of 53.3 − 57.6 μM of each oxidant. The presence of Fe^{2+} accelerated all the processes, as shown in Fig. 19c and d. This was due to the following reasons; (i) the parallel generation of more oxidizing radicals from the activation of PS and PMS by Fe^{2+}, e.g., via reaction (15) and (ii) the production of more $^{\bullet}OH$ from photo-Fenton reaction (21) and the Fenton's reaction (36) between added and Fe^{2+} and H_2O_2 [2,5]. However, the two latter reactions are optimal at pH = 3.0, drastically decreasing their rate at pH = 7.4 where the processes were assessed. This explains the low enhancement of the percentage of DEA and DIA concentrations for UVC/H_2O_2/Fe^{2+} respect to UVC/H_2O_2 highlighted in Fig. 19c and d, respectively. The rise of the percent of each herbicide was determined with increasing the UVC fluence (with production of more oxidizing radicals) by PS/UVC for several aqueous matrices and in both cases, Fig. 19e and f disclose lesser herbicide decay in the order: pure water > tap water > WWTP effluent > lake water, according to the greater consumption of the oxidant with higher amounts of their anions and organic components, as pointed out above.

$$Fe^{2+} + H_2O_2 \rightarrow Fe^{3+} + {}^{\bullet}OH + OH^{-} \quad (36)$$

The above results make evident that there is not a general rule to know whether activated PS or PMS has higher oxidation power to remove herbicides. It depends not only of their reaction rate with the herbicides, but also of the experimental conditions tested, including the activation method used, the pH, and the aqueous matrix. The assessment of their behavior upon given conditions is needed to decide their better suitability for treatment. In general, the oxidation power of PS and PMS is superior to that H_2O_2, but in some specific cases, e.g., with UVC, the latter upgraded PMS.

6. Conclusions and prospects

It has been shown that the thermal, catalytic, UV, photocatalytic, and electrochemical activations of PS and PMS are very effective to remove herbicides in synthetic and real waters and wastewaters. Currently, the performance of these systems has been assessed with small reactors at laboratory scale based on an academic study but giving scarce information over their economic cost. Techno-economic studies are needed to be made to benchmark these technologies with other AOPs, particularly for analogous treatments with H_2O_2 that are usually compared. No knowledge enough of these processes has been developed yet for their feasible industrial application and this is a research challenge that requires a large attention in the next future. Pre-pilot flow plants should be at least considered for their subsequent scale up if the processes became viable. These flow plants should be automatized for an adequate control with injection of effluents and oxidants and well-designed with a good hydrodynamics to appropriately mix the above components and achieve the maximum efficiency by using good systems for the absorption of light irradiation or electrochemical cells if they are checked. The use of sunlight and alternative energetic sources should give an additional value of economic interest for their practical application.

For all the sulfate-based AOPs, it was found a higher percentage of herbicide decay with decreasing its concentration because the main generated $SO_4^{\bullet-}$ and $^{\bullet}OH$ oxidants can more rapidly remove lower amount of organic matter. Other operating parameters such as decreasing pH and increasing temperature, the PS or PMS dosage, the quantity of catalyst or photocatalyst, light intensity, and applied *I* or *j* depending on the activation procedure also accelerated the herbicide abatement due to the progressive production of more oxidizing agents. A pseudo-first-order decay of the herbicide was always found. A high number of papers have analyzed the effect of selected scavengers to elucidate the role of the oxidizing species generated. In general, $SO_4^{\bullet-}$ predominated in acidic and neutral conditions, being $^{\bullet}OH$ more significant in alkaline media. Other oxidizing agents as $O_2^{\bullet-}$ and $^1O_2$ were detected with several catalysts and pre-eminently by photocatalysts under the reduction of O_2 by the photogenerated e_{CB}^-. This was confirmed by their corresponding EPR spectra with DMPO or TEMP. Clear examples have been provided for the treatment of glyphosate with

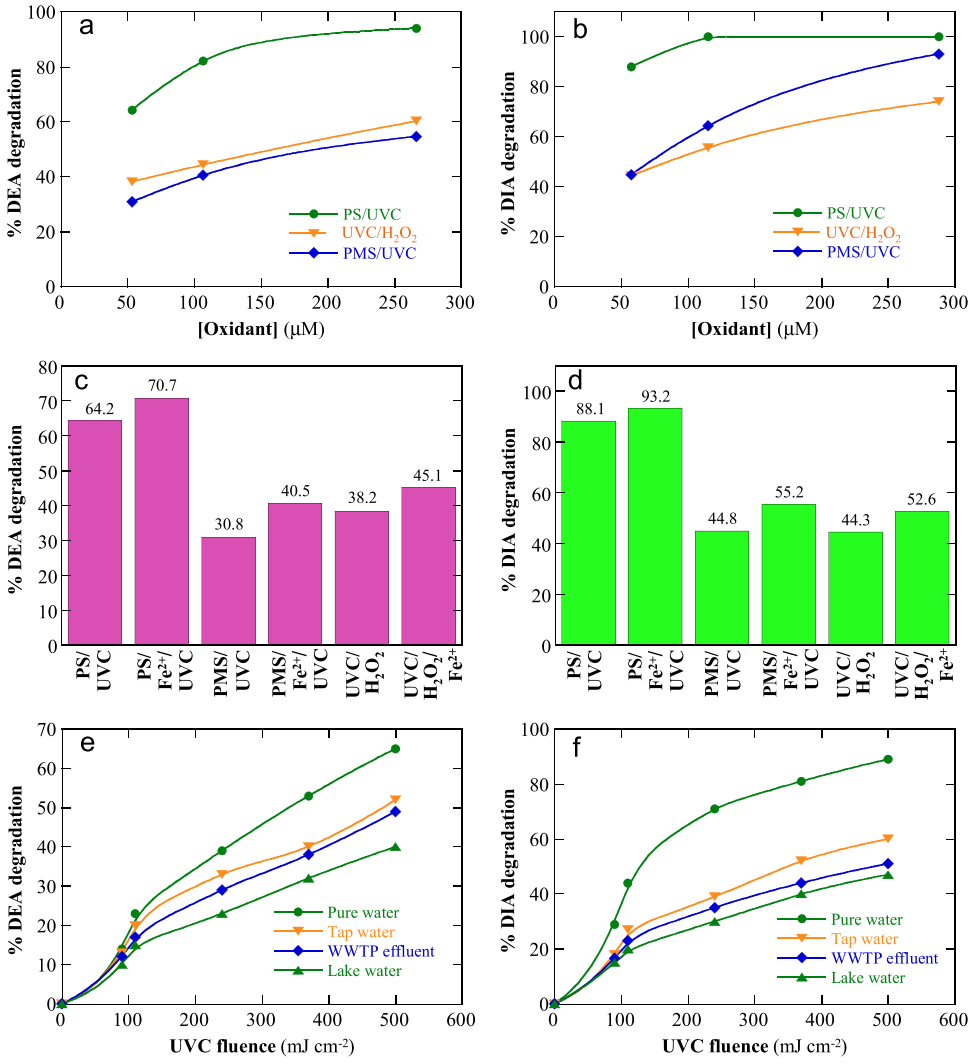

Fig. 19. Variation of the percent of (a) DEA and (b) DIA degradations with the concentration of PS, H_2O_2, or PMS as oxidant, activated by a 0.1 mW cm^{-2} UVC light ($\lambda = 254$ nm) using a stirred tank photoreactor. The assays were made with 1.0 mg L^{-1} of each s-triazine at pH = 7.4 and results are given after 500 mJ cm^{-2} of UVC fluence. Effect of 0.50 mg L^{-1} Fe^{2+} for the above (c) DEA and (d) DIA trials with 53.3–57.6 μM of each oxidant. Change of the percent of (e) DEA and (f) DIA degradation with the applied UVC fluence for the PS/UVC process of 1.0 mg L^{-1} of each pollutant with 53.3 and μM oxidant in pure water (pH = 7.4), tap water, WWTP effluent, and lake water. The pH of the three latter aqueous matrices (close to neutral) was not initially adjusted. Adapted from ref. [186].

PS activated with $NiCo_2S_4/Co_9S_8/NiS$ and the degradation of atrazine with photocatalysts activating PMS. Many works have studied the effect of common inorganic anions contained in real waters and wastewater like Cl^-, NO_3^-, SO_4^{2-}, HCO_3^-, CO_3^{2-}, and $H_2PO_4^-$, over the loss of herbicide concentration in all activated processes. These studies informed over the effectiveness of the charge transfer reactions of $SO_4^{\bullet-}$ and $^{\bullet}OH$ with such anions, thus allowing interpreting their oxidative role in real effluents. In general, HCO_3^- and CO_3^{2-} showed a strong inhibitory influence over herbicide removal because of their rapid scavenging of $SO_4^{\bullet-}$ and $^{\bullet}OH$. However, in some cases, low contents of these ions produced buffered neutral solutions that favored a more rapid attack of generated oxidants on the herbicide. Low degradation relevance was found for NO_3^-, SO_4^{2-}, and $H_2PO_4^-$ due to their slow reactions with $SO_4^{\bullet-}$ and $^{\bullet}OH$ In contrast, Cl^- presented a contradictory effect because low concentrations accelerated the degradation due to the formation of the extra oxidant active chlorine, whereas large concentrations inhibited the process acting as scavenger of the oxidizing radicals generated. In electrochemical activation, Cl^- was quickly oxidized at the anode in parallel to PS or PMS and produced large quantities of active chlorine that strongly accelerated the herbicide removal. It has been well-proven the negative influence of the addition of humic acid, as component model of NOM, by its competitive oxidation with the herbicides, although positive effects have been described in some processes with UV activation of PMS due to the extra decomposition of this oxidant by the photoexcited by-products of humic acid. These findings over the addition of inorganic anions and humic acid supported the smaller herbicide destruction found for real waters and wastewaters in front of pure water, but with different relative order for tap water, lake water, river water, groundwater, and/or WWTP effluent depending on the sample analyzed with a variable content of the above compounds. It is also noticeable the academic efforts made by many researchers to identify the primary aromatic and heteroaromatic intermediates, as well as the final carboxylic acids, detected by GC-MS, LC-MS, or LC-MS/MS during the destruction of herbicides. From these products, reasonable reaction sequences for their degradation or mineralization have been proposed that can serve to analyze the evolution of their toxicity during the treatment.

Thermal activation has shown better performance than other methods to generate $SO_4^{\bullet-}$ and $^{\bullet}OH$ at high temperature, but its cost should be evaluated for practical application in view of the expensive water heating. For iron ions activation, the catalytic use of adding MBQ, citric acid, and hydroxylamine with PS and *p*-benzoquinone with PMS to enhance Fe^{2+} regeneration has been well-proven. However, the presence of such extra organic compounds to the treated solution is not recommended in practice because it presupposes an increasing of its organic matter that is more difficulty mineralized by the generated oxidants. The combination of PS/Fe^{2+} and hydroxylamine as catalyst should be more widely explored at neutral pH since it seems a useful method to treat little volumes of real wastewaters. An important feature of solid catalysts used for activation is their stability and reusability that can be lost by the corrosion of their surface with leaching of components

and/or the lowering of active sites by deposition of the by-products formed. In this way, 0.15 M S-nZVI/biochar and Fe_3O_4/sepiolite were hetero-catalysts very stable for PS activation, as well as $LaFe_{0.9}Co_{0.1}O_3$, $NiCo_2S_4/Co_9S_8$/NiS, and CoS/rGO for PMS activation. For CoS/rGO, the higher $k_1 = 0.405\ min^{-1}$ was found for pentachlorophenol, although using a MOF like S-BUC-21 (Fe) particles, the best $k_1 = 0.521\ min^{-1}$ for atrazine decay was obtained for PMS/photocatalyst. Further research of new hetero-catalysts should be focused to develop reusable materials, a requirement for their possible application in practice.

Comparative treatments with activated PS and PMS did not show any clear tendency about the process with higher oxidation power to remove herbicides. It depended not only of their reaction rate with the herbicides, but also of many experimental conditions including the activation method used, the pH, and the aqueous matrix. Then, trials have to be checked under comparable conditions to decide the best treatment. In general, activated PS and PMS showed a superior oxidation power than similar activated H_2O_2 processes, but the latter upgraded PMS in some specific cases, e.g., with UVC activation.

Declaration of Competing Interest

The authors declare that they have no known competing financial interests or personal relationships that could have appeared to influence the work reported in this paper.

Data availability

Data will be made available on request.

References

[1] M.C. Vagi, A.S. Petsas, Recent advances on the removal of priority organochlorine and organophosphorus biorecalcitrant pesticides defined by Directive 2013/39/EU from environmental matrices by using advanced oxidation processes: an overview (2007-2018), J. Environ. Chem. Eng. 2019 (2019), 102940, https://doi.org/10.1016/j.jece.2019.102940.

[2] E. Brillas, Recent development of electrochemical advanced oxidation of herbicides. A review on its application to wastewater treatment and soil remediation, J. Clean. Prod. 290 (2021), 125841, https://doi.org/10.1016/j.jclepro.2021.125841.

[3] R. Mahour, M.F. Khan, S. Forbes, L.A. Perez-Estrada, Pesticides and herbicides, Water Environ. Res. 86 (2014) 1545–1578, https://doi.org/10.2175/106143014×14031280668777.

[4] M.A. Rodrigo, M.A. Oturan, N. Oturan, Electrochemically assisted remediation of pesticides in soils and water: a review, Chem. Rev. 114 (2014) 8720–8745, https://doi.org/10.1021/cr500077e.

[5] E. Brillas, A review on the photoelectro-Fenton process as efficient electrochemical advanced oxidation for wastewater remediation. Treatment with UV light, sunlight, and coupling with conventional and other photo-assisted advanced technologies, Chemosphere 250 (2020), 126198, https://doi.org/10.1016/j.chemosphere.2020.126198.

[6] E. Brillas, Fenton, photo-Fenton, electro-Fenton, and their combined treatments for the removal of insecticides from waters and soils. A review, Sep. Purif. Rechn. 284 (2022), 120290, https://doi.org/10.1016/j.seppur.2021.120290.

[7] C.A. Martínez-Huitle, M.A. Rodrigo, I. Sirés, O. Scialdone, A critical review on latest innovations and future challenges of electrochemical technology for the abatement of organics in water, Appl. Catal. B: Environ. 328 (2023), 122430, https://doi.org/10.1016/j.apcatb.2023.122430.

[8] A.R. Ribeiro, O.C. Nunes, M.F.R. Pereira, A.M.T. Silva, An overview on the advanced oxidation processes applied for the treatment of water pollutants defined in the recently launched Directive 2013/39/EU, Environ. Int. 75 (2015) 33–51, https://doi.org/10.1016/j.envint.2014.10.027.

[9] P.V. Nidheesh, G. Divyapriya, N. Oturan, C. Trellu, M.A. Oturan, Environmental applications of boron-doped diamond electrodes: 1, Appl. Water Wastewater Treat., ChemElectroChem 6 (2019) 2124–2242, https://doi.org/10.1002/celc.201801876.

[10] M. Malakootian, A. Shahesmaeili, M. Faraji, H. Amiri, S. Silva Martinez, S, 2020. Advanced oxidation processes for the removal of organophosphorus pesticides in aqueous matrices: a systematic review and meta-analysis, Process Saf. Environ.: Prot. 134 (2020) 292–307, https://doi.org/10.1016/j.psep.2019.12.004.

[11] S. Sheikhi, R. Dehghanzadeh, H. Aslan, Advanced oxidation processes for chlorpyrifos removal from aqueous solution: a systematic review, J. Environ. Health Sci. Eng. 19 (2021) 1249–1262, https://doi.org/10.1007/s40201-021-00674-1.

[12] S. Guerra-Rodríguez, E. Rodrñiguez, D.,N. Singh, J. Rodríguez-Chueca, Assessment of sulfate radical-based advanced oxidation processes for water and wastewater treatment: a review, Water 10 (2018) 182, https://doi.org/10.3390/w10121828.

[13] A. Hassani, J. Scaria, F. Ghanbari, P.V. Nidheesh, Sulfate radicals-based advanced oxidation processes for the degradation of pharmaceuticals and personal care products: a review on relevant activation mechanisms, performance, and perspectives, Environ. Res. 217 (2023), 114789, https://doi.org/10.1016/j.envres.2022.114789.

[14] A.J. dos Santos, E. Brillas, P.L. Cabot, I. Sirés, Simultaneous persulfate activation by electrogenerated H_2O_2 and anodic oxidation at a boron-doped diamond anode for the treatment of dye solutions, Sci. Total Environ. 747 (2020), 141541, https://doi.org/10.1016/j.scitotenv.2020.141541.

[15] A.J. dos Santos, I. Sirés, E. Brillas, Removal of bisphenol A from acidic sulfate medium and urban wastewater using persulfate activated with electroregenerated Fe^{2+}, Chemosphere 263 (2021), 128271 https://doi.org/10.1016/j.chemosphere.2020.128271.

[16] M. Gagol, A. Przyjazny, G. Boczkaj, Wastewater treatment by means of advanced oxidation processes based on cavitation - A review, Chem. Eng. J. 338 (2018) 599–627, https://doi.org/10.1016/j.cej.2018.01.049.

[17] Y. Zhou, Y. Xiang, Y. He, Y. Yang, J. Zhang, L. Luo, H. Peng, C. Dai, F. Zhu, L. Tang, Applications and factors influencing of the persulfate-based advanced oxidation processes for the remediation of groundwater and soil contaminated with organic compounds, J. Hazard. Mater. 359 (2018) 396–407, https://doi.org/10.1016/j.jhazmat.2018.07.083.

[18] E.M. Diaz Kirmser, D.O. Mártire, M.C. Gonzalez, J.A. Rosso, Degradation of the herbicides clomazone, paraquat, and glyphosate by thermally activated peroxydisulfate, J. Agric. Food Chem. 58 (2010) 12858–12862, https://doi.org/10.1021/jf103054h.

[19] C. Tan, N. Gao, Y. Deng, N. An, J. Deng, Heat-activated persulfate oxidation of diuron in water, Chem. Eng. J. 203 (2012) 294–300, https://doi.org/10.1016/j.cej.2012.07.005.

[20] Y. Ji, C. Dong, D. Kong, J. Lu, Q. Zhou, Heat-activated persulfate oxidation of atrazine: implications for remediation of groundwater contaminated by herbicides, Chem. Eng. J. 263 (2015) 45–54, https://doi.org/10.1016/j.cej.2014.10.097.

[21] C. Jiang, Y. Yang, L. Zhang, D. Lu, L. Lu, X. Yang, T. Cai, Degradation of atrazine, simazine and ametryn in an arable soil using thermal-activated persulfate oxidation process: optimization, kinetics, and degradation pathway, J. Hazard. Mater. 400 (2020), 123201, https://doi.org/10.1016/j.jhazmat.2020.123201.

[22] J. Li, E. Liang, T. Huang, X. Zhao, T. Wang, Insights into atrazine degradation by thermally activated persulfate: evidence from dual C-H isotope analysis and DFT simulations, Chem. Eng. J. 454 (2023), 140207, https://doi.org/10.1016/j.cej.2022.140207.

[23] X. Yang, X. Ding, L. Zhou, H.-H. Fan, X. Wang, C. Ferronato, J.-M. Chovelon, G. Xiu, New insights into clopyralid degradation by sulfate radical: pyridine ring cleavage pathways, Water Res 171 (2020), 115378, https://doi.org/10.1016/j.watres.2019.115378.

[24] J. Cai, M. Zhou, W. Yang, Y. Pan, X. Lu, K.G. Serrano, Degradation and mechanism of 2,4-dichlorophenoxyacetic acid (2,4-D) by thermally activated persulfate oxidation, Chemosphere 212 (2018) 784–793, https://doi.org/10.1016/j.chemosphere.2018.08.127.

[25] W. Ren, X. Huang, L. Wang, X. Liu, Z. Zhou, Y. Wang, C. Lin, M. He, W. Ouyang, Degradation of simazine by heat-activated peroxydisulfate process: a coherent study on kinetics, radicals and models, Chem. Eng. J. 426 (2021), 131876, https://doi.org/10.1016/j.cej.2021.131876.

[26] X. Yang, X. Cao, L. Zhang, Y. Wu, L. Zhou, G. Xiu, C. Ferronato, J.-M. Chovelon, Sulfate radical-based oxidation of the aminopyralid and picloram herbicides: the role of amino group on pyridine ring, J. Hazard. Mater. 405 (2021), 124181, https://doi.org/10.1016/j.jhazmat.2020.124181.

[27] V. Rybnikova, N. Singhal, K. Hanna, Remediation of an aged PCP-contaminated soil by chemical oxidation under flow-through conditions, Chem. Eng. J. 201 (2018) 202–211, https://doi.org/10.1016/j.cej.2016.12.120.

[28] C.A.L. Graça, M.G. Maniero, L.M. De Andrade, J.R. Guimaraes, A.C.S.C. Teixeira, Evaluation of amicarbazone toxicity removal through degradation processes based on hydroxyl and sulfate radicals, J. Environ. Sci. Health A 54 (2019) 1126–1143, https://doi.org/10.1080/10934529.2019.1643693.

[29] L. Bu, Z. Shi, S. Zhou, Modeling of Fe(II)-activated persulfate oxidation using atrazine as a target contaminant, Sep. Purif. Technol. 169 (2016) 59–65, https://doi.org/10.1016/j.seppur.2016.05.037.

[30] L. Bu, C. Bi, Z. Shi, S. Zhou, Significant enhancement on ferrous/persulfate oxidation with epigallocatechin-3-gallate: simultaneous chelating and reducing, Chem. Eng. J. 321 (2017) 642–650, https://doi.org/10.1016/j.cej.2017.04.001.

[31] L. Chen, X. Hu, Y. Yang, C. Jiang, C. Bian, C. Liu, M. Zhang, T. Cai, Degradation of atrazine and structurally related s-triazine herbicides in soils by ferrous-activated persulfate: kinetics, mechanisms and soil-types effects, Chem. Eng. J. 351 (2018) 523–531, https://doi.org/10.1016/j.cej.2018.06.045.

[32] X. Wang, Y. Wang, N. Chen, Y. Shi, L. Zhang, Pyrite enables persulfate activation for efficient atrazine degradation, Chemosphere 244 (2020), 125568, https://doi.org/10.1016/j.chemosphere.2019.125568.

[33] Y. An, X. Li, Z. Liu, Y. Li, Z. Zhou, X. Liu, Constant oxidation of atrazine in Fe(III)/PDS system by enhancing Fe(III)/Fe(II) cycle with quinones: reaction mechanism, degradation pathway and DFT calculation, Chemosphere 317 (2023), 137883, https://doi.org/10.1016/j.chemosphere.2023.137883.

[34] C. Liang, Y.-Y. Guo, Y.-R. Pan, A study of the applicability of various activated persulfate processes for the treatment of 2,4-dichlorophenoxyacetic acid, Int. J. Environ. Sci. Technol. 11 (2014) 483–492, https://doi.org/10.1007/s13762-013-0212-5.

[35] S. Rodriguez, A. Santos, A. Romero, F. Vicente, Kinetic of oxidation and mineralization of priority and emerging pollutants by activated persulfate, Chem. Eng. J. 213 (2012) 225–234, https://doi.org/10.1016/j.cej.2012.09.077.

[36] C. Tan, N. Gao, W. Chu, C. Li, M.R. Templeton, Degradation of diuron by persulfate activated with ferrous ion, Sep. Purif. Technol. 95 (2012) 44–48, https://doi.org/10.1016/j.seppur.2012.04.012.

[37] L. Zhou, W. Zheng, Y. Ji, J. Zhang, C. Zeng, Y. Zhang, Q. Wang, X. Yang, Ferrous-activated persulfate oxidation of arsenic(III) and diuron in aquatic system, J. Hazard. Mater. 263 (2013) 422–430, https://doi.org/10.1016/j.jhazmat.2013.09.056.

[38] C.S. Liu, K. Shih, C.X. Sun, F. Wang, Oxidative degradation of propachlor by ferrous and copper ion activated persulfate, Sci. Total Environ. 416 (2012) 507–512, https://doi.org/10.1016/j.scitotenv.2011.12.004.

[39] Q. Wang, Y. Shao, N. Gao, W. Chu, J. Deng, X. Shen, X. Lu, Y. Zhu, X. Wei, Degradation of alachlor with zero-valent iron activating persulfate oxidation, J. Taiwan Inst. Chem. Eng. 63 (2016) 379–385, https://doi.org/10.1016/j.jtice.2016.03.038.

[40] Q. Wang, Y. Shao, N. Gao, S. Liu, L. Dong, P. Rao, W. Chu, B. Xu, N. An, J. Deng, Impact of zero valent iron/persulfate preoxidation on disinfection byproducts through chlorination of alachlor, Chem. Eng. J. 380 (2020), 122435, https://doi.org/10.1016/j.cej.2019.122435.

[41] C.A.L. Graça, L.T.N. Fugita, A.C. de Velosa, A.C.S.C. Teixeira, Amicarbazone degradation promoted by ZVI-activated persulfate: study of relevant variables for practical application, Environ. Sci. Pollut. Res. 25 (2018) 5474–5483, https://doi.org/10.1007/s11356-017-0862-9.

[42] S. Wu, H. He, X. Li, C. Yang, G. Zeng, B. Wu, S. He, L. Lu, Insights into atrazine degradation by persulfate activation using composite of nanoscale zero-valent iron and graphene: Performances and mechanisms, Chem. Eng. J. 341 (2018) 126–136, https://doi.org/10.1016/j.cej.2018.01.136.

[43] Z. Jiang, J. Li, D. Jiang, Y. Gao, Y. Chen, W. Wang, B. Cao, Y. Tao, L. Wang, Y. Zhang, Removal of atrazine by biochar-supported zero-valent iron catalyzed persulfate oxidation: reactivity, radical production and transformation pathway, Environ. Res. 184 (2020), 109260, https://doi.org/10.1016/j.envres.2020.109260.

[44] S. Deng, L. Liu, G. Cagnetta, J. Huang, G. Yu, Mechanochemically synthesized S-ZVI^{bm} composites for the activation of persulfate in the pH-independent degradation of atrazine: effects of sulfur dose and ball-milling conditions, Chem. Eng. J. 423 (2021), 129789, https://doi.org/10.1016/j.cej.2021.129789.

[45] Q. Jiang, Y. Zhang, S. Jiang, Y. Wang, H. Li, W. Han, J. Qu, L. Wang, Y. Hu, Graphene-like carbon sheet-supported nZVI for efficient atrazine oxidation degradation by persulfate activation, Chem. Eng. J. 403 (2021), 126309, https://doi.org/10.1016/j.cej.2020.126309.

[46] Y. Zhang, Q. Jiang, S. Jiang, H. Li, R. Zhang, J. Qu, S. Zhang, W. Han, One-step synthesis of biochar supported nZVI composites for highly efficient activating persulfate to oxidatively degrade atrazine, Chem. Eng. J. 420 (2021), 129868, https://doi.org/10.1016/j.cej.2021.129868.

[47] Q. Jiang, S. Jiang, H. Li, R. Zhang, Z. Jiang, Y. Zhang, A stable biochar supported S-nZVI to activate persulfate for effective dichlorination of atrazine, Chem. Eng. J. 431 (2022), 133937, https://doi.org/10.1016/j.cej.2021.133937.

[48] Z. Yin, G. Cagnetta, J. Huang, Mechanochemically sulfidated zero-valent iron as persulfate activation catalyst in permeable reactive barriers for groundwater remediation - A feasibility study, Chemosphere 311 (2023), 137081, https://doi.org/10.1016/j.chemosphere.2022.137081.

[49] X. Wei, N. Gao, C. Li, Y. Deng, S. Zhou, L. Li, Zero-valent iron (ZVI) activation of persulfate (PS) for oxidation of bentazon in water, Chem. Eng. J. 285 (2016) 660–670, https://doi.org/10.1016/j.cej.2015.08.120.

[50] Y. Xie, J. Dai, G. Chen, Feasibility study on applying the iron-activated persulfate system as a pre-treatment process for clofibric acid selective degradation in municipal wastewater, Sci. Total Environ. 739 (2020), 140020, https://doi.org/10.1016/j.scitotenv.2020.140020.

[51] X. Li, M. Zhou, Y. Pan, Enhanced degradation of 2,4-dichlorophenoxyacetic acid by pre-magnetization Fe-C activated persulfate: influential factors, mechanism and degradation pathway, J. Hazard. Mater. 353 (2018) 454–465, https://doi.org/10.1016/j.jhazmat.2018.04.035.

[52] X. Xiong, B. Sun, J. Zhang, N. Gao, J. Shen, J. Li, X. Guan, Activating persulfate by Fe^0 coupling with weak magnetic field: performance and mechanism, Water Res 62 (2014) 53–62, https://doi.org/10.1016/j.watres.2014.05.042.

[53] S. Rodriguez, A. Santos, A. Romero, Oxidation of priority and emerging pollutants with persulfate activated by iron: effect of iron valence and particle size, Chem. Eng. J. 318 (2017) 197–205, https://doi.org/10.1016/j.cej.2016.06.057.

[54] W. Hayat, Z.-H. Liu, Y.-P. Wan, X. Du, S. Huang, Y. Zhang, The degradation of fenuron in water by activated persulfate oxidation: an analysis of efficiency, influential parameters and potential applicability, Chem. Eng. J. 445 (2022), 136688, https://doi.org/10.1016/j.cej.2022.136688.

[55] Y. Liu, J. Lang, T. Wang, A. Jawad, H. Wang, A. Khan, Z. Chen, Z. Chen, Enhanced degradation of isoproturon in soil through persulfate activation by Fe-based layered double hydroxide: different reactive species comparing with activation by homogenous Fe(II, Environ. Sci. Pollut. Res. 25 (2018) 26394–26404, https://doi.org/10.1007/s11356-018-2637-3.

[56] J. Peng, X. Lu, X. Jiang, Y. Zhang, Q. Chen, B. Lai, G. Yao, Degradation of atrazine by persulfate activation with copper sulfide (CuS): kinetics study, degradation pathways and mechanism, Chem. Eng. J. 354 (2018) 740–752, https://doi.org/10.1016/j.cej.2018.08.038.

[57] X. Hou, G. Zhan, X. Huang, N. Wang, Z. Ai, L. Zhang, Persulfate activation induced by ascorbic acid for efficient organic pollutants oxidation, Chem. Eng. J. 382 (2020), 122355, https://doi.org/10.1016/j.cej.2019.122355.

[58] W. Song, J. Li, C. Fu, Z. Wang, X. Zhang, J. Yang, W. Hogland, L. Gao, Kinetics and pathway of atrazine degradation by a novel method: persulfate coupled with dithionite, Chem. Eng. J. 373 (2019) 803–813, https://doi.org/10.1016/j.cej.2019.05.110.

[59] X. Xu, W. Chen, S. Zong, X. Ren, D. Liu, Atrazine degradation using Fe_3O_4-sepiolite catalyzed persulfate: reactivity, mechanism and stability, J. Hazard. Mater. 377 (2019) 62–69, https://doi.org/10.1016/j.jhazmat.2019.05.029.

[60] S. Zong, X. Xu, G. Ran, J. Liu, Comparative study of atrazine degradation by magnetic clay activated persulfate and H_2O_2, RSC Adv. 10 (2020) 11410–11417, https://doi.org/10.1039/d0ra00345j.

[61] D. Li, J. Ali, A. Shahzad, E. Abdelnasser Gendy, H. Nie, W. Jiang, H. Xiao, Z. Chen, S. Wang, Persulfate coupled with Cu^{2+}/LDH-MoS_4: a novel process for the efficient atrazine abatement, mechanism and degradation pathway, Chem. Eng. J. 436 (2022), 134933, https://doi.org/10.1016/j.cej.2022.134933.

[62] G. Xue, L. Zhang, X. Fan, K. Luo, S. Guo, H. Chen, X. Li, Q. Jian, Responses of soil fertility and microbiomes of atrazine contaminated soil to remediation by hydrochar and persulfate, J. Hazard. Mater. 435 (2022), 128944, https://doi.org/10.1016/j.jhazmat.2022.128944.

[63] D. Zhang, Z. An, Y. Zhang, Y. Hu, J. Zhan, H. Zhou, M. Wu, MoS_2@SiO_2 enhanced persulfate oxidation for the degradation of triazine herbicides in fixed-bed reactor, J. Water Process Eng. 52 (2023), 103523, https://doi.org/10.1016/j.jwpe.2023.103523.

[64] H. Zheng, J. Du, H. Zhong, Q. Yuan, J. Zhang, W. Kang, Q. Sun, M. Tao, W. Xiao, D.D. Dionysiou, Y. Huang, Enhanced persulfate activation by sulfur-modified Fe_3O_4 composites for atrazine degradation: erformance and mechanism, Process Saf. Environ. Prot. 170 (2023) 1052–1065, https://doi.org/10.1016/j.psep.2022.12.074.

[65] C. Chu, J. Yang, D. Huang, J. Li, A. Wang, P.J.J. Alvarez, J.-H. Kim, Cooperative pollutant adsorption and persulfate-driven oxidation on hierarchically ordered porous carbon, Environ. Sci. Technol. 53 (2019) 10352–10360, https://doi.org/10.1021/acs.est.9b03067.

[66] H. Chen, Z. Zhang, M. Feng, W. Liu, W. Wang, Q. Yang, Y. Hu, Degradation of 2,4-dichlorophenoxyacetic acid in water by persulfate activated with FeS (mackinawite), Chem. Eng. J. 313 (2017) 498–507, https://doi.org/10.1016/j.cej.2016.12.075.

[67] M. Kermani, F. Mohammadi, B. Kakavandi, A. Esrafili, Z. Rostamifasih, Simultaneous catalytic degradation of 2,4-D and MCPA herbicides using sulfate radical-based heterogeneous oxidation over persulfate activated by natural hematite (α-Fe_2O_3/PS), J. Phys. Chem. Solids 117 (2018) 49–59, https://doi.org/10.1016/j.jpcs.2018.02.009.

[68] M. Cao, Y. Hou, E. Zhang, S. Tu, S. Xiong, Ascorbic acid induced activation of persulfate for pentachlorophenol degradation, Chemosphere 229 (2019) 200–205, https://doi.org/10.1016/j.chemosphere.2019.04.135.

[69] G. Asgari, A. Seid-Mohammadi, M.R. Samargandi, R. Jamshidi, Mineralization, kinetics, and degradation pathway of pentachlorophenol degradation from aqueous media via persulfate/dithionite process, Arab. J. Chem. 14 (2021), 103357, https://doi.org/10.1016/j.arabjc.2021.103357.

[70] Y. Liu, X. Ji, J. Yang, W. Tang, Y. Zhu, Y. Wang, Y. Zhang, Y. Zhang, J. Duan, W. Li, Degradation of the typical herbicide atrazine by UV/persulfate: kinetics and mechanisms, Environ. Sci. Pollut. Res. 29 (2022) 43928–43941, https://doi.org/10.1007/s11356-022-18717-x.

[71] M.G. Antoniou, H.R. Andersen, Comparison of UVC/$S_2O_8^{2-}$ with UVC/H_2O_2 in terms of efficiency and cost for the removal of micropollutants from groundwater, Chemosphere 119 (2015) 581–588, https://doi.org/10.1016/j.chemosphere.2014.03.029.

[72] M.S. Khandarkhaeva, D.G. Aseev, M.R. Sizykh, A.A. Batoeva, Oxidation of atrazine by photoactivated potassium persulfate in aqueous solutions, Russ. J. Phys. Chem. A 90 (2016) 2177–2182, https://doi.org/10.1134/S003602441611011X.

[73] W. Qin, Z. Lin, L. Sun, X. Yuan, D. Xia, A preliminary study on the integrated UV/ozone/persulfate process for efficient abatement of atrazine, 558-546, Ozone.: Sci. Eng. 42 (2020), https://doi.org/10.1080/01919512.2020.1746631.

[74] F. Lai, F.-X. Tian, B. Xu, W.-K. Ye, Y.-Q. Gao, C. Chen, H.-B. Xing, B. Wang, M.-J. Xie, X.-J. Hu, A comparative study on the degradation of phenylurea herbicides by UV/persulfate process: kinetics, mechanisms, energy demand and toxicity evaluation associated with DBPs, Chem. Eng. J. 428 (2022), 132088, https://doi.org/10.1016/j.cej.2021.132088.

[75] F. Sadeghi, A. Fadaei, F. Mohammadi-Moghadam, S. Hemati, G. Mardani, Photocatalytic degradation of trifluralin in aqueous solutions by UV/$S_2O_8^{2-}$ and UV/ZnO processes: a comparison of removal efficiency and cost estimation, Int. J. Chem. Eng. 2021 (2021), 9964291, https://doi.org/10.1155/2021/9964291.

[76] C.W. Luo, J. Ma, J. Jiang, Y.Z. Liu, Y. Song, Y. Yang, Y. Guan, D. Wu, Simulation and comparative study on the oxidation kinetics of atrazine by UV/H_2O_2, UV/HSO_5^- and UV/$S_2O_8^{2-}$, Water Res 80 (2015) 99–108, https://doi.org/10.1016/j.watres.2015.05.019.

[77] C.A.L. Graça, A.C.D. Velosa, A.C.S.C. Teixeira, Amicarbazone degradation by UVA-activated persulfate in the presence of hydrogen peroxide or Fe^{2+}, Catal. Today 280 (2017) 80–85, https://doi.org/10.1016/j.cattod.2016.06.044.

[78] N. Garkusheva, G. Matafonova, I. Tsenter, S. Beck, V. Batoev, K. Linden, Simultaneous atrazine degradation and E. coli inactivation by simulated solar photo-Fenton-like process using persulfate, J. Environ. Sci. Health A 52 (2017) 849–855, https://doi.org/10.1080/10934529.2017.1312188.

[79] S. Popova, G. Matafonova, V. Batoev, Simultaneous atrazine degradation and E. coli inactivation by UV/$S_2O_8^{2-}$/Fe^{2+} process under KrCl excilamp (222 nm) irradiation, Ecotoxicol. Environ. Saf. 169 (2019) 169–177, https://doi.org/10.1016/j.ecoenv.2018.11.014.

[80] S.A. Popova, G.G. Matafonova, V.B. Batoev, Generation of radicals in ferrous-persulfate system using KrCl excilamp, ChemChemTech 62 (2019) 119–123, https://doi.org/10.6060/ivkkt.20196205.5819.

[81] S.A. Popova, I.M. Tsenter, N.M. Garkusheva, G.G. Matafonova, V.B. Batoev, Water treatment and disinfection by UV radiation of the led matrix (365 nm) in the ferrous-persulfate system, ChemChemTech 65 (2022) 134–143, https://doi.org/10.6060/ivkkt.20226502.6457.

[82] I. Sánchez-Montes, J. Carneiro Doerenkamp, Y. Núñez de la Rosa, P. Hammer, R. C. Rocha-Filho, J.M. Aquino, Effective Fenton-like degradation of the tebuthiuron herbicide by ferrocene functionalized g-C_3N_4, J. Photochem. Photobiol. A: Chem. 435 (2023), 114276, https://doi.org/10.1016/j.jphotochem.2022.114276.

[83] M.H. Pérez, L.P. Vega, H. Zúñiga-Benítez, G.A. Peñuela, Comparative degradation of alachlor using photocatalysis and photo-Fenton, Water Air Soil Pollut. 229 (2018) 346, https://doi.org/10.1007/s11270-018-3996-6.

[84] A. Ghavi, G. Bagherian, H. Rezaei-Vahidian, Degradation of paraquat herbicide using hybrid AOP process: statistical optimization, kinetic study, and estimation of electrical energy consumption, Environ. Sci. Eur. 13 (2021) 117, https://doi.org/10.1186/s12302-021-00555-2.

[85] E. Brillas, S. Garcia-Segura, Recent progress of applied TiO_2 photoelectrocatalysis for the degradation of organic pollutants in wastewaters, J. Environ. Chem. Eng. 11 (2023), 109635, https://doi.org/10.1016/j.jece.2023.109635.

[86] J. An, C. Xia, H. Chen, D. Hu, Activation of persulfate by irradiated magnetite: implications for abatement of atrazine in aqueous solution, Res, Environ. Sci. 31 (2018) 130–135, https://doi.org/10.13198/j.issn.1001-6929.2017.03.39.

[87] J. Chen, H. Zhu, Q. Ren, S. Chen, Y. Ding, Z. Jin, C. Xiong, W. Guo, X. Jia, Efficient degradation of atrazine residues in wastewater by persulfate assisted Ag_3VO_4/Bi_2MoO_6/diatomite under visible light, J. Environ. Chem. Eng. 10 (2022), 107938, https://doi.org/10.1016/j.jece.2022.107938.

[88] B. Mendoza-Reyes, S. Mendiola-Alvarez, J.L. Guzmán-Mar, M. Villanueva-Rodríguez, E.J. Ruiz-Ruiz, L. Hinojosa-Reyes, Enhanced photocatalytic oxidation of a phenoxyacetic acid herbicide using TiO_2-FeOOH/Fe_2O_3 assisted with sulfate radicals, Int. J. Environ. Sci. Technol. 20 (2023) 967–980, https://doi.org/10.1007/s13762-022-04095-x.

[89] M.M. Haque, N. Muneer, D.W. Bahnemann, Semiconductor-mediated photocatalyzed degradation of a herbicide derivative, chlorotoluron, in aqueous suspensions, Environ. Sci. Technol. 40 (2006) 4765–4770, https://doi.org/10.1021/es060051h.

[90] M.A. Rahman, M. Muneer, Heterogeneous photocatalytic degradation of picloram, dicamba, and floumeturon in aqueous suspensions of titanium dioxide, J. Environ. Sci. Health B 40 (2005) 147–267, https://doi.org/10.1081/PFC-200045546.

[91] D. Akgün, M. Dükkanci, g-C_3N_4 supported Ag/AgCl@MIL-88A MOF based triple composites for highly efficient diuron photodegradation under visible LED light irradiation, J. Water Process Eng. 51 (2023), 103469, https://doi.org/10.1016/j.jwpe.2022.103469.

[92] J.A. Osajima, H.M. Ishiki, K. Takashima, The photocatalytic degradation of imazapyr, Mon. fur Chem. 139 (2008) 7–11, https://doi.org/10.1007/s00706-007-0728-9.

[93] E. Durna, N. Genç, Removal of metribuzin by sulfate radical-based photooxidation: multi-objective optimization by central composite design, Water Environ. J. 33 (2019) 265–275, https://doi.org/10.1111/wej.12397.

[94] S. Navarro, J. Fenoll, N. Vela, E. Ruiz, G. Navarro, Photocatalytic degradation of eight pesticides in leaching water by use of ZnO under natural sunlight, J. Hazard. Mater. 172 (2009) 1303–1310, https://doi.org/10.1016/j.jhazmat.2009.07.137.

[95] J. Fenoll, P. Sabater, G. Navarro, G. Pérez-Lucas, S. Navarro, Photocatalytic transformation of sixteen substituted phenylurea herbicides in aqueous semiconductor suspensions: intermediates and degradation pathways, J. Hazard. Mater. 244–245 (2013) 370–379, https://doi.org/10.1016/j.jhazmat.2012.11.055.

[96] L. Bu, S. Zhu, S. Zhou, Degradation of atrazine by electrochemically activated persulfate using BDD anode: role of radicals and influencing factors, Chemosphere 195 (2018) 236–244, https://doi.org/10.1016/j.chemosphere.2017.12.088.

[97] J. Li, J. Yan, G. Yao, Y. Zhang, X. Li, B. Lai, Improving the degradation of atrazine in the three-dimensional (3D) electrochemical process using $CuFe_2O_4$ as both particle electrode and catalyst for persulfate activation, Chem. Eng. J. 361 (2019) 1317–1332, https://doi.org/10.1016/j.cej.2018.12.144.

[98] J. Cai, M. Zhou, Q. Zhang, Y. Tian, G. Song, The radical and non-radical oxidation mechanism of electrochemically activated persulfate process on different cathodes in divided and undivided cell, J. Hazard. Mater. 416 (2021), 125804, https://doi.org/10.1016/j.jhazmat.2021.125804.

[99] X. Sun, Z. Liu, Z. Sun, Electro-enhanced degradation of atrazine via Co-Fe oxide modified graphite felt composite cathode for persulfate activation, Chem. Eng. J. 433 (2022), 133789, https://doi.org/10.1016/j.cej.2021.133789.

[100] J. Zhou, J. Liu, T. Liu, G. Liu, J. Li, D. Chen, Y. Feng, Electrochemical activation of persulfate by Al-doped blue TiO_2 nanotubes for the multipath degradation of atrazine, J. Hazard. Mater. 445 (2023), 130578, https://doi.org/10.1016/j.jhazmat.2022.130578.

[101] J. Cai, M. Zhou, Y. Liu, A. Savall, K. Groenen Serrano, Indirect electrochemical oxidation of 2,4-dichlorophenoxyacetic acid using electrochemically-generated persulfate, Chemosphere 204 (2018) 163–169, https://doi.org/10.1016/j.chemosphere.2018.04.004.

[102] J. Mehralipour, M. Kermani, Optimization of photo-electro/persulfate/nZVI process on 2,4 dichlorophenoxyacetic acid degradation via central composite design: a novel combination of advanced oxidation process, J. Environ. Health Sci. Eng. 19 (2021) 941–957, https://doi.org/10.1007/s40201-021-00661-6.

[103] J. Mehralipour, M. Kermani, Ultrasonic coupling with electrical current to effective activation of persulfate for 2, 4 dichlorophenoxyacetic acid herbicide degradation: modeling, synergistic effect, and a by-product study, J. Environ. Health Sci. Eng. 19 (2021) 625–639, https://doi.org/10.1007/s40201-021-00633-w.

[104] Y. Yu, S. Zhou, L. Bu, Z. Shi, S. Zhu, Degradation of diuron by electrochemically activated persulfate, Water Air Soil Pollut. 227 (2016) 279, https://doi.org/10.1007/s11270-016-2978-9.

[105] E. Vieira Dos Santos, C. Sáez, P. Cañizares, C.A. Martínez-Huitle, M.A. Rodrigo, Treating soil-washing fluids polluted with oxyfluorfen by sono-electrolysis with diamond anodes, Ultrason. Sonochem. 34 (2017) 115–122, https://doi.org/10.1016/j.ultsonch.2016.05.029.

[106] Y. Ji, C. Dong, D. Kong, J. Lu, New insights into atrazine degradation by cobalt catalyzed peroxymonosulfate oxidation: kinetics, reaction products and transformation mechanisms, J. Hazard. Mater. 285 (2015) 491–500, https://doi.org/10.1016/j.jhazmat.2014.12.026.

[107] Y. Fan, Y. Ji, G. Zheng, J. Lu, D. Kong, X. Yin, Q. Zhou, Degradation of atrazine in heterogeneous Co_3O_4 activated peroxymonosulfate oxidation process: kinetics, mechanisms, and reaction pathways, Chem. Eng. J. 330 (2017) 831–839, https://doi.org/10.1016/j.cej.2017.08.020.

[108] J. Li, M. Xu, G. Yao, B. Lai, Enhancement of the degradation of atrazine through $CoFe_2O_4$ activated peroxymonosulfate (PMS) process: kinetic, degradation intermediates, and toxicity evaluation, Chem. Eng. J. 348 (2018) 1012–1024, https://doi.org/10.1016/j.cej.2018.05.032.

[109] Y. Hong, J. Peng, X. Zhao, Y. Yan, B. Lai, G. Yao, Efficient degradation of atrazine by CoMgAl layered double oxides catalyzed peroxymonosulfate: optimization, degradation pathways and mechanism, Chem. Eng. J. 370 (2019) 354–363, https://doi.org/10.1016/j.cej.2019.03.127.

[110] F. Ji, H. Zhang, X. Wei, Y. Zhang, B. Lai, Efficient degradation of atrazine by Co-NZ catalyst prepared by electroless plating in the presence of peroxymonosulfate: characterization, performance and mechanistic consideration, Chem. Eng. J. 359 (2019) 1316–1326, https://doi.org/10.1016/j.cej.2018.11.049.

[111] X. Li, X. Liu, C. Lin, H. Zhang, Z. Zhou, G. Fan, J. Ma, Cobalt ferrite nanoparticles supported on drinking water treatment residuals: an efficient magnetic heterogeneous catalyst to activate peroxymonosulfate for the degradation of atrazine, Chem. Eng. J. 367 (2019) 208–218, https://doi.org/10.1016/j.cej.2019.02.151.

[112] R. Zhang, Y. Wan, J. Peng, G. Yao, Y. Zhang, B. Lai, Efficient degradation of atrazine by $LaCoO_3/Al_2O_3$ catalyzed peroxymonosulfate: performance, degradation intermediates and mechanism, Chem. Eng. J. 372 (2019) 796–808, https://doi.org/10.1016/j.cej.2019.04.188.

[113] J. Zhu, J. Wang, C. Shan, J. Zhang, L. Lv, B. Pan, Durable activation of peroxymonosulfate mediated by Co-doped mesoporous $FePO_4$ via charge redistribution for atrazine degradation, Chem. Eng. J. 375 (2019), 122009, https://doi.org/10.1016/j.cej.2019.122009.

[114] H. Cai, J. Li, H. Yin, G. Yao, B. Lai, Degradation of atrazine in aqueous solution through peroxymonosulfate activated by Co-modified nano-titanium dioxide, Water Environ. Res 92 (2020) 1363–1375, https://doi.org/10.1002/wer.1324.

[115] X. Dong, B. Ren, X. Zhang, X. Liu, Z. Sun, C. Li, Y. Tan, S. Yang, S. Zheng, D. D. Dionysiou, Diatomite supported hierarchical 2D $CoNi_3O_4$ nanoribbons as highly efficient peroxymonosulfate catalyst for atrazine degradation, Appl. Catal. B: Environ. 272 (2020), 118971, https://doi.org/10.1016/j.apcatb.2020.118971.

[116] B. Liu, W. Guo, H. Wang, Q. Si, Q. Zhao, H. Luo, N. Ren, Activation of peroxymonosulfate by cobalt-impregnated biochar for atrazine degradation: the pivotal roles of persistent free radicals and ecotoxicity assessment, J. Hazard. Mater. 398 (2020), 122768, https://doi.org/10.1016/j.jhazmat.2020.122768.

[117] J. Li, G. Gou, H. Zhao, C. Liu, N. Li, L. Li, B. Tan, B. Lai, Efficient peroxymonosulfate activation by $CoFe_2O_4$-CeO_2 composite: performance and catalytic mechanism, Chem. Eng. J. 435 (2022), 134840, https://doi.org/10.1016/j.cej.2022.134840.

[118] H. Lu, H. Shi, Q. Xie, L. Li, Y. Xiao, L. Jia, D. Li, Surface modification of Co_3O_4 nanosheets to promote peroxymonosulfate activation for degradation of atrazine, Catal. Lett. 152 (2022) 3347–3353, https://doi.org/10.1007/s10562-021-03874-4.

[119] L. Yang, Y. Wei, Y. Peng, Y. Liu, Z. Shu, Y. Wang, Q. Meng, C. Zhao, H. Zhao, F. Yang, B. Lai, Carbonized resin with Fe&Co bimetal for peroxymonosulfate activation to degrade atrazine, Sep. Purif. Technol. 292 (2022), 121049, https://doi.org/10.1016/j.seppur.2022.121049.

[120] Y.-H. Guan, J. Ma, Y.-M. Ren, Y.-L. Liu, J.-Y. Xiao, I.-Q. Lin, C. Zhang, Efficient degradation of atrazine by magnetic porous copper ferrite catalyzed peroxymonosulfate oxidation via the formation of hydroxyl and sulfate radicals, Water Res 47 (2013) 5431–5438, https://doi.org/10.1016/j.watres.2013.06.023.

[121] G. Wang, C. Cheng, J. Zhu, L. Wang, S. Gao, X. Xia, Enhanced degradation of atrazine by nanoscale $LaFe_{1-x}CuO_{3-\delta}$ perovskite activated peroxymonosulfate: performance and mechanism, Sci. Total Environ. 673 (2019) 565–575, https://doi.org/10.1016/j.scitotenv.2019.04.098.

[122] H. Song, S. Pan, Y. Wang, Y. Cai, W. Zhang, Y. Shen, C. Li, MXene-mediated electron transfer in Cu(II)/PMS process: from Cu(III) to Cu(I), Sep. Purif. Technol. 297 (2022), 121428, https://doi.org/10.1016/j.seppur.2022.121428.

[123] P. Xu, P. Wang, X. Li, R. Wei, X. Wang, C. Yang, T. Shen, T. Zheng, G. Zhang, Efficient peroxymonosulfate activation by CuO-Fe_2O_3/MXene composite for atrazine degradation: performance, coexisting matter influence and mechanism, Chem. Eng. J. 440 (2022), 135863, https://doi.org/10.1016/j.cej.2022.135863.

[124] H. Zheng, J. Bao, Y. Huang, L. Xiang, B. Ren, J. Du, M.N. Nadagouda, D. D. Dionysiou, Efficient degradation of atrazine with porous sulfurized Fe_2O_3 as

catalyst for peroxymonosulfate activation, Appl. Catal. B: Environ. 259 (2019), 118056, https://doi.org/10.1016/j.apcatb.2019.118056.
[125] Y. Feng, J. Zhong, L. Zhang, Y. Fan, Z. Yang, K. Shih, H. Li, D. Wu, B. Yan, Activation of peroxymonosulfate by Fe^0@Fe_3O_4 core-shell nanowires for sulfate radical generation: electron transfer and transformation products, Sep. Purif. Technol. 247 (2020), 116942, https://doi.org/10.1016/j.seppur.2020.116942.
[126] P. Wang, X. Liu, W. Qiu, F. Wang, H. Jiang, M. Chen, W. Zhang, J. Ma, Catalytic degradation of micropollutant by peroxymonosulfate activation through Fe(III)/Fe(II) cycle confined in the nanoscale interlayer of Fe(III)-saturated montmorillonite, Water Res 182 (2020), 116030, https://doi.org/10.1016/j.watres.2020.116030.
[127] F. Wang, S.-S. Liu, Z. Feng, H. Fu, M. Wang, P. Wang, W. Liu, C.-C. Wang, High-efficient peroxymonosulfate activation for rapid atrazine degradation by FeS_x@MoS_2 derived from MIL-88A(Fe), J. Hazard. Mater. 440 (2022), 129723, https://doi.org/10.1016/j.jhazmat.2022.129723.
[128] J. Ali, D. Li, A. Shahzad, M. Wajid Ullah, J. Ifthikar, M. Asif, C. Yanan, X. Lei, Z. Chen, S. Wang, MoS_4-LDH: a dual center Fe-based layered double hydroxide catalyst for efficient atrazine removal and peroxymonsulfate activation, Chem. Eng. J. 456 (2023), 141161, https://doi.org/10.1016/j.cej.2022.141161.
[129] H. Zhang, R. Zhang, Z. Wu, F. Yang, M. Luo, G. Yao, Z. Ao, B. Lai, Cobalt-doped boosted the peroxymonosulfate activation performance of $LaFeO_3$ perovskite for atrazine degradation, Chem. Eng. J. 452 (2023), 139427, https://doi.org/10.1016/j.cej.2022.139427.
[130] H. Zhang, X. Liu, J. Ma, C. Lin, C. Qi, X. Li, Z. Zhou, G. Fan, Activation of peroxymonosulfate using drinking water treatment residuals for the degradation of atrazine, J. Hazard. Mater. 344 (2018) 1220–1228, https://doi.org/10.1016/j.jhazmat.2017.11.038.
[131] H. Zhang, X. Liu, C. Lin, X. Li, Z. Zhou, G. Fan, J. Ma, Peroxymonosulfate activation by hydroxylamine-drinking water treatment residuals for the degradation of atrazine, Chemosphere 224 (2019) 689–697, https://doi.org/10.1016/j.chemosphere.2019.02.186.
[132] C. Li, Y. Huang, X. Dong, Z. Sun, X. Duan, B. Ren, S. Zheng, D.D. Dionysiou, Highly efficient activation of peroxymonosulfate by natural negatively-charged kaolinite with abundant hydroxyl groups for the degradation of atrazine, Appl. Catal. B: Environ. 247 (2019) 10–23, https://doi.org/10.1016/j.apcatb.2019.01.079.
[133] Y. Feng, L. Zhang, Z. Yang, Y. Fan, K. Shih, H. Li, Y. Liu, D. Wu, Nonradical degradation of microorganic pollutants by magnetic N-doped graphitic carbon: a complement to the unactivated peroxymonosulfate, Chem. Eng. J. 392 (2020), 123724, https://doi.org/10.1016/j.cej.2019.123724.
[134] Y. Huang, L. Lai, W. Huang, H. Zhou, J. Li, C. Liu, B. Lai, N. Li, Effective peroxymonosulfate activation by natural molybdenite for enhanced atrazine degradation: role of sulfur vacancy, degradation pathways and mechanism, J. Hazard. Mater. 435 (2022), 128899, https://doi.org/10.1016/j.jhazmat.2022.128899.
[135] C. Ding, G. Zeng, Y. Tao, X. Long, D. Gong, N. Zhou, R. Zeng, X. Liu, Y. Deng, M.-E. Zhong, Environmental-friendly hydrochar-montmorillonite composite for efficient catalytic degradation of dicamba and alleviating its damage to crops, Sci. Total Environ. 856 (2023), 158917, https://doi.org/10.1016/j.scitotenv.2022.158917.
[136] N. Jaafarzadeh, F. Ghanbari, M. Ahmadi, Efficient degradation of 2,4-dichlorophenoxyacetic acid by peroxymonosulfate/magnetic copper ferrite nanoparticles/ozone: a novel combination of advanced oxidation processes, Chem. Eng. J. 320 (2017) 436–447, https://doi.org/10.1016/j.cej.2017.03.036.
[137] J. Zhou, X. Guo, X. Zhou, J. Yang, S. Yu, X. Niu, Q. Chen, F. Li, Y. Liu, Boosting the efficiency of Fe-MoS_2/peroxymonosulfate catalytic systems for organic pollutants remediation: insights into edge-site atomic coordination, Chem. Eng. J. 433 (2022), 134511, https://doi.org/10.1016/j.cej.2022.134511.
[138] J. Zuo, J. Shen, J. Kang, P. Yan, B. Wang, S. Wang, D. Fu, W. Wang, T. She, S. Zhao, Z. Chen, B-doped $NiFe_2O_x$ based on the activation of peroxymonosulfate for degrading 2,4-dichlorophenoxyacetic acid in water, Chem. Eng. J. 459 (2023), 141565, https://doi.org/10.1016/j.cej.2023.141565.
[139] Q. Yi, L. Bu, Z. Shi, S. Zhou, Epigallocatechin-3-gallate-coated Fe_3O_4 as a novel heterogeneous catalyst of peroxymonosulfate for diuron degradation: performance and mechanism, Chem. Eng. J. 302 (2016) 417–425, https://doi.org/10.1016/j.cej.2016.05.025.
[140] N.T. Dung, V.D. Thao, N.N. Huy, Decomposition of glyphosate in water by peroxymonosulfate activated with CuCoFe-LDH material, Vietnam J. Chem. 59 (2021) 813–822, https://doi.org/10.1002/vjch.202100045.
[141] N.T. Dung, P.T.H. Hanh, V.D. Thao, L.V. Ngan, N.T. Thuy, D.T.M. Thanh, N. T. Phuong, K.A. Lin, N.N. Huy, Decomposition and mineralization of glyphosate herbicide in water by radical and non-radical pathways through peroxymonosulfate activation using Co_3O_4/g-C_3N_4: a comprehensive study, Environ. Sci.: Water Res. Technol. 9 (2022) 221–234, https://doi.org/10.1039/d2ew00688j.
[142] J. Li, Z. Ni, Q. Gao, X. Yang, Y. Fang, R. Qiu, M. Zhu, S. Zhang, Core-shell structured cobalt-nickel bimetallic sulfide with dual redox cycles to activate peroxymonosulfate for glyphosate removal, Chem. Eng. J. 453 (2023), 129972, https://doi.org/10.1016/j.cej.2022.139972.
[143] L. Xue, L. Hao, H. Ding, R. Liu, D. Zhao, J. Fu, M. Zhang, Complete and rapid degradation of glyphosate with $Fe_3Ce_1O_x$ catalyst for peroxymonosulfate activation at room temperature, Environ. Res. 201 (2021), 111618, https://doi.org/10.1016/j.envres.2021.111618.
[144] B. Liu, Y. Wang, X. Hao, J. Wang, Z. Yang, Q. Yang, Ternary transition metal organic frameworks (MOFs) CuZn-MIL101 (Fe) for peroxymonosulfate activation to degradation of 2-methyl-4-chlorophenoxyacetic acid (MCPA): a non-radical pathway dominated by singlet oxygen, J. Environ. Chem. Eng. 11 (2023), 109175, https://doi.org/10.1016/j.jece.2022.109175.
[145] C. Liu, L. Chen, D. Ding, T. Cai, From rice straw to magnetically recoverable nitrogen doped biochar: efficient activation of peroxymonosulfate for the degradation of metolachlor, Appl. Catal. B: Environ. 254 (2019) 312–320, https://doi.org/10.1016/j.apcatb.2019.05.014.
[146] C. Liu, L. Chen, D. Ding, T. Cai, Sulfate radical induced catalytic degradation of metolachlor: efficiency and mechanism, Chem. Eng. J. 368 (2019) 606–617, https://doi.org/10.1016/j.cej.2019.03.001.
[147] C. Marinescu, M. Ben Ali, A. Hamdi, Y. Cherifi, A. Barras, Y. Coffinier, S. Somacescu, V. Raditoiu, S. Szunerits, R. Boukherroub, Cobalt phthalocyanine-supported reduced graphene oxide: a highly efficient catalyst for heterogeneous activation of peroxymonosulfate for rhodamine B and pentachlorophenol degradation, Chem. Eng. J. 336 (2018) 465–475, https://doi.org/10.1016/j.cej.2017.12.009.
[148] L. Amirache, F. Barka-Bouaifel, P. Borthakur, M.R. Das, H. Ahouari, H. Vezin, A. Barras, B. Ouddane, S. Szunerits, R. Boukherroub, Cobalt sulfide-reduced graphene oxide: an efficient catalyst for the degradation of rhodamine B and pentachlorophenol using peroxymonosulfate, J. Environ. Chem. Eng. 9 (2021), 106018, https://doi.org/10.1016/j.jece.2021.106018.
[149] N. Zhou, J. Zu, L. Yang, X. Shu, J. Guan, Y. Deng, D. Gong, C. Ding, M.-E. Zhong, Cobalt (0/II) incorporated N-doped porous carbon as effective heterogeneous peroxymonosulfate catalyst for quinclorac degradation, J. Colloid Interface Sci. 563 (2020) 197–207, https://doi.org/10.1016/j.jcis.2019.12.067.
[150] J. Zhang, C. Wang, N. Huang, M. Xiang, L. Jin, Z. Yang, S. Li, Z. Lu, C. Shi, B. Cheng, H. Xie, H. Li, Humic acid promoted activation of peroxymonosulfate by Fe_3S_4 for degradation of 2,4,6-trichlorophenol: an experimental and theoretical study, J. Hazard. Mater. 434 (2022), 128913, https://doi.org/10.1016/j.jhazmat.2022.128913.
[151] F.J. Rivas, R.R. Solís, Chloride promoted oxidation of tritosulfuron by peroxymonosulfate, Chem. Eng. J. 349 (2018) 728–736, https://doi.org/10.1016/j.cej.2018.05.117.
[152] X. Cheng, H. Liang, A. Ding, X. Tang, B. Liu, X. Zhu, Z. Gan, D. Wu, G. Li, Ferrous iron/peroxymonosulfate oxidation as a pretreatment for ceramic ultrafiltration membrane: control of natural organic matter fouling and degradation of atrazine, Water Res 113 (2017) 32–41, https://doi.org/10.1016/j.watres.2017.01.055.
[153] P. Wang, X. Liu, W. Qiu, F. Wang, H. Jiang, M. Chen, W. Zhang, J. Ma, Catalytic degradation of micropollutant by peroxymonosulfate activation through Fe(III)/Fe(II) cycle confined in the nanoscale interlayer of Fe(III)-saturated montmorillonite, Water Res 182 (2020), 116030, https://doi.org/10.1016/j.watres.2020.116030.
[154] X. Li, J. Ma, Y. Gao, X. Liu, Y. Wei, Z. Liang, Enhanced atrazine degradation in the Fe(III)/peroxymonosulfate system via accelerating Fe(II) regeneration by benzoquinone, Chem. Eng. J. 427 (2022), 131995, https://doi.org/10.1016/j.cej.2021.131995.
[155] J. Hu, H. Chen, H. Dong, L. Zhu, Z. Qiang, J. Yu, Transformation of iopamidol and atrazine by peroxymonosulfate under catalysis of a composite iron corrosion product (Fe/Fe_3O_4): electron transfer, active species and reaction pathways, J. Hazard. Mater. 403 (2021), 123553, https://doi.org/10.1016/j.jhazmat.2020.123553.
[156] X. Li, X. Liu, X. Huang, C. Lin, M. He, W. Ouyang, Activation of peroxymonosulfate by WTRs-based iron-carbon composites for atrazine removal: performance evaluation, mechanism insight and byproduct analysis, Chem. Eng. J. 421 (2021), 127811, https://doi.org/10.1016/j.cej.2020.127811.
[157] Y. Guan, W. Sun, P. Wang, Radical production ratio and atrazine degradation kinetics in PMS/Fe^0, Syst., J. Harbin Inst. Technol. 54 (2022) 50–58, https://doi.org/10.11918/202102008.
[158] O.M. Rodriguez-Narvaez, M.O.A. Pacheco-Alvarez, K. Wróbel, J. Paramo-Vargas, E.R. Bandala, E. Brillas, J.M. Peralta-Hernandez, Development of a Co^{2+}/PMS process involving target contaminant degradation and PMS decomposition, Int. J. Environ. Sci. Technol. 17 (2020) 17–26, https://doi.org/10.1007/s13762-019-02427-y.
[159] J. Li, Y. Wan, Y. Li, G. Yao, B. Lai, Surface Fe(III)/Fe(II) cycle promoted the degradation of atrazine by peroxymonosulfate activation in the presence of hydroxylamine, Appl. Catal. B: Environ. 256 (2019), 117782, https://doi.org/10.1016/j.apcatb.2019.117782.
[160] J.M. Dangwang Dikdim, Y. Gong, G.B. Noumi, J.M. Sieliec, X. Zhao, N. Ma, M. Yang, J.B. Tchatchueng, Peroxymonosulfate improved photocatalytic degradation of atrazine by activated carbon/graphitic carbon nitride composite under visible light irradiation, Chemosphere 217 (2019) 833–842, https://doi.org/10.1016/j.chemosphere.2018.10.177.
[161] Z. Shen, H. Zhou, Z. Pan, Y. Guo, Y. Yuan, G. Yao, B. Lai, Degradation of atrazine by Bi_2MoO_6 activated peroxymonosulfate under visible light irradiation, J. Hazard. Mater. 400 (2020), 123187, https://doi.org/10.1016/j.jhazmat.2020.123187.
[162] Z. Shen, H. Zhou, P. Zhou, H. Zhang, Z. Xiong, Y. Yu, G. Yao, B. Lai, Degradation of atrazine in water by Bi_2MoO_6 and visible light activated Fe^{3+}/peroxymonosulfate coupling System, J. Hazard. Mater. 425 (2022), 127781, https://doi.org/10.1016/j.jhazmat.2021.127781.
[163] Q. Yang, J. An, Z. Xu, S. Liang, H. Wang, Performance and mechanism of atrazine degradation using Co_3O_4/g-C_3N_4 hybrid photocatalyst with peroxymonosulfate under visible light irradiation, Colloids Surf. A: Physicochem. Eng. Asp. 614 (2021), 126161, https://doi.org/10.1016/j.colsurfa.2021.126161.
[164] D. Roy, S. Neogi, S. De, Visible light assisted activation of peroxymonosulfate by bimetallic MOF based heterojunction MIL-53(Fe/Co)/CeO_2 for atrazine

degradation: pivotal roles of dual redox cycle for reactive species generation, Chem. Eng. J. 430 (2022), 133069, https://doi.org/10.1016/j.cej.2021.133069.
[165] R. Tang, D. Gong, Y. Deng, S. Xiong, J. Deng, L. Li, Z. Zhou, J. Zheng, L. Su, L. Yang, π-π Stacked step-scheme PDI/g-C_3N_4/TiO_2@Ti_3C_2 photocatalyst with enhanced visible photocatalytic degradation towards atrazine via peroxymonosulfate activation, Chem. Eng. J. 427 (2022), 131809, https://doi.org/10.1016/j.cej.2021.131809.
[166] K. Wei, A. Armutlulu, Y. Wang, G. Yao, R. Xie, B. Lai, Visible-light-driven removal of atrazine by durable hollow core-shell TiO_2@$LaFeO_3$ heterojunction coupling with peroxymonosulfate via enhanced electron-transfer, Appl. Catal. B: Environ. 303 (2022), 120889, https://doi.org/10.1016/j.apcatb.2021.120889.
[167] Y. Deng, L. Li, H. Zeng, R. Tang, Z. Zhou, Y. Sun, C. Feng, D. Gong, J. Wang, Y. Huang, Unveiling the origin of high-efficiency charge transport effect of C_3N_5/C_3N_4 homojunction for activating peroxymonosulfate to degrade atrazine under visible light, Chem. Eng. J. 457 (2023), 141261, https://doi.org/10.1016/j.cej.2022.141261.
[168] Z. Li, W. Ai, Y. Zhang, J. Zhang, W. Liu, D. Zhong, Y. Cai, E. Johansson, G. Boschloo, W. Jin, L. Yang, Magnetic carbon nanotube modified S-scheme TiO_{2-x}/g-C_3N_4/CNFe heterojunction coupled with peroxymonosulfate for effective visible-light-driven photodegradation via enhanced interfacial charge separation, Sep. Purif. Technol. 308 (2023), 122897, https://doi.org/10.1016/j.seppur.2022.122897.
[169] Z.-C. Zhang, F.-X. Wang, F. Wang, C.-C. Wang, P. Wang, Efficient atrazine degradation via photoactivated SR-AOP over S-BUC-21(Fe): the formation and contribution of different reactive oxygen species, Sep. Purif. Technol. 307 (2023), 122864, https://doi.org/10.1016/j.seppur.2022.122864.
[170] A. Abdelhaleem, W. Chu, Monuron photodegradation using peroxymonosulfate activated by non-metal-doped TiO_2 under visible LED and the modeling via a parallel-serial kinetic approach, Chem. Eng. J. 338 (2018) 411–421, https://doi.org/10.1016/j.cej.2018.01.036.
[171] R.R. Solís, F.J. Rivas, O. Gimeno, J.-L. Pérez-Bote, Synergism between peroxymonosulfate and $LaCoO_3$-TiO_2 photocatalysis for oxidation of herbicides. operational variables and catalyst characterization assessment, J. Chem. Technol. Biotechnol. 92 (2017) 2159–2170, https://doi.org/10.1002/jctb.5228.
[172] L. Yin, J. Wei, Y. Qi, Z. Tu, R. Qu, C. Yan, Z. Wang, F. Zhu, Degradation of pentachlorophenol in peroxymonosulfate/heat system: kinetics, mechanism, and theoretical calculations, Chem. Eng. J. 434 (2022), 134736, https://doi.org/10.1016/j.cej.2022.134736.
[173] K.H. Chan, W. Chu, Degradation of atrazine by cobalt-mediated activation of peroxymonosulfate: different cobalt counteranions in homogenous process and cobalt oxide catalysts in photolytic heterogeneous process, Water Res 43 (2009) 2513–2521, https://doi.org/10.1016/j.watres.2009.02.029.
[174] S. Guerra-Rodríguez, A.R.L. Ribeiro, R.S. Ribeiro, E. Rodríguez, A.M.T. Silva, J. Rodríguez-Chueca, UV-A activation of peroxymonosulfate for the removal of micropollutants from secondary treated wastewater, Sci. Total Environ. 770 (2021), 145299, https://doi.org/10.1016/j.scitotenv.2021.145299.
[175] Y. Lu, W. Xu, H. Nie, Y. Zhang, N. Deng, J. Zhang, Mechanism and kinetic analysis of degradation of atrazine by US/PMS, Int. J. Environ. Res. Public Health 16 (2019) 1781, https://doi.org/10.3390/ijerph16101781.
[176] S. Wu, H. Li, X. Li, H. He, C. Yang, Performances and mechanisms of efficient degradation of atrazine using peroxymonosulfate and ferrate as oxidants, Chem. Eng. J. 353 (2018) 533–541, https://doi.org/10.1016/j.cej.2018.06.133.
[177] G. Shi, S.K. Ong, Oxidation of 2,4-dichlorophenoxyacetic acid by persulfate or peroxymonosulfate with iron(II) as an activator, J. Hazard. Toxic. Rad. Waste 26 (2022), 04021036, https://doi.org/10.1061/(ASCE)HZ.2153-5515.0000645.
[178] Z.-H. Diao, W.-X. Zhang, J.-Y. Liang, S.-T. Huang, F.-X. Dong, L. Yan, W. Qian, W. Chu, Removal of herbicide atrazine by a novel biochar based iron composite coupling with peroxymonosulfate process from soil: synergistic effect and mechanism, Chem. Eng. J. 409 (2021), 127684, https://doi.org/10.1016/j.cej.2020.127684.
[179] N. Jaafarzadeh, F. Ghanbari, M. Ahmadi, Catalytic degradation of 2,4-dichlorophenoxyacetic acid (2,4-D) by nano-Fe_2O_3 activated peroxymonosulfate: influential factors and mechanism determination, Chemosphere 169 (2017) 568–576, https://doi.org/10.1016/j.chemosphere.2016.11.038.
[180] L. Gao, Y. Guo, J. Huang, B. Wang, S. Deng, G. Yu, Y. Wang, Simulating micropollutant abatement during cobalt mediated peroxymonosulfate process by probe-based kinetic models, Chem. Eng. J. 441 (2022), 135970, https://doi.org/10.1016/j.cej.2022.135970.
[181] J.M. Jazic, T. Durkic, B. Basic, M. Watson, T. Apostolovic, A. Tubic, J. Agbaba, Degradation of a chloroacetanilide herbicide in natural waters using UV activated hydrogen peroxide, persulfate and peroxymonosulfate processes, Environ. Sci.: Water Res. Technol. 6 (2020) 2800–2815, https://doi.org/10.1039/d0ew00358a.
[182] C. Wang, W. Li, N. Gao, W. Yang, L. Yu, Comparing the degradation of ametryn in three different systems and identification of radical species, Chin. J. Environ. Eng. 11 (2017) 4520–4526, https://doi.org/10.12030/j.cjee.201606059.
[183] J.A. Khan, X. He, N.S. Shah, H.M. Khan, E. Hapeshi, D. Fatta-Kassinos, D. D. Dionysiou, Kinetic and mechanism investigation on the photochemical degradation of atrazine with activated H_2O_2, $S_2O_8^{2-}$ and HSO_5^-, Chem. Eng. J. 252 (2014) 393–403, https://doi.org/10.1016/j.cej.2014.04.104.
[184] C. Luo, J. Ma, J. Jiang, Y. Liu, Y. Song, Y. Yang, Y. Guan, D. Wu, Simulation and comparative study on the oxidation kinetics of atrazine by UV/H_2O_2, UV/HSO_5^- and UV/$S_2O_8^{2-}$, Water Res 80 (2015) 99–108, https://doi.org/10.1016/j.watres.2015.05.019.
[185] B.R. Gonçalves, A. Della-Flora, C. Sirtori, R.M.F. Sousa, M.C. Starling, J. A. Sánchez Pérez, E.M. Saggioro, S.F. Sales Junior, A.G. Trovó, Influence of water matrix components and peroxide sources on the transformation products and toxicity of tebuthiuron under UVC-based advanced oxidation processes, Sci. Total Environ. 859 (2023), 160120, https://doi.org/10.1016/j.scitotenv.2022.160120.
[186] J.A. Khan, X. He, N.S. Shah, M. Sayed, H.M. Khan, D.D. Dionysiou, Degradation kinetics and mechanism of desethyl-atrazine and desisopropyl-atrazine in water with $^{\bullet}OH$ and $SO_4^{\bullet-}$ based-AOPs, Chem. Eng. J. 325 (2017) 485–494, https://doi.org/10.1016/j.cej.2017.05.011.
[187] J. Andersen, M. Pelaez, L. Guay, Z. Zhang, K. O'Shea, D.D. Dionysiou, NF-TiO_2 photocatalysis of amitrole and atrazine with addition of oxidants under simulated solar light: emerging synergies, degradation intermediates, and reusable attributes, J. Hazard. Mater. 260 (2013) 569–575, https://doi.org/10.1016/j.jhazmat.2013.05.056.
[188] K. Govindan, M. Raja, M. Noel, E.J. James, Degradation of pentachlorophenol by hydroxyl radicals and sulfate radicals using electrochemical activation of peroxomonosulfate, peroxodisulfate and hydrogen peroxide, J. Hazard. Mater. 272 (2014) 42–51, https://doi.org/10.1016/j.jhazmat.2014.02.036.